MASS SPECTROMETRIC IMAGING OF LARGE PEPTIDES BY MALDI-LIT-MS^n

By

DANIEL PATRICK MAGPARANGALAN

A DISSERTATION PRESENTED TO THE GRADUATE SCHOOL
OF THE UNIVERSITY OF FLORIDA IN PARTIAL FULFILLMENT
OF THE REQUIREMENTS FOR THE DEGREE OF
DOCTOR OF PHILOSOPHY

UNIVERSITY OF FLORIDA

2010

To my parents

ACKNOWLEDGMENTS

There are many people to whom I owe a debt of gratitude. First I want to thank my advisor, Rick, for accepting me into his research group and teaching me how to be a great scientist. The environment Rick fostered allowed me to learn the many facets of mass spectrometry, in addition to skills necessary for a good scientist: how to question, and critically think about a problem.

And it goes without saying that without the members of the Yost group, both past and present, made this experience worth the journey. First is my former manager at Mallinckrodt, David Berberich (a former Yostie) who introduced me to the art of mass spectrometry. Then, all of the current and graduated students made the years a joy as we worked hard and enjoyed the fruits of our labors at ASMS. I'd like to especially thank Tim and Dodge for all the mass spectrometry knowledge you imparted to me over the years. I can only hope I have paid that debt back to the group by helping the current graduate students.

In addition to Rick, I'd like to thank Dieter at BMS. His invaluable insights helped push this project to fruition.

Also I would like to thank Mari, Jae, Ed, George (recently at) and Jae at Thermo. Their help and support were instrumental in getting this project (and the instrument) on its way.

Finally, thank you all my friends, family, and finally my fiancée Shawnee. Without your love and support, it would have been a difficult time indeed.

TABLE OF CONTENTS

page

LIST OF TABLES

LIST OF FIGURES

Abstract of Dissertation Presented to the Graduate School
of the University of Florida in Partial Fulfillment of the
Requirements for the Degree of Doctor of Philosophy

MASS SPECTROMETRIC IMAGING OF LARGE PEPTIDES BY MALDI-LIT-MS^n

By

Daniel Patrick Magparangalan

December 2010

Chair: Richard A. Yost
Major: Chemistry

Mass spectrometric imaging (MSI) is a powerful analytical tool that probes a tissue surface to determine analyte distribution throughout the tissue section. After sampling a tissue section at spatially defined positions and collecting a mass spectrum at each position, three-dimensional chemical image maps are constructed by plotting each individual ion's response versus its location. The majority of MSI instruments utilize a time-of-flight mass spectrometer for these experiments. However, these instruments are incapable of performing multiple stages of mass spectrometry (MS^n). This limitation results in limited structural elucidation capabilities and lower analyte selectivity.

Linear ion traps (LIT) are capable of performing MS^n; however, commercial ion traps have a limited upper *m/z* limit (*m/z* 4000). This work describes the extension of the upper mass limit of an LIT past *m/z* 4000 for the analysis of amyloid β (Aβ) peptides (molecular weights ranging from 4100 to 4600 Da) for both in vitro and in vivo analysis. These peptides have been associated with dementia cases, and particularly Alzheimer's Disease. Initial work demonstrated the ability to extend the mass range of the instrument past *m/z* 4000.

Aβ peptides were analyzed in situ using two different strategies. Intact peptide analysis was achieved after performing a series of washes that reduced endogenous interfering ions (particularly lipids). The Aβ peptides were located in the cortex and hippocampus regions of the brain. The comparison of the mass spectral image of Aβ 1–40 in a Tg2576 mouse brain section to a serial section stained with Thioflavin S indicated a good correlation between the two images. Images of the 1–38 and 1–42 fragments also illustrated localization in the cortex and hippocampus regions of the brain. In addition, MS^2 and MS^3 images of selected product fragments of the Aβ 1–40 peptide fragment demonstrated similar localization. Spatial resolution was improved by using smaller step size at a cost of longer analysis times.

In addition to examining intact Aβ peptides, these peptides were digested to form smaller molecules whose molecular weights were well within the mass range of an unmodified LIT. Various sample preparation strategies were explored and the digested fragment Aβ 29–40 was identified by using MS^3 on the tissue section. However, analyte migration was noted after the tryptic digestion. A strategy for reducing analyte migration during tissue digestion and the results are presented in this work.

CHAPTER 1
INTRODUCTION

Background and Significance

Peptides and proteins play a major role within the body as messengers, transporters or building blocks that form the structural backbone of cells and tissues [1]. A greater abundance of a specific biomolecule versus health-state levels could be the first symptom for a patient that is not exhibiting any symptoms. For example, increased levels of certain amyloid β (Aβ) fragments are suspected to play a major role in the progression of Alzheimer's Disease (AD). The levels of certain Aβ peptides build up over a long period of time; however, the disease may not present any clinical symptoms until treatment is futile. Thus, the analysis of endogenous proteins and peptides is important for the study of many disease states and determination of new biomarkers.

Peptide and protein analysis requires several steps of sample preparation. Analysis of endogenous proteins and peptides are typically performed by homogenizing a tissue sample, extracting the peptides, performing a chromatographic separation, and then analyzing the peptides by mass spectrometry. Based upon the mass spectrometer platform, a digestion step may be necessary as some mass spectrometers have a limited upper molecular weight detection limit. During the sample preparation process, however, all spatial information is lost. An alternative analytical method, fluorescence microscopy, can localize of specific proteins [2]; however, this imaging approach lacks the chemical information offered by mass spectrometry and requires tagging the protein of interest.

A complementary technique to established imaging techniques is mass spectrometric imaging (MSI) [3-5]. MSI employs a microscopically focused ionization

source to simultaneously desorb and ionize molecules at a spatially-defined point on the tissue; the ions are then transferred to the mass analyzer, and a mass spectrum is generated for that point (similar to a pixel). The tissue sample is then rastered underneath the microprobe and a mass spectrum is collected at each defined interval. Images are generated by selecting an ion of interest and creating a position-specific, two-dimensional ion map, typically with a color gradient used to indicate the third dimension (ion signal intensity). Figure 1-1 illustrates the localization of two different endogenous lipids in a coronal rat brain section. These images demonstrate the ability of the mass spectrometer to distinguish two unique molecules in the tissue section and produce spatial information for the user.

A significant advantage of MSI over other imaging techniques is molecular selectivity without the need for fluorescently- or radio-labeled compounds, especially when performed in conjunction with tandem mass spectrometry or high resolution accurate mass analysis. Although fluorescently/radio-labeled compounds offer excellent selectivity, the detection is based on the label. For example, a pharmaceutical company may be interested in the distribution of a peptide that treats cancer. However, if the fluorescently or radio-labeled peptide is metabolized within the body, detection of the metabolite would be impossible if cleaved from the radio-label, and the labeled peptide could not be differentiated from a metabolite that retained the label.

The ability to probe discrete sections of tissue for peptides, proteins, and exogenous compounds is a powerful investigative tool for diseased-state studies. Compound-specific images generated from MSI offer insights into peptide distribution with little sample preparation and high molecular selectivity. However, MSI does suffer

from a few drawbacks. MSI lacks a separation step that eliminates a portion of the 'clutter' that inhabits a tissue section (e.g., heme, salts, etc.) Second, MSI is limited to in situ studies. Because experiments cannot be performed on live organisms, the effects of a drug compound on the peptide levels in a brain section cannot be determined in real time as when in vivo studies are performed. Despite these two limitations, MSI offers a complementary analytical technique to established methods to ascertain the biological functions of peptides and proteins within disease-state tissues.

A typical workflow for MSI employing ionization by matrix-assisted laser desorption/ionization (MALDI) is illustrated in Figure 1-2. Tissue samples are sectioned at a specific thickness and mounted onto a sample stage, after which a MALDI matrix is applied. In the source region, a microprobe interrogates a series of spatially defined spots on the tissue, where the size of the spot is most often defined by the diameter of the focused laser beam (typically 50–200 µm). The mass spectrum is then collected for each spot and saved for future data processing, resulting in mass-to-charge (*m/z*) specific ion maps illustrating the distribution of the analyte within the tissue [6].

MSI Workflow

MSI requires significantly less sample preparation than other imaging techniques such as autoradiography or fluorescence techniques; however, optimizing sample preparation and instrumental parameters is important to generating quality mass spectrometric images. For example, poor tissue handling can lead to analyte degradation due to enzymatic processes within the tissue section [7]. Several topics such as sample handling and sectioning, matrix selection, and MSI analysis modes will be discussed in the following sections.

Post-dissection Tissue/Organ Preparation and Storage

It is important to immediately preserve the tissue and whole organs after sacrificing the animal to reduce any post-mortem enzymatic processes that occur. Even three minutes is sufficient time for low-level peptides to degrade beyond the point of detection [8]. When surgically removing tissue and whole organs from the host animal, care must be taken to preserve the original shape of the tissue, lest spatial information be lost. After excision of the tissue, the tissue may be loosely wrapped in aluminum foil prior to immersion in liquid nitrogen for 30 to 60 seconds. Quick submersion is not suggested, as tissue may undergo tissue cracking and degradation. In addition, direct submersion is discouraged to prevent sample adhesion to the walls of the Dewar. Finally, freshly dissected tissue should not be immediately placed in small plastic tubing; otherwise, the tissue may mold to conform to the shape of the tube when frozen. Whole tissues and organs can be stored at -80 °C for at least a year with little sample degradation [7].

Tissue Sectioning and Mounting

Although histological sectioning is typically performed on formalin-fixed, paraffin-embedded tissue, fresh-frozen sectioning of the tissue is the preferred method for MSI experiments. Use of paraffin or OCT (optimal cutting temperature medium) for tissue mounting to the sample stage can cause ion suppression during MSI data collection [7]. To avoid contamination of the tissue sections from the embedding medium, one can deposit several drops of deionized water to the sample stage and then immediately position the tissue onto the drops, thereby freeze-mounting the tissue to the sample stage [9]. Fresh-frozen sectioning of tissue thus avoids additional sample preparation steps.

Tissue sectioning is performed in a cryostat with a microtome. The cryostat is held at a temperature ranging from -20 °C to -30 °C, depending on the tissue type. Tearing of the tissue usually occurs at warmer temperatures; thus, lowering the cryostat temperature should improve tissue section quality. In addition, tissue section thickness can affect the amount of analyte that may be extracted from the tissue (and in turn analyte response) during MALDI experiments because a molecule must travel a longer distance within thicker tissue sections (although thicker sections may also provide more analyte) [10].

Tissue sections are transferred to the sample plate (or microscope glass slide) by picking up the tissue with a set of forceps or using an artistic brush [7]. Additionally, samples may be transferred by placing the plate or microscope slide directly on top of the tissue section and allowing the tissue to naturally adhere to the sample plate surface. For time-of-flight mass spectrometry experiments, a conductive surface must be used to avoid inaccuracies in mass measurement due to surface charging [11, 12]. Because time-of-flight mass spectrometers measure the flight time of an ion, any unaccounted changes in kinetic energy of the ion can change its velocity and cause errors in mass analysis. However, other mass analyzers (such as ion traps) do not have this limitation and can use either conductive or non-conductive surfaces; thus, conventional glass microscope slides are an option as well as stainless steel MALDI sample plates [6]. Tools used for the transfer and mounting of the tissue should be kept within the cryostat to avoid warming of the tissue.

After the tissue section has been transferred to the microscope slide, the tissue is gently heated (e.g., placing a finger against the back of the microscope slide), then

placed back into the cryostat to thaw-mount the tissue to the sample plate surface. After thaw-mounting, tissue sections should be stored at -80 °C until analysis to prevent any enzymatic processes from occurring.

Tissue Section Preparation, MALDI Matrix Selection, and Deposition

Tissue sample preparation is the last step prior to insertion into the MSI instrument. This section will focus on the selection and application of the MALDI matrix to the tissue section. Although a single general purpose protocol will often generate adequate MSI results, ideally each MSI experiment should be individually optimized to tune the experiment for in situ peptide analysis from various tissue types.

Tissue preparation

Prior to matrix application, the tissue may undergo washing, followed by drying in a desiccator to remove excess water. The washing step may be performed to remove endogenous salts that can potentially inhibit MALDI matrix crystal formation. In addition, washing the tissue can remove some endogenous compounds (e.g., lipids) and improve signal-to-noise. For example, a tissue section can be rinsed (or immersed) in 80% to 100% ethanol for 30 seconds [7]. However, care must be taken to limit the immersion, as analytes may migrate, or worse, wash away. As a final step prior to matrix application, the tissue section is placed in a desiccator or under vacuum to remove any excess water (typically from 30 minutes to an hour). Additional water in the tissue sample may result in uneven matrix solvent evaporation, which may lead to uneven co-crystallization of the matrix and analyte. Uneven co-crystallization may result in ‘hot spots’ that lead to regions of artificially higher signal.

MALDI matrix selection

Two properties are necessary for performing optimal MALDI experiments: 1) the matrix should absorb at the wavelength of the laser to limit in-source fragmentation and 2) the matrix should co-crystallize with the target analyte so that the analyte is desorbed into the gas phase upon ablation of the matrix. UV-absorbing compounds that are commonly used with MALDI, and in turn with MSI, are 2,5-dihydroxybenzoic acid (DHB), α-cyano-4-hydroxycinnamic acid (CHCA), and 3,5-dimethoxy-4-hydroxycinnamic acid or sinapinic acid (SA) [7]. Figure 1-3 illustrates the chemical structure of these three compounds. Selection of a specific MALDI matrix is often based upon the analyte of interest. SA is typically used for proteins and large peptides, CHCA is typically used for smaller molecules, and DHB is used as a general-purpose matrix. However, a drawback to using all matrices is the abundance of low *m/z* matrix and cluster ions. Alternative higher molecular weight matrices such as porphyrins [13] also absorb in the UV region but produce less interference in the low *m/z* region [14]. Other options include the use of ionic matrices, which have been reported to have the advantage of continuous matrix coverage over a tissue section [15, 16].

MALDI matrix application methods

Crystal size and coating uniformity play a larger role for MSI applications than standard MALDI experiments. Spatial resolution (the effective pixel dimension of an image) is limited not just by the raster step size of the tissue and the diameter of the laser spot, but also by the size of individual MALDI matrix crystals. Thus DHB, with its elongated crystals, potentially offers a poorer spatial resolution than CHCA or SA, which have small spherical crystals. In addition, coating uniformity will affect the variability of the ion signal across the tissue. An excess of matrix in one location can potentially lead

to an unexpected enhancement or suppression of the ion signal. Uniform matrix deposition should reduce any matrix-related variations in signal.

MALDI matrix coating uniformity and crystal size can be optimized by the choice of matrix, the MALDI matrix solvent solution, and the MALDI matrix application technique. Although dried-droplet matrix application requires the least amount of equipment (a pipettor), it is by far the most irreproducible and time-consuming of the matrix deposition techniques. Other common matrix application techniques for MSI found in the literature include pneumatic spraying [6], inkjet printing [17], acoustic matrix deposition [18], sublimation [19], and solvent-free matrix dry-coating [20]. Of these methods, pneumatic spraying is by far the most common technique. Pneumatic spraying can be performed with a TLC sprayer, a Meinhard nebulizer, or even an artistic airbrush, as each can produce even, homogenous layers of small matrix crystals across the entire tissue section [21]. Commercial devices can further increase matrix crystal reproducibility by automating the matrix coating process.

Spatial Resolution: Relationship between Laser Spot Size and Raster Step Size

Selection of a specific MSI sampling methodology is based upon the size of the tissue sample and information needed. Figure 1-4 illustrates the various MSI image collection strategies available. Typically, the raster step size in an imaging experiment is set equivalent to the spot size of the laser. The spatial resolution is then limited by the spot size of the laser (assuming that the MALDI matrix crystals are not larger than the spot size). To increase the spatial resolution, the raster step size can be decreased. During such an oversampling experiment, the raster step size is reduced to smaller than the diameter of the laser spot. This has a disadvantage, however, of increasing the

analysis time. However, the increase in analysis time can be mitigated by using a more directed approach of interrogating a smaller region of the tissue.

In some cases, the raster step size is increased to be greater than the diameter of the laser spot. Whole-body tissue sections commonly utilize such an approach due to the large area that must be examined. For example, Khatib-Shahidi, et al. [22] used a raster step size of 500 µm for analyzing whole-body rat tissue sections. Although analysis time decreases by in increasing the raster step, spatial resolution is reduced.

MSI Instrumentation

Two primary components are necessary for MSI, 1) a microprobe (i.e., a microscopically focused ionization source to generate ions at a spatially defined point in the tissue section), and 2) a mass analyzer. In the following sections, various microprobe ion sources and mass analyzers typically associated with MSI are presented. In addition, sample preparation and post-acquisition data processing techniques are discussed.

Microprobe Ionization Sources

Three aspects that must be considered when selecting an ionization source are ionization efficiency, spatial resolution, and sampling rate. In general, it is important to optimize ionization efficiency to generate the greatest number of ions from a given spot without causing in-source fragmentation. The size of the microprobe spot defines the spatial resolution, sensitivity, and overall image quality of the MS image. Finally, the sampling rate will affect the overall analysis time for each tissue section.

Optimization of each parameter is important; however, the interconnectivity of the parameters needs to be considered. For example, decreasing the spot size to increase spatial resolution will result in less analyte ablated, thus increasing the detection limit for

the instrument (provided that the laser fluence remains constant). Furthermore, a decrease in step size results in an increase in total analysis time (for example given identical scan areas, a 50% decrease of step size would result in a four times increase in analysis time). The three most common sources for MSI are matrix-assisted laser desorption/ionization (MALDI), secondary ion mass spectrometry (SIMS) and desorption electrospray ionization (DESI). Although SIMS offers spatial resolution superior to the other two sources, SIMS does not produce intact ions for peptides in the mass range of interest in this study. For this reason, SIMS will not be discussed here (although more information can be found in a review paper by Solon et al.) [23]. The following sections will focus on the two ionization sources (MALDI and DESI) most commonly used for MSI as well as emerging ionization sources.

Matrix-assisted laser desorption/ionization (MALDI)

The most commonly used ionization source for MSI is matrix-assisted laser desorption/ionization (MALDI). MALDI is a soft ionization technique that employs a laser to produce predominantly singly-charged ions [24, 25]. The key to MALDI is the application of a matrix to the sample. Prior to the introduction of MALDI, laser desorption of intact analytes from tissue was difficult due to the harsh ionization process that caused a high degree of fragmentation—high energies needed for desorption of the molecules into the gas phase. Karas and Hillenkamp found that addition of a large excess of an organic matrix that absorbs at the laser wavelength greatly increased ionization efficiency and as well as the likelihood of forming intact molecular ion species. With this discovery, the analysis of high molecular weight biomolecules (e.g., peptides and proteins) became the most common application for MALDI.

The MALDI matrix typically employed is a small organic acid that co-crystallizes with the analyte and absorbs light at the wavelength of the laser. As the majority of the energy is absorbed by the organic matrix, sample fragmentation is minimized. MALDI matrices typically used are 2,5-dihydroxybenzoic acid (DHB), α-cyano-4-hydroxycinnamic acid (CHCA), and sinapinic acid (SA). The selection of a specific MALDI matrix is based on the tissue type and analyte of interest. Further discussion of MALDI matrix selection can be found in the tissue preparation section.

During the laser ablation of the matrix surface, charged analytes (i.e., ions) are generated and then transferred to the mass spectrometer. The singly-charged ions produced by MALDI are preferred as the mass spectrum is cleaner and easier to interpret (as opposed to an ESI source that can generate a variety of multiply charged species). This is important for tissue analysis as there is a wide abundance of endogenous molecules.

MALDI experiments typically use a pulsed UV laser (e.g., N_2 laser with a 337 nm wavelength) as the ionization source. The laser energy and the number of laser shots required for a MALDI experiment are optimized with respect to MALDI matrix selection and tissue type for each experiment. For example, DHB typically requires more laser energy when compared to a ‘hotter’ matrix, such as CHCA or SA [26].

Although the repetition rate of the laser does not play a direct role in the image quality, higher repetition rates increase sample throughput, with optimal rates employed near the scan rate of the mass analyzer. This is important when performing experiments on larger tissue sections, such as MSI over whole-body tissue sections. For example, depending upon the rastering pattern and repetition rate of the laser,

whole-body tissue experiments can take upwards of 5 days (~115,000 pixels over the entire tissue section at a lateral resolution of 250 µm with an acquisition rate of ~4 s/pixel) [22].

Desorption electrospray ionization (DESI)

A recent alternative method to MALDI is desorption electrospray ionization (DESI) [27, 28], an atmospheric pressure surface sampling technique that, unlike MALDI, does not require a matrix. Charged droplets are emitted from the electrospray source and strike the tissue surface at an angle, thus desorbing compounds as ions that are then transferred into the mass spectrometer. The tissue surface is rastered beneath the DESI emitter [29].

The primary advantages of the DESI technique are that there is little sample preparation required (no MALDI matrix application) and experiments are performed at atmospheric pressure. A further advantage is that specimen size is not limited, so subdivision of whole-body tissue sections is unnecessary for DESI-MS experiment. In contrast, a MALDI-MSI experiment may require the division of a whole body section into pieces that will fit onto the MALDI target plate. This may require computer-stitching programs that can degrade image quality.

A disadvantage of DESI is that many parameters must be optimized prior to a DESI experiment (multiple spray angles and sample distance from both the ESI emitter and to the mass spectrometer) [30]. Also, the sampling rate must be optimized to balance length of analysis time vs. signal response. In addition, the image quality is much lower than MALDI-MSI experiments due to the poor spatial resolution (250 µm) [31]. Finally, inaccurate localization of desorbed ions is a possibility due to the DESI process. For example during a scan performed from left to right on a surface, it was

noted that analytes were washed toward the right [29]. The washing affect is due to the impact of the DESI plume onto the surface as well as analyte-surface interaction, which can result in an MSI representation that is shifted in the direction of the DESI spray [32]. Despite these challenges, DESI has potential for increased use within the MSI field.

Emerging ionization sources

An advantage of atmospheric pressure ionization sources for surface sample analysis is the ability to sample a surface without moving it into the vacuum region, which is usually small to limit the volume to be evacuated for a standard MALDI target plate, typically ~8 x ~13 cm. Another alternative atmospheric pressure source amendable to MSI experiments is a liquid microjunction surface-sampling probe (LMJ-SSP) [33, 34]. This probe consists of an inner and outer sampling tube that forms a microjunction at the surface of the tissue section as solvent is delivered to the surface and then drawn away toward the mass spectrometer. Thus, the effective resolution of this probe is the diameter of the sampling tube (~500 µm). This technique has been used to sample various organs in a whole-body tissue sections; however, no MS images have been published using this technique [33, 34]. A disadvantage of this technique is that the sampling solvent will bias against analytes not compatible with the solvent. As a consequence, incorrect assumptions may be drawn if ion maps of two analytes are compared.

Another alternative microprobe source is nanostructure-initiator mass spectrometry (NIMS) [35]. Although it is not an atmospheric pressure technique, this technique has a similar advantage as SIMS in that no matrix application step is necessary. But unlike SIMS, NIMS is a soft ionization technique; thus, analytes are less likely to undergo fragmentation during the ionization process. And with a similar lateral

spatial resolution (150 µm), NIMS has the potential to generate image maps comparable to MALDI-MSI. This technique however is still relatively new; thus, only one application of NIMS to drugs and metabolites has appeared [36].

Mass Analyzers

Several mass analyzers are in use for MSI experiments. The most common mass analyzer for MSI found in the literature is the time-of-flight (ToF) mass analyzer [37]. However, other mass analyzers offer their own advantages that should not be discounted. For experiments examining compounds in a matrix as complex as tissue, tandem mass spectrometry and/or high resolution mass spectrometry is almost a necessity. This is due to lack of clean-up separation steps prior to mass analysis, such as extraction and LC prior to MS for removal of interfering compounds. Therefore, linear ion traps (LIT) [6], Fourier transform ion cyclotron resonance (FT-ICR) [38], orbitrap [9], QqToF [37], and ToF/ToF [39] instruments are effective when performing MSI experiments for peptide studies in tissue.

Time-of-flight (ToF) mass analyzers

ToF mass analyzers offer reasonably high mass accuracy (< 20 ppm), mass resolution (> 10,000) and a large *m/z* window (up to *m/z* 10,000 in reflectron mode and up to *m/z* 100,000 in linear mode). Fast 'scan times' of the ToF allow for increased sample throughput when paired with a high repetition rate laser. In addition, the pulsed nature of the MALDI laser is well-suited for use with a ToF, as a complete mass spectrum can be recorded for each laser pulse. However, these advantages are balanced by an increased number of laser shots necessary to obtain an adequate signal-to-noise ratio due to the spot-to-spot variability noted in MALDI experiments

(typically 80 to over 700 laser shots per spot in MS mode and 400 to 8000 laser shots in MS/MS mode) [37, 40].

A second drawback of the ToF mass analyzer is the limited structural elucidation capabilities and limited ability to distinguish between analyte and interfering species at the same nominal *m/z* (isobaric species). Most MSI experiments employ a single ToF analyzer, and thus provide only molecular weight information (no structural information). At most, a ToF instrument can provide two stages of mass spectrometry by coupling a second ToF analyzer to form a ToF/ToF [39] or adding a quadrupole mass filter to form a QqToF [22, 37, 41-44]. QqToF and ToF/ToF instruments offer higher analyte selectivity than stand-alone ToFs because they provide collision-induced dissociation (CID) for monitoring product ions in MS/MS. However in some cases, MS^3 (or even further stages) may be required to elucidate a compound's structure or to distinguish between isobaric species [6]. In this case, an ion trap is necessary.

Linear ion trap (LIT) mass analyzers

Although it lacks the wide mass range of a ToF mass analyzer, an ion trap (either a 3-D quadrupole ion trap or a linear ion trap) offers advanced structural elucidation and analyte selectivity by providing two or more stages of tandem mass spectrometry (MS/MS and MS^n) capabilities. Some of the earliest MALDI-MSI experiments were performed on a 3-D quadrupole ion trap, studying the levels of paclitaxil spiked into rat liver sections [4]. Selecting an ion of interest and inducing fragmentation enables the identification of an analyte or differentiation from a potentially interfering peak [6]. Positive identification is especially important in MALDI analysis as there are typically many interfering MALDI matrix-related peaks after matrix application. This overlap makes distinguishing analyte from matrix difficult or impossible, particularly at trace

levels. An additional advantage is that intermediate pressure MALDI-LIT (~70 mTorr) requires fewer laser shots per pixel (~10 laser shots or less) [6]. This both decreases analysis time and reduces the amount of matrix ablated from the tissue surface, which in turn increases the number of times that a tissue sample may be analyzed.

Ion traps are not without drawbacks. Most commercial systems have an upper *m/z* limit of 4000 (although here we have modified the linear ion trap to scan up to *m/z* 5500) [45]. This upper *m/z* cutoff could preclude detection of peptide/protein-based therapeutic drugs or detection of proteins affected by the administration of a drug. In this case, on-tissue enzymatic digestion is an option [46]. However, most drug molecules have molecular weights of less than 1000 Da, and thus are well within the *m/z* range of the linear ion trap instrument.

In addition to the *m/z* limitation, space-charging of ions within the trap can cause mass shifts in the mass spectrum. Although using an LIT as opposed to a 3-D trap largely alleviates the space-charging issues [47], highly abundant background compounds (such as those found during tissue imaging experiments) may impact analyte identification. Despite these challenges, ion traps are a remarkably useful tool for mass spectrometric images because of the ease with which they perform tandem mass spectrometry (MS/MS and MS^n).

Triple quadrupole and other hybrid quadrupole mass analyzers

Although triple quadrupole (QqQ) mass analyzers are widely utilized for quantitation, QqQ instruments are not typically coupled to a MALDI source. An early laser microprobe system employed laser desorption on a QqQ system [48]. The strength of a QqQ instrument is the use of MS/MS to perform selected reaction monitoring (SRM) and/or multiple reaction monitoring (MRM) experiments. In particular,

MRM scans on a QqQ instrument allow for high selectivity for detection of a compound with 100% duty cycle. Coupling a high repetition rate laser (1kHz) to a QqQ instrument increases sample throughput [49, 50].

Whereas there are few MALDI-QqQ instruments, hybrid quadrupole instruments have been employed for MSI experiments, for example a QqLIT [51, 52]. Here, a linear ion trap replaces Q_3 to serve as either a mass filter or an ion trap. This is key because tandem mass spectrometry is almost a necessity for peptide analysis due to the abundance of interfering ions in tissue and the need for structural elucidation. The QqToF instrument, mentioned previously, is another example of a quadrupole hybrid instrument.

High resolution mass analyzers

An alternative method to positively identify an analyte is accurate mass analysis with a high resolution mass analyzer (mass resolution > 100,000). Two options are to use an orbitrap [9, 53] or an FT-ICR [38] instrument. Both mass analyzers offer superior mass accuracy (< 2 ppm) and mass resolution, when compared to an ion trap or ToF. The higher mass accuracy and mass resolution often allows the user to distinguish between analyte and background peaks at the same nominal mass [54]. This is of particular importance with peptide studies, due to the number of isobaric endogenous species in tissue.

One drawback to using an instrument with high mass accuracy is the low sample throughput for the instrument. Sample throughput for MSI experiments can be defined as the number of pixels (i.e., spatially-defined data points) per unit time. ToF instruments typically provide spatially defined mass spectra at a rate of 30–50 pixels/min [38] with ion traps having a similar throughput (60–70 pixels/min) [6]. In

contrast, four pixels/min is the norm for an FT-ICR experiment. Thus for a profiling experiment, it could take eight hours, or even more at higher spatial resolution, to obtain FT-ICR mass spectrometric data over an entire tissue section even for a modest 1700 pixels [38]. An orbitrap experiment requires much less time than an FT-ICR (25 pixels/min, especially if the scanned mass range is narrowed); however, the sample throughput is still not comparable to either a ToF or an LIT [9].

Linear Ion Trap Mass Spectrometry

Ion Trap Theory and Fundamentals

The linear ion trap is a complex mass analyzer that relies upon oscillating radio frequency (RF) pulses to trap ions injected into the trap. The potential of an ion to be trapped within the RF field is illustrated by the Mathieu stability diagram (Figure 1-5) [55]. This figure illustrates the solutions to the reduced Mathieu equation (Equations 1-1 and 1-2) [56-58].

$$a_x = -a_y = -8eU/mr_0^2\Omega_0^2 \quad \text{(Equation 1-1)}$$

$$q_x = -2q_y = -4eV/mr_0^2\Omega_0^2 \quad \text{(Equation 1-2)}$$

Where a and q describe dimensionless parameters that describe regions where an ion is stable within the ion trap. V is the zero-to-peak RF peak voltage, U describes the DC potential placed on the quadrupole rods, Ω_0 is the drive frequency of the RF voltage, r_0 is the internal radio of the LIT, and m is the ion mass.

After trapping, ions are cooled to the center of the trap using a buffer gas (typically helium). These ions are stored within the trap until they reach a boundary and are ejected from the trap. To simplify the instrument's power supplies, DC power supplies

are typically eliminated. Thus, the a_x term is set to zero and thus ions fall along the q_x axis.

Initial commercial ion traps utilized the right hand edge of the ion trap to eject ions (q_{eject} of 0.908). This however led to poor mass resolution. In addition, use of a q_{eject} of 0.908 limited the ion trap to an upper *m/z* limit of ~650. Later discoveries determined that a supplementary voltage applied across the end caps of a three-dimensional ion trap created a hole in the RF field [59]. Ions scanned along the q_x line would leave the trap upon reaching that hole. This type of scan (mass selective instability scan with resonant ejection) dramatically improved mass resolution and increased the upper mass limit of an ion trap to *m/z* 2000 when a q_{eject} of 0.88 is employed.

Linear Ion Trap (LIT) Description

Improvements of trapping design lead to the development of the 2D ion trap. The 2D ion trap consists of three sections, (Figure 1-6) [47]. Ions enter through the front section of the ion trap and then are trapped within the center section. During ion trapping and isolation, the front and back sections of the LIT are held at a higher positive voltage (for positive ions) or negative voltage (for negative ions) to reduce ion leakage through the axial ends of the trap. During ejection, ions are ejected through two slits in the center section rods and are detected by two electron multipliers. Compared to a 3D trap, the 2D trap holds more ions due to the stretched geometry in the z direction. Also more ions are detected as ions are ejected from both sides of the trap (radially).

MALDI Source for the LIT

A conventional ESI-LIT has two sets of quadrupole rods in front of the LIT to guide ions from the high-pressure source region to the low-pressure trapping region.

Modifications of the first set of quadrupole rods (q00) were necessary to permit MALDI operation. Figure 1-7 illustrates the MALDI modification to the LIT. A hole was bored into one of the q00 rods to allow the laser beam to strike the sample plate. To accelerate the ion passage through q00, a set of auxiliary rods extracts ions produced at the sample surface and accelerates them down toward q0. This is different from the ESI-LIT, where the pressure differential is sufficient to draw any ions toward the lower pressure region of the instrument.

Initial versions of the LIT system in the lab utilized a fiber optic cable to transmit laser light to the sample plate. This however was found to be insufficient for experiments as it was necessary to perform constant alignment checks to achieve optimal laser transmission. The current laboratory setup utilizes a series of mirrors, neutral density filters and lenses to direct, focus and attenuate the laser to the sample plate surface (Figure 1-8).

The instrument is fitted with a 337 nm, 60 Hz N_2 laser (model MNL-100; LTB Lasertechnik Berlin GmbH). The laser spot size for this instrument is approximately 100 µm with an upper laser energy transmission of 70 µJ per pulse. However, laser energies ranging from 2 µJ to 10 µJ are sufficient for most MSI experiments.

Peptide Fragmentation and Identification

Structural elucidation of peptides can be performed by fragmentation of a peptide ion and subsequently analyzing the resulting peptide fragment ions. Fragmentation of the peptide ion into smaller fragments is commonly performed by collision-induced dissociation (CID) [57]. In a CID experiment, parent ions are isolated within the trap, after which activation energy is applied across the quadrupole rods at a frequency corresponding to the oscillation frequency of the ion. The amplitude of the applied

activation energy is enough to increase the amplitude of ion oscillation from the center of the trap, but not enough to eject it from the trap. The ions will collide with the helium buffer gas, picking up enough internal energy to fragment and form characteristic product ions, which are subsequently ejected from the trap to create a product ion MS/MS spectrum.

Figure 1-9 illustrates an example of MS/MS fragmentation of a five amino acid residue peptide. Fragmentation of a peptide generally takes place at one of the bonds along the peptide backbone (indicated by the dotted lines). After fragmentation, one or more of six types of fragment ions may be generated, termed a, b, c, x, y, or z type ions. The most common ions formed from a low energy CID experiment are b and y type ions. In this example, if a cleavage occurs at the dotted line, a protonated b_3 (Figure 1-9B) and y_2 (Figure 1-9C) ion may result. The subscript number indicates the number of amino acid residues remaining in the peptide fragment. Multiple stages of mass spectrometry may be performed to glean further information on a peptide's sequence.

Alternatives to CID experiments include electron capture dissociation (ECD) and electron transfer dissociation (ETD) [60, 61]. These fragmentation experiments can offer further information of the peptide backbone, such as sites of phosphorylation or glycosylation and typically generate c and z type ions. Examination of the ions resulting from a tandem mass spectrometry experiment allows scientists to perform structural elucidation and identification of a peptide.

Amyloid β Peptides

Amyloid β (Aβ) peptides originate from the amyloid precursor protein (APP). In the normal (non-AD) brain, APP is cleaved and eventually cleared away. However, it is

suspected that in brains afflicted by Alzheimer's Disease (AD), the cleavage of the APP is affected and strands of Aβ 1–42 are preferentially formed [62]. These fragments are aggregate more often than their 1-37, 1-38, and 1-40 isoforms. Figure 1-10 illustrates the suggested formation of the amyloid plaques [63]. Over a period of time, these fragments aggregate into soluble oligomers that eventually aggregate into insoluble plaques (Figure 1-11, see chapter 3 for more information). Figure 1-12 illustrates the potential fragments formed from APP and the enzymes involved with the cleavage [64]. The Aβ hypothesis suggests that these plaques are responsible for the progression of AD [62].

Several methods are available for the analysis of Aβ peptides. Thioflavin S is a common stain that stains the plaques green under a confocal fluorescence microscope as demonstrated in Figure 1-11 [65]. Selectivity for individual amyloid isoforms can be achieved if a fluorescently-tagged antibody is used [66]. Chemical information can be obtained if tissue sections containing the plaques are first digested and then LC-MS or MALDI-MS is performed .

These techniques are adequate if spatial or chemical information is needed. However, histological methods lack any chemical information of the tissues surrounding the Aβ plaques. Conversely, typical MS experiments lack spatial information due to the sample preparation steps necessary for MS analysis. MSI experiments on a ToF instrument have been demonstrated for Aβ plaques [67-69], however ToF instruments lack MS^n for peptide sequencing.

To resolve these limitations, this dissertation will present work demonstrating the ability of a linear ion trap to analyze and locate these high molecular weight peptides

within the tissue section. Several strategies will be offered for Aβ peptide analysis that may be applied to other peptide studies.

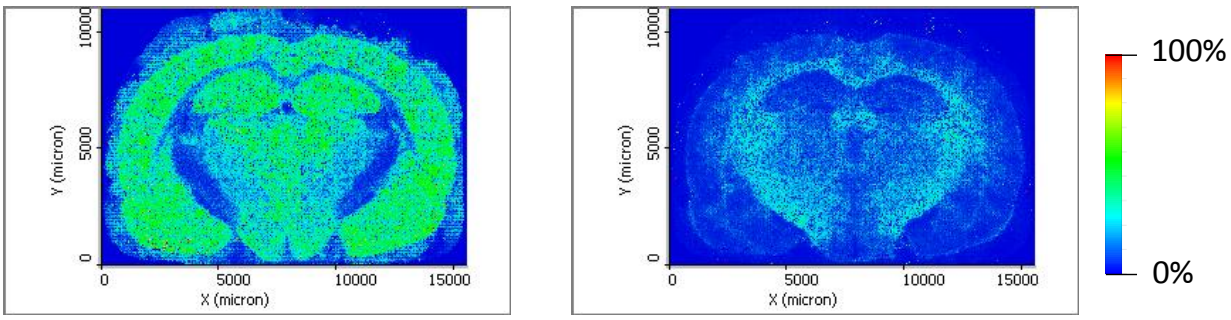

m/z 772.7
PC 16:0/16:0
$[M+K]^+$

m/z 810.7
PC 18:0/18:1
$[M+Na]^+$

Figure 1-1. Example of two MS images of phosphatidylcholine (PC) 16:0/16:0 and PC 18:0/18:1 within the same brain section. Tandem mass spectrometry confirmed the identity of the two lipids.

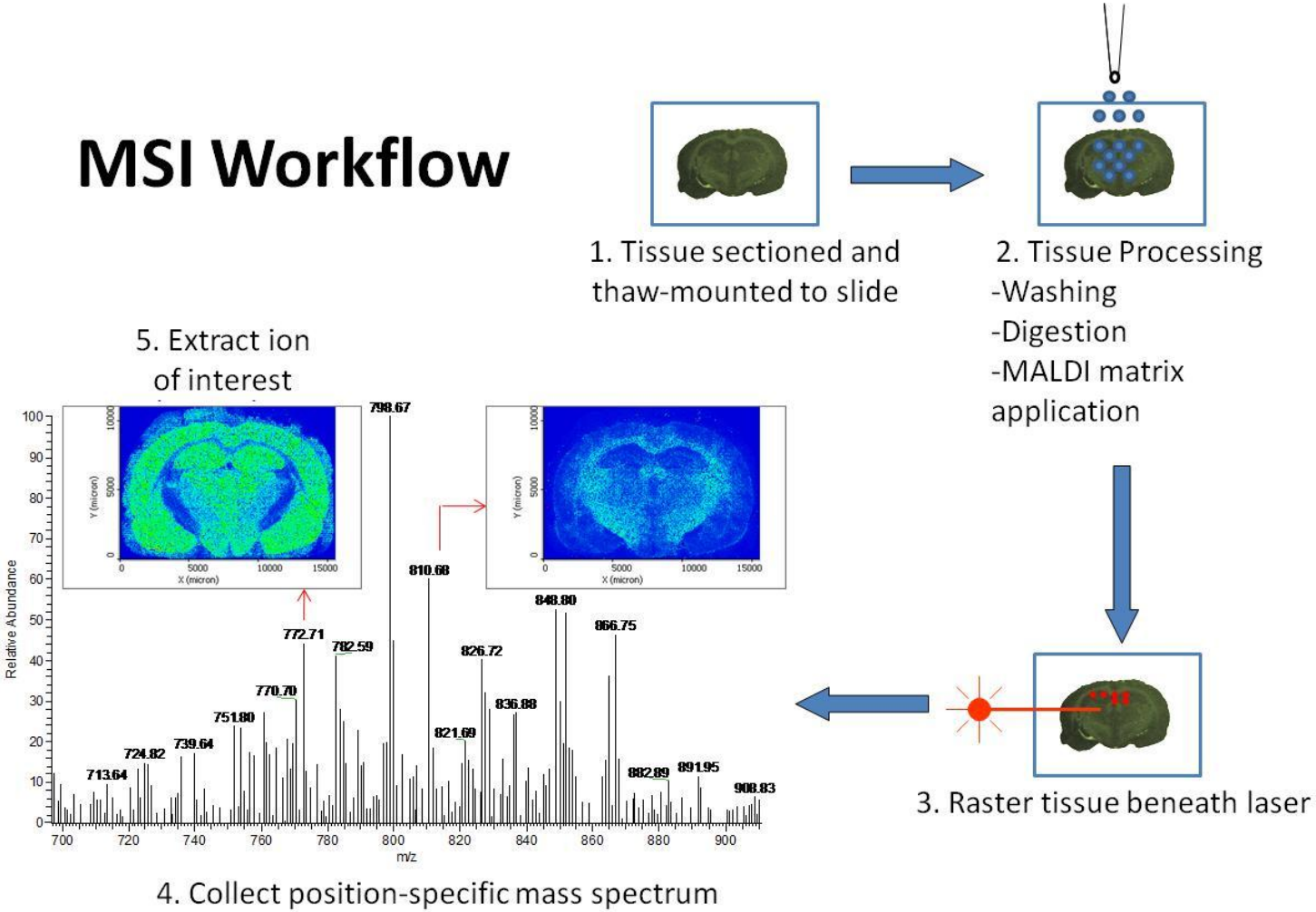

Figure 1-2. Workflow of an example MSI experiment. In this case (1) the brain is sectioned at a thickness of 10 µm. Following sectioning, the brain section is prepared (2) for MALDI-MS analysis. Washing and digestion are two optional steps, performed if the method requires. Finally, the MALDI matrix application is performed prior to insertion into the mass spectrometer. As the tissue section rasters(3) beneath the laser, a mass spectrum is collected at each spot (4). Following MS analysis, ions are selected for imaging (5).

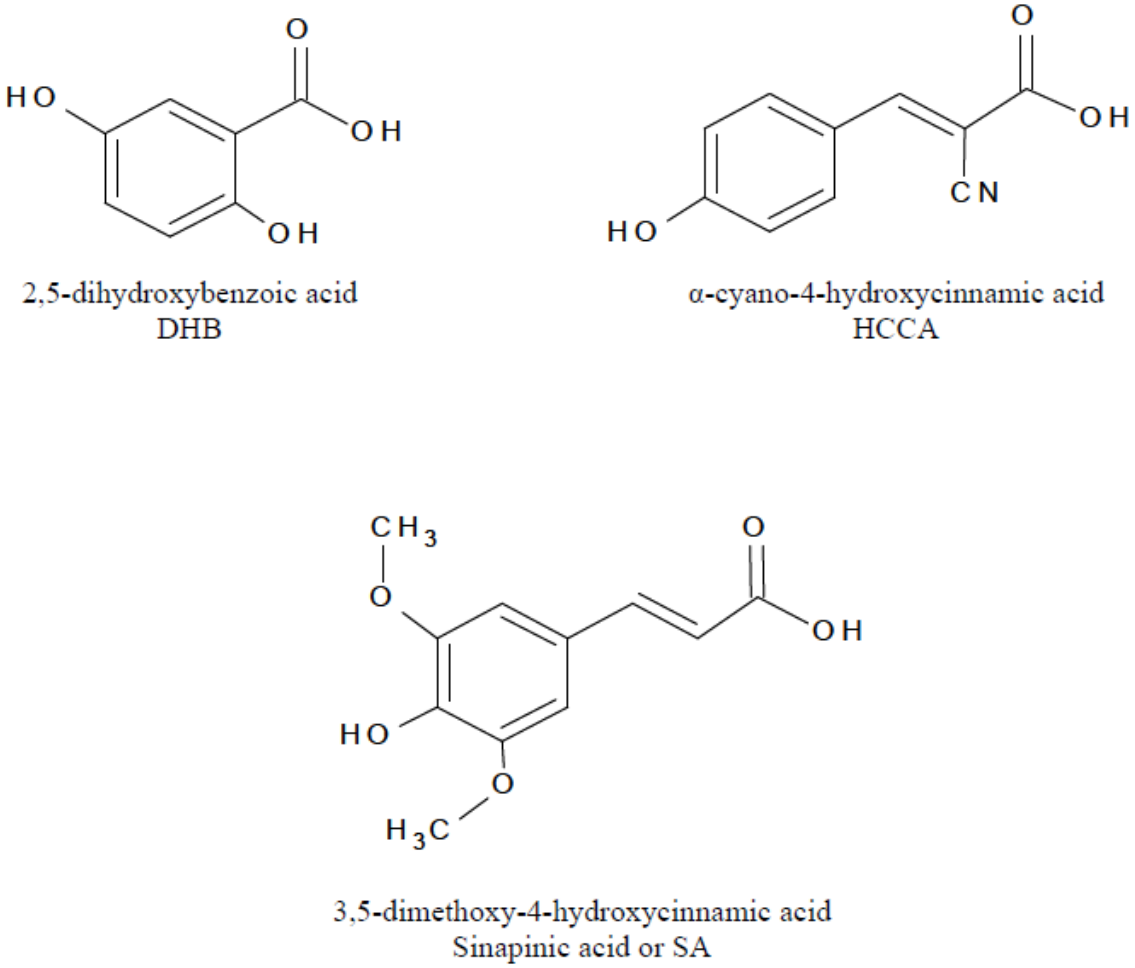

Figure 1-3. Chemical structures of three common MALDI matrix molecules.

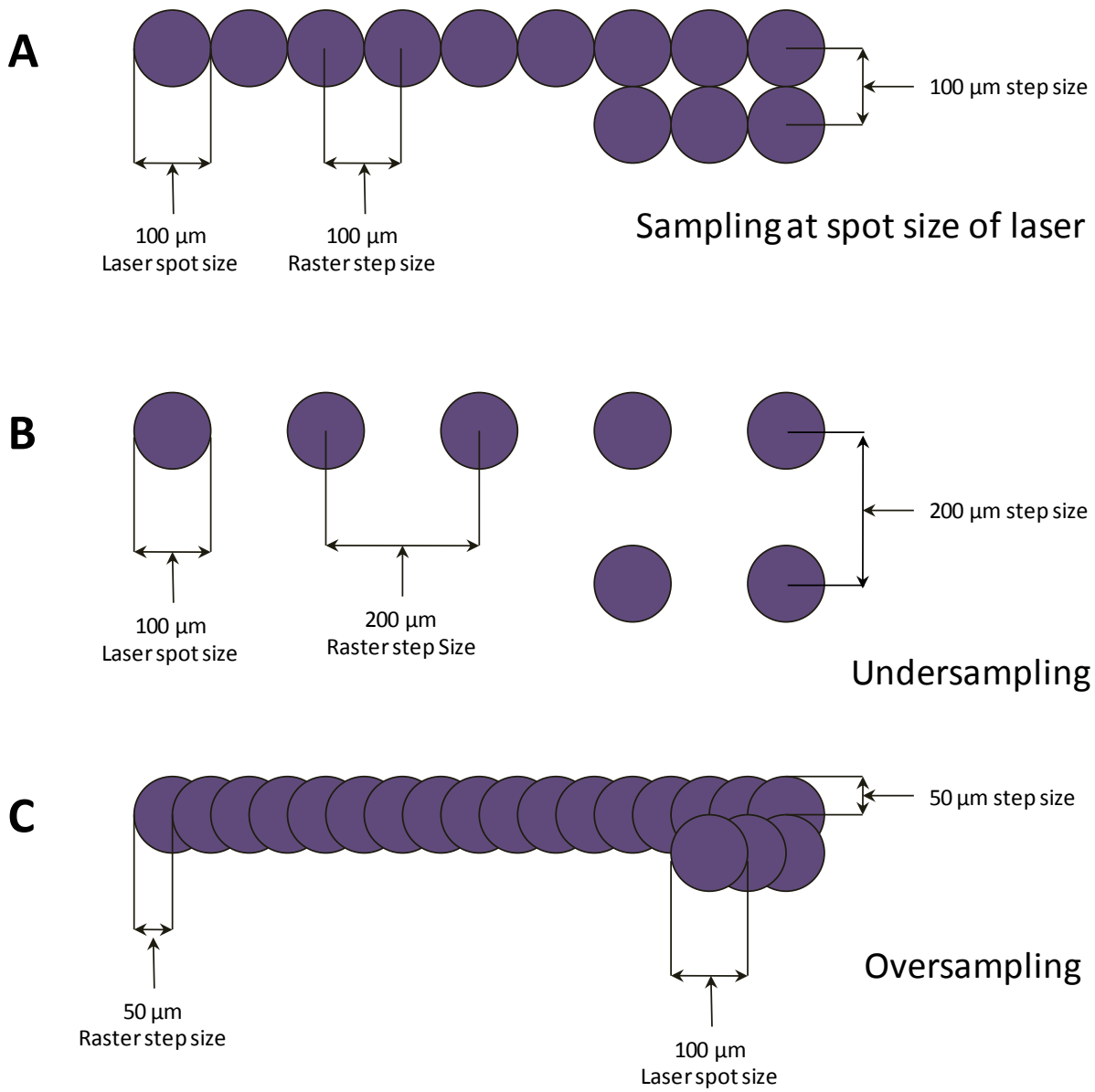

Figure 1-4. Illustration of various sampling techniques for MSI. Typically the tissue is moved at a raster step size equivalent to the laser spot size, A. However for cases when a large area must be analyzed, undersampling may be necessary to avoid unacceptably long analysis times, B. Undersampling is any case where the raster step size is greater than the laser spot size. For cases where the molecule may reside in areas smaller than the spot size of the laser, oversampling may be useful. In this case, the raster step size is decreased to less than that of the laser spot size. Oversampling can improve image resolution at the cost of dramatically increasing analysis times.

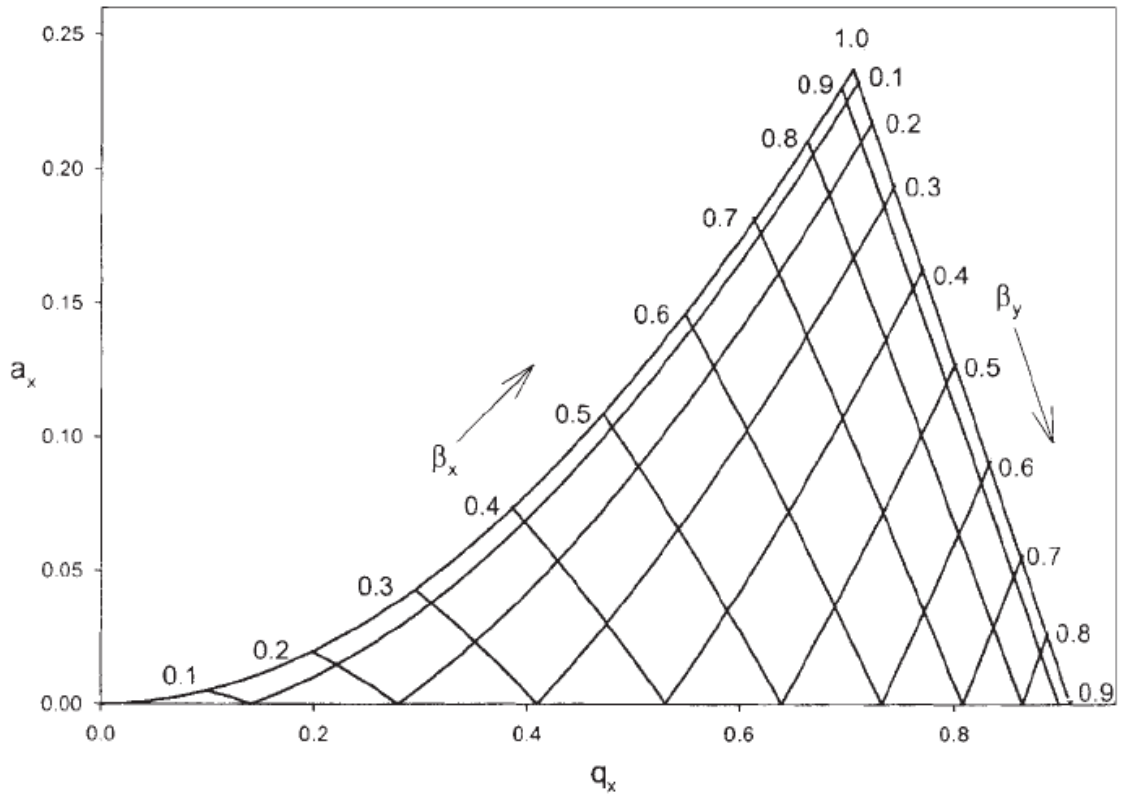

Figure 1-5. Mathieu stability diagram. Ions injected inside the trap are trapped if the trapping field and ion characteristics lie within the shaded region of the diagram. Adapted from Douglas et al. [58].

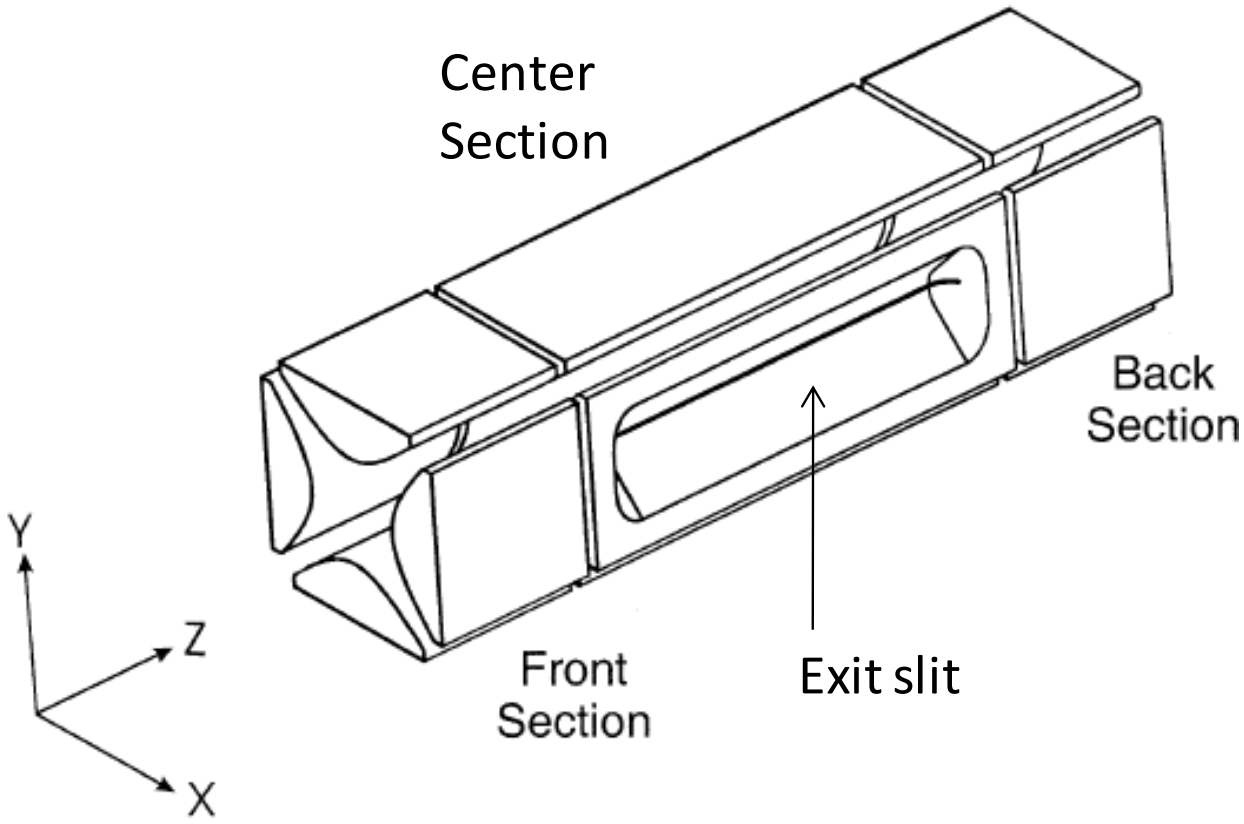

Figure 1-6. Schematic of a 2D linear ion trap. Ions are trapped within the center section of the trap and then subsequently radially ejected through two slits in the center section. Adapted from Schwartz et al. [47].

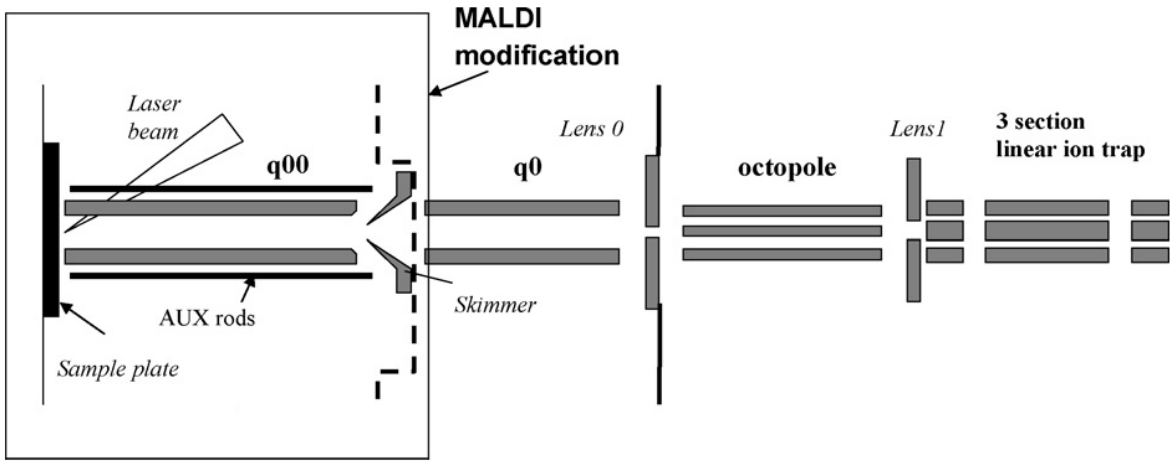

Figure 1-7. Schematic of MALDI LTQ system. The box region indicates the area where the MALDI modification occurred. Adapted from Garrett et al. [6].

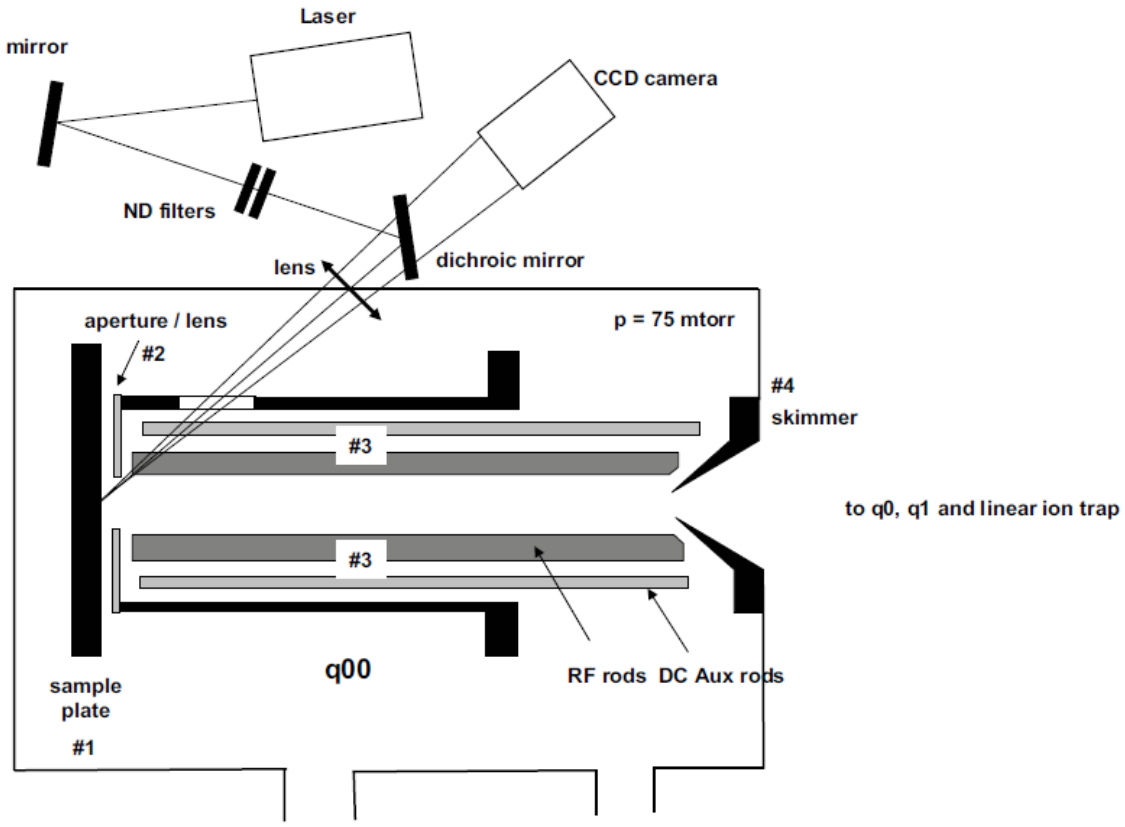

Figure 1-8. Current instrument setup of the MALDI source region. A series of mirrors, neutral density (ND) filters and lenses guide and attenuate the laser beam to the sample plate. Adapted from Strupat et al. [53].

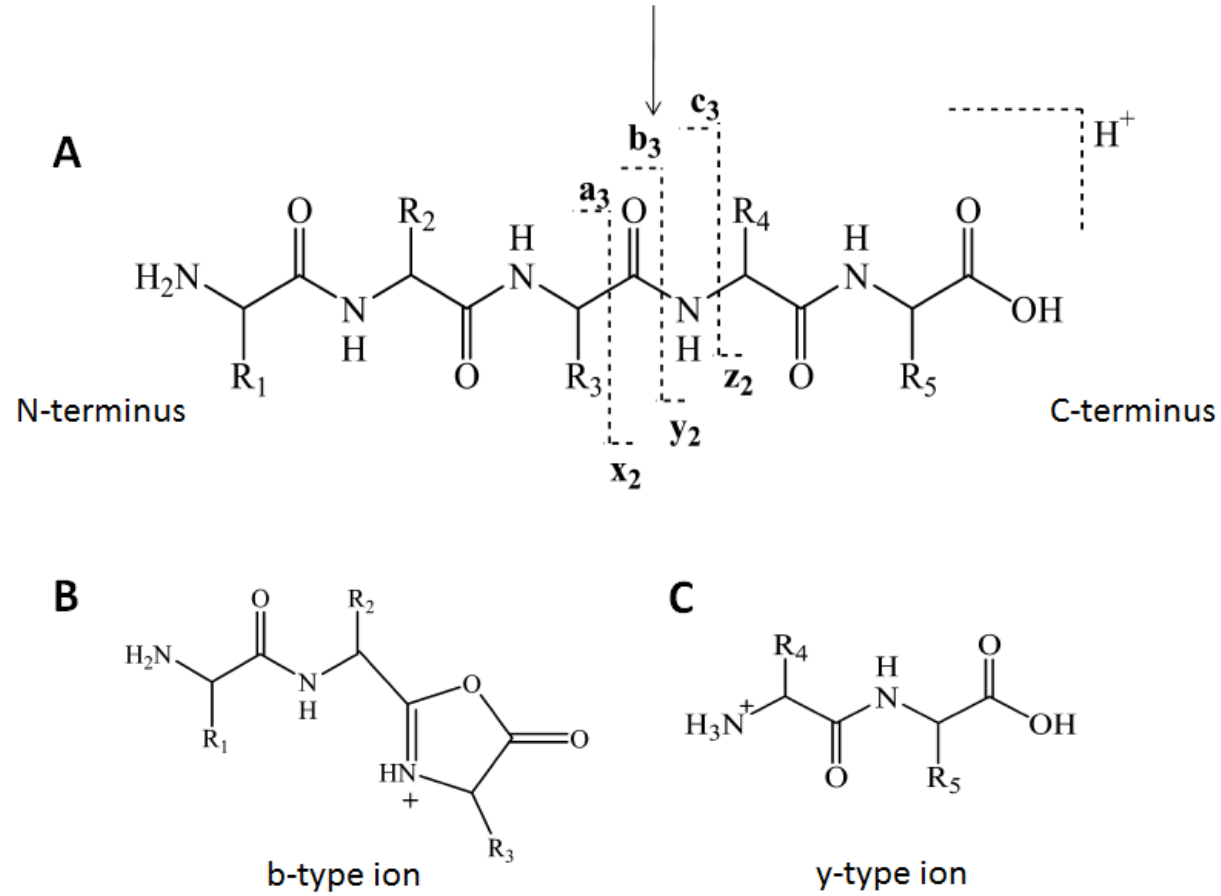

Figure 1-9. Nomenclature for peptide fragments generated by tandem mass spectrometry. The top structure, A, illustrates an example peptide with five amino acid residues (R_1 through R_5). If fragmentation occurs at the dotted line denoted by the arrow, a protonated b_3, B, or y_2, C, ion may result.

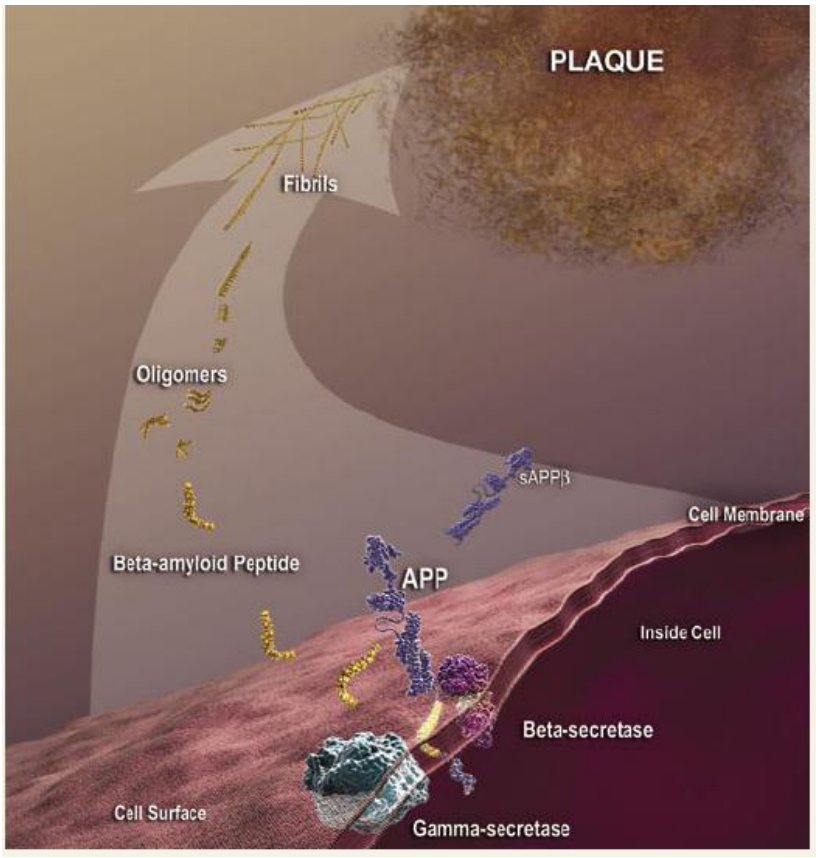

Figure 1-10. Illustration of process that converts APP to amyloid beta plaques. Adapted from the National Institute on Aging [63].

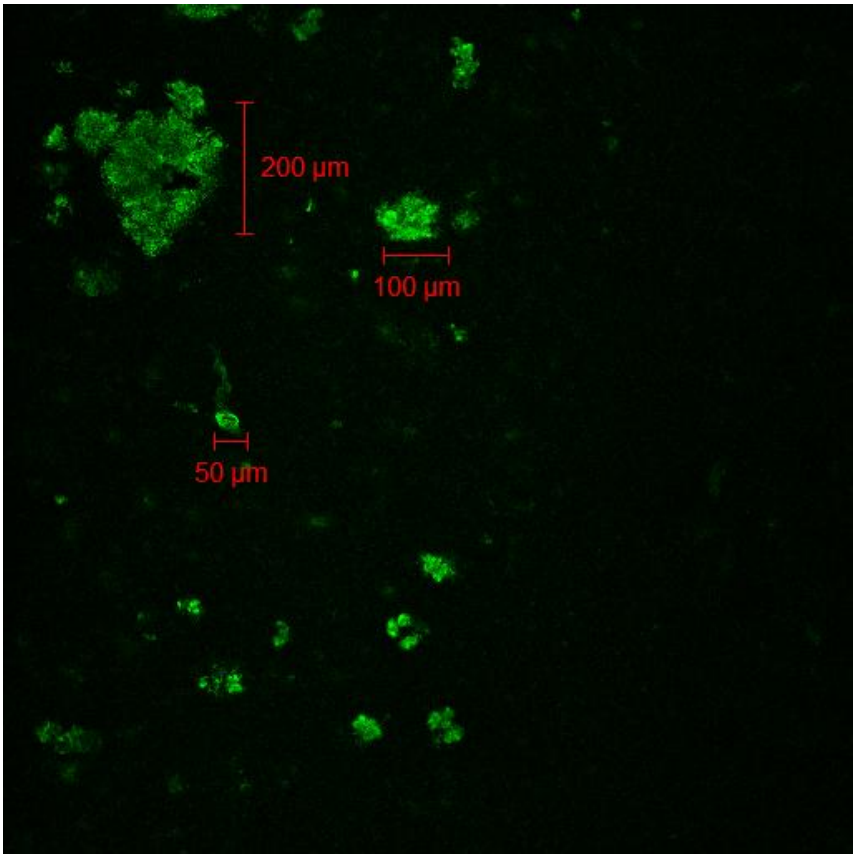

Figure 1-11. Histological stain of amyloid β plaques in a 30 month old Tg2576 mouse.

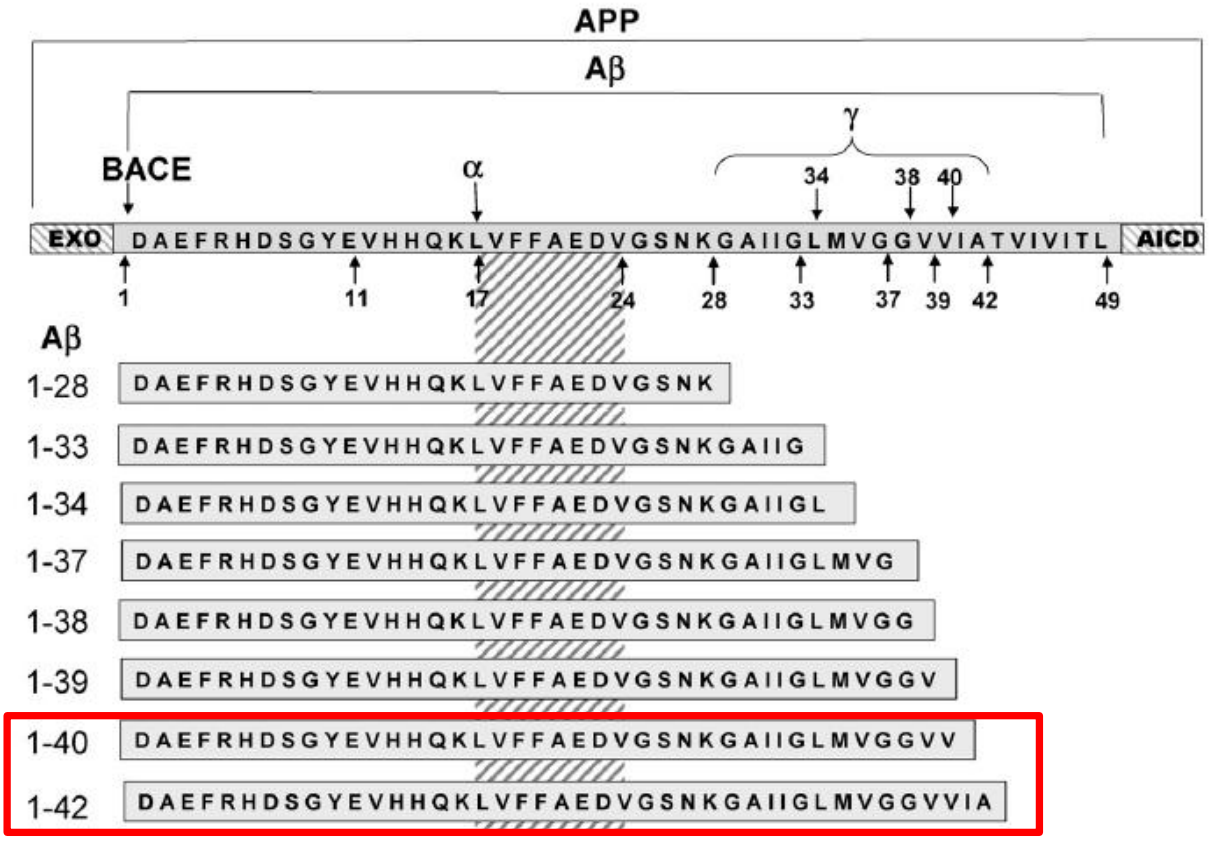

Figure 1-12. Cleavage of APP forms amyloid beta fragments of varying lengths. Aβ plaques primarily consist of Aβ 1–40 and 1–42 peptides (indicated by the red box). Adapted from Ford et al. [64].

CHAPTER 2
ANALYSIS OF LARGE PEPTIDES BY MALDI USING A LINEAR QUADRUPOLE ION TRAP WITH MASS RANGE EXTENSION[†]

Overview

Analysis of large peptides can be used to discover or to monitor biomarkers for various diseases. For example, the levels of such peptides can determine the effectiveness of an experimental drug or the progress of a disease. Many mass spectrometric methods for monitoring these peptides use MALDI-ToF instruments due to their high molecular weights, although such instruments typically lack MS/MS or MS^n capabilities. Here, the *m/z* range of a MALDI-LIT instrument was extended to *m/z* 5500 for the MS or MS^n analysis of large peptides. Instrument performance was examined using amyloid β 1–40 and 1–42 (avg. MW 4330.8 and 4515.0, respectively), large peptides that comprise the bulk of neuritic plaques and are potential biomarkers for Alzheimer's Disease. The amyloid β 1–40 was detected in the full-scan mass spectrum with sufficient resolution to distinguish and match the expected isotopic pattern. The MS/MS product ion spectra of both peptides matched the expected fragmentation patterns; up to MS^4 experiments were performed to verify the identity of the peptides. These experiments clearly demonstrate the advantages of this approach, including MS^n experiments for structural elucidation and simplified spectra due to singly-charged parent ions, for large peptides.

[†] Reproduced in part with permission from Analytical Chemistry, Vol. 82 (3), Magparangalan, D. P., Garrett, T. G., Drexler, D. M., Yost, R. A. Pages 930-934. Copyright 2010 Analytical Chemistry

Mass Range Extension on a Linear Ion Trap

There is much interest in large peptides as biomarkers for various diseases. The levels of such peptides can determine a drug's efficacy in clinical trials, assist in early stage disease diagnosis, or monitor the progress of a patient's treatment [70-72]. The analyses of these biomarkers are typically performed using mass spectrometry.

Mass spectrometry offers accurate mass analysis and analyte fragmentation techniques to facilitate peptide identification and elucidation of a peptide's structure. As these peptides can have a high molecular weight, the ionization techniques typically employed are electrospray ionization (ESI) and matrix-assisted laser desorption/ionization (MALDI) [64, 70, 71, 73, 74]. ESI generates multiply-charged ions that are then transferred to the mass analyzer. Thus, large peptides and proteins can be detected using mass analyzers with a limited mass-to-charge (*m/z*) range. Conversely, MALDI predominately generates singly-charged ions. The choice of ionization source is dependent on the mass spectrometer's upper *m/z* cutoff. In addition to accurate mass analysis and enhanced mass resolution, time of flight (ToF) mass spectrometers have a high upper *m/z* cutoff (up to *m/z* ~ 10,000 in reflectron mode) that enables the coupling of a MALDI source to observe high MW singly-charged ions. Unfortunately, MS/MS capabilities for structural elucidation are limited with a ToF mass spectrometer; at best, it can perform MS^2, and that typically requires a ToF-ToF tandem instrument.

In comparison, linear ion trap (LIT) mass spectrometers provide multiple stages of MS (MS^n), which enhance selectivity, structural elucidation, and identification. However, an LIT has a lower *m/z* cutoff (typically *m/z* 2000 or 4000) compared to a ToF. When ESI sources are coupled to LITs, this is not typically a limitation, as analytes

introduced into the MS are multiply-charged species whose *m/z* falls within the LIT *m/z* window. One disadvantage of multiple charging is increased complexity of the MS and MS^n spectra.

Here we evaluate a MALDI-LIT MS with an extended *m/z* range. There are several techniques for extending the mass range of an LIT. The following equation gives the upper *m/z* limit, $(m/z)_{max}$, of an LIT operated in mass-selective instability mode [56]:

$$(m/z)_{max} = \frac{4V_{max}}{q_{eject}\, r_0^2\, \Omega^2} \qquad \text{(Equation 2-1)}$$

where V_{max} is the zero-to-peak RF peak voltage level, r_0 is the internal radius of LIT, Ω_0 is the drive frequency of the RF voltage, and q_{eject} is the point on the stability diagram where the ion becomes unstable and is ejected. From equation 1, the *m/z* range can be extended in four ways: (i) increasing the maximum RF voltage, (ii) decreasing the trapping dimensions, (iii) decreasing the RF drive frequency, or (iv) decreasing the q_{eject} [75]. For these studies, the q_{eject} was lowered to achieve a higher *m/z* cutoff (*m/z* 5500).

To test the effectiveness of the instrument modification for the analysis of large peptides, fragments of the amyloid β peptide population were selected. Amyloid β peptides (Aβ) comprise the bulk of neuritic plaques that are characteristic of Alzheimer's disease [76, 77]. These peptides are produced by the sequential cleavage of the amyloid β precursor protein by the aspartyl protease β-secretase and the presenilin-dependent protease γ-secretase [78]. An analytical technique that can monitor the

levels of such peptide fragments could be used for biomarker determination in Alzheimer's disease [79, 80].

This chapter describes the effect of lowering the qeject of the LIT mass spectrometer to facilitate analysis of singly-charged amyloid β peptide fragments. This approach allows for multiple stages of fragmentation (MSn) to be performed in order to enhance selectivity and structural elucidation. The use of MALDI for ionization offers the potential for mass spectrometric imaging of these markers in intact tissue.

Experimental Methods

Sinapinic acid (SA, 3,5-dimethoxy-4-hydroxycinnamic acid) was purchased from Sigma-Aldrich (St. Louis, MO) and used as the MALDI matrix for all analyses. Ammonium hydroxide and HPLC-grade acetonitrile and water were purchased from Fisher Scientific (Fairlawn, NJ). Trifluoroacetic acid (TFA) was purchased from Acros Organics (Morris Plains, NJ). The analytes [Aβ 1–40 and Aβ 1–42] and ProteoMass™ MALDI calibration kit were purchased from Sigma-Aldrich. Uniformly ^{15}N-labeled Aβ 1–40 and ^{15}N-labeled Aβ 1–42 were purchased from rPeptide (Athens, GA). Analytes were prepared at a concentration of 100 μg/mL in 1% ammonium hydroxide (aq). Sinapinic acid MALDI matrix solution was prepared at a concentration of 20 mg/mL in 50:50:0.1 acetonitrile:water:TFA (v:v:v). The dried droplet method was employed to deposit 1.5 μL of sample analyte and 1.5 μL of matrix onto the MALDI well plate.

A Finnigan LTQ linear ion trap fitted with an intermediate pressure vMALDI source (San Jose, CA) was used for all experiments. The MALDI source has a nitrogen laser (337 nm) with a frequency of 20 Hz and maximum energy of 250 μJ/pulse. For collection of full-scan mass spectra, a laser power of 12% was used so as to limit

space-charging of the peptide ions within the trap (laser output for the vMALDI instrument is measured as % laser power). To increase the number of ions available for MS^n experiments, the laser power was increased to 25%; an isolation window of 12 AMU and a CID energy of 20 (arb) during the MS^n experiments was required for adequate sensitivity at this extended mass range. A more detailed description of this instrument has been previously published [6].

Each MS scan consisted of 3 laser shots, and approximately 50 scans were averaged to generate a mass spectrum for the sample spot. The sample was automatically moved in a circular raster pattern underneath the laser spot. Simulated spectra were generated using Qual Browser software (ver. 2.0.7) from Thermo Fisher. Expected fragment ions were determined using ProteinProspector [81].

When scanning in normal mass mode (up to *m/z* 2000), the instrument has a q_{eject} of 0.88 [47]. In high mass mode, the q_{eject} is lowered to 0.44, which allows for analysis of ions of *m/z* 150 to 4000. In order to analyze ions beyond *m/z* 4000, the q_{eject} was further lowered to 0.30. This allows for analysis of ions from *m/z* 300 to 5500. Although a decrease in q_{eject} should allow for an upper mass limit of over 5800, the instrument software limits the mass range of the instrument to 5500. The q_{eject} value was lowered through an engineering software patch provided by Thermo. Lowering the q_{eject} value is related to two parameters that are derived from q, namely β and ω [56]. To lower $q_{eject,}$ a reduced β value and a lower resonance ejection frequency (ω) during the mass selective instability scan are required. For a q_{eject} of 0.300, the corresponding β is approximately 0.2161 and the resonance ejection frequency is 130.61 kHz. (For

comparison, at a qeject of 0.44, β is equal to approximately 0.3244 and the resonance ejection frequency is 196.07 kHz.)

Since the mass range was extended past the normal mass calibration range, a rough two-point calibration was performed using bradykinin (Sigma-Aldrich) and Aβ 1–42. Afterward, the instrument was calibrated using the high mass standard within the calibration kit with Aβ 1–42 added.

Results and Discussion

Two issues were addressed to extend the *m/z* range of the instrument beyond *m/z* 4000 — space-charging within the trap and mass resolution. Both issues are related, as increased space-charge decreases mass resolution. Although the LIT has a larger volume to collect ions when compared to a 3-D Paul trap, there is still a finite number of ions that can be collected before loss of resolution due to space-charging occurs [47]. Space-charge effects can be overcome by tailoring the number of laser shots per spot and/or the % laser power of each shot. In these studies, the optimum full-scan MS conditions to prevent space-charging were three laser shots at 12% laser power.

Full-scan Mass Spectra of High MW peptides

After the instrument conditions (laser power, number of laser shots) were optimized, the full-scan spectrum of Aβ 1–40 was acquired with the instrument (Figure 2-1). The monoisotopic *m/z* of the $[M+H]^+$ Aβ 1–40 ion is 4327.3. The isotope pattern of the recorded Aβ 1–40 peptide spectrum (Figure 2-1A) closely matches the isotope pattern of the simulated spectrum (Figure 2-1B). The simulated spectrum was generated using the QualBrowser software included with the LTQ instrument. The

mass resolution for the $[M+H]^+$ ion of the peptide was determined to be 6000 FWHM (full width at half-max).

The detection of amyloid β peptide with an AP/MALDI 3-D ion trap has been previously reported [82]. However, only the +2 charge state was detected due to the upper mass limit of the ion trap. With this instrument, the singly-charged ion is detected in the full-scan mass spectrum with little interference from the background.

MS^n Experiments

To take full advantage of the capabilities of the LIT, MS^2 experiments were performed on the $[M+H]^+$ ion of both the Aβ 1–40 and Aβ 1–42 peptides (Figure 2-2). MS-Product within ProteinProspector was used to identify several of the major ions for both spectra [81].

It is worth noting that optimal isolation of parent ions for MS/MS analysis required an isolation window of 12 Da centered on the most abundant isotope of the Aβ peptide. The widening of the isolation window is a consequence of increasing the % laser power for the MS^n experiment. The % laser power for the MS^n experiments was increased (~25% laser power, twice that for full-scan MS experiments) to increase the number of Aβ peptide ions available for subsequent isolation and fragmentation. With the increased number of ions due to the higher laser power, space-charge broadened the frequency distribution of the ions during the isolation step. The isolation window was therefore widened to ensure that all the Aβ peptide ions were isolated. After the isolation step, the effects of space-charge are greatly reduced, as all ions outside the isolation window have been ejected from the trap. This reduces the ion population within the trap to levels below which space-charge is an issue.

The dominant ions in the MS^2 spectra of the $[M+H]^+$ Aβ 1–40 ion (aside from the loss of water and ammonia) include the y_{33}, y_{37}, y_{39}, b_{22}, and b_{23} ions (Figure 2-2A). For the MS^2 fragmentation of the $[M+H]^+$ Aβ 1–42 ion, the major fragments detected were the y_{35}, y_{39}, y_{41}, b_{22}, and b_{23} ions (Figure 2-2B). The dominance of the y ions in the mass spectra can be explained by preferential fragmentation adjacent to acidic amino acid residues (aspartic acid and glutamic acid) [83].

The MS^2 spectra of the Aβ 1–40 and Aβ 1–42 $[M+H]^+$ ions provide minimal structural information due to preferential cleavage adjacent to acidic amino acids present in the peptide. Therefore, to elucidate further the peptide's structure, additional stages of mass spectrometry are necessary. The y_{33} ion present in Figure 2-2A was isolated and fragmented; the MS^3 mass spectrum is displayed in Figure 2-3A. The fragmentation coverage of the y_{33} fragment ion is much higher, with a number of y-type ions and ions due to internal fragmentation observed. Further coverage of the peptide was achieved by isolating and fragmenting the $(b_{23}y_{33})_{16}$ ion for an MS^4 experiment (Figure 2-3B). In this fashion, identification of the Aβ peptide was demonstrated with MALDI/MS^n. Although acidic amino acid residues caused limited fragmentation coverage in MS^2, additional stages of mass spectrometry overcame this obstacle. This technique could be useful for the identification of unknown peptides, particularly for those not in peptide databases.

Isotopically Labeled Standards

Isotopically-labeled standards are typically used as internal calibrants for quantitative mass spectrometry. Although a single stage of MS can be used for quantitation, analyte specificity can be significantly improved by using tandem MS. The

selectivity of MS^n is of particular value when sample pretreatment and/or chromatographic separation is not available, as in MALDI imaging studies [84]. However, using alternating MALDI/MS/MS experiments of an analyte and its isotopically-labeled standard provides poor reproducibility [85]. This poor precision was attributed to laser shot-to-shot variability and non-homogenous MALDI matrix crystals. To improve precision, the $[M+H]^+$ ions of the analyte and its isotopically labeled standard were isolated for MS/MS in a single scan using a wide isolation window.

Although it is a simple matter to widen the isolation window to encompass the analyte and its isotopically-labeled standard when they differ by only a few AMU, a mass window wide enough to encompass a peptide and its uniformly ^{15}N-labeled analog is more challenging because of the large *m/z* difference. (The difference between the $[M+H]^+$ ions of the Aβ 1–40 and its uniformly ^{15}N-labeled standard is 53 *m/z* units).

Several experiments were performed to examine the capabilities of the instrument to accommodate a wide isolation window. Equal concentrations of Aβ 1–40 and its ^{15}N analog were spotted onto a MALDI well plate spot. Figure 2-4A shows the full-scan spectrum of this mixture. To isolate and fragment both ions in one event, an isolation window of *m/z* 80 was used for the MS/MS experiment centered at *m/z* 4355 (the midway point between Aβ 1–40 and its ^{15}N analog); the MS/MS spectrum is shown in Figure 2-4B. A drawback to this method is trapping and fragmenting unwanted ions that fall in the *m/z* range between the analyte and its isotopically-labeled compound; the fragment ions from these interferences may mask the analyte/internal standard response. Nevertheless, in this case the b and y fragment ion peaks were readily identified in the MS/MS spectrum. In addition, equal intensities for both the analyte, ^{15}N

analog, and their respective fragments were maintained in both the full scan MS and MS/MS spectra.

Conclusions

The experiments and data reported here demonstrate the potential for amyloid β peptide analysis on a linear ion trap by intermediate pressure MALDI employing mass range extension. The isotope pattern of the full-scan MS matches that of the expected spectrum, and MS^n experiments confirm the identity of the peptides. Wide isolation and fragmentation of an amyloid β peptide and its ^{15}N analog were also demonstrated; with this approach, quantitation of the amyloid β peptide would be feasible.

With the extended mass range, limitations such as increased space-charging and loss of mass resolution were noted. However, careful instrument optimization minimized the effects of these two issues.

While all analytes were analyzed on a stainless steel MALDI plate, preliminary experiments suggest that analysis of large molecular weight peptides from intact tissue will be possible. Analysis of large peptides from intact tissue poses several problems, as a tissue section presents an extremely complex sample matrix. Optimizing MALDI extraction efficiency and reducing background interferences are among the many issues to address for tissue studies. MALDI extraction efficiency will require careful selection of MALDI matrix compound and solvents, as well as optimization of MALDI matrix application conditions. Although sample background will be increased due to the number of potentially interfering species present in tissue, MS^n experiments should prove useful to enhance selectivity and provide sample elucidation and identification.

Furthermore, the use of MALDI/MS^n on the LIT offers potential for imaging these peptides in intact tissue.

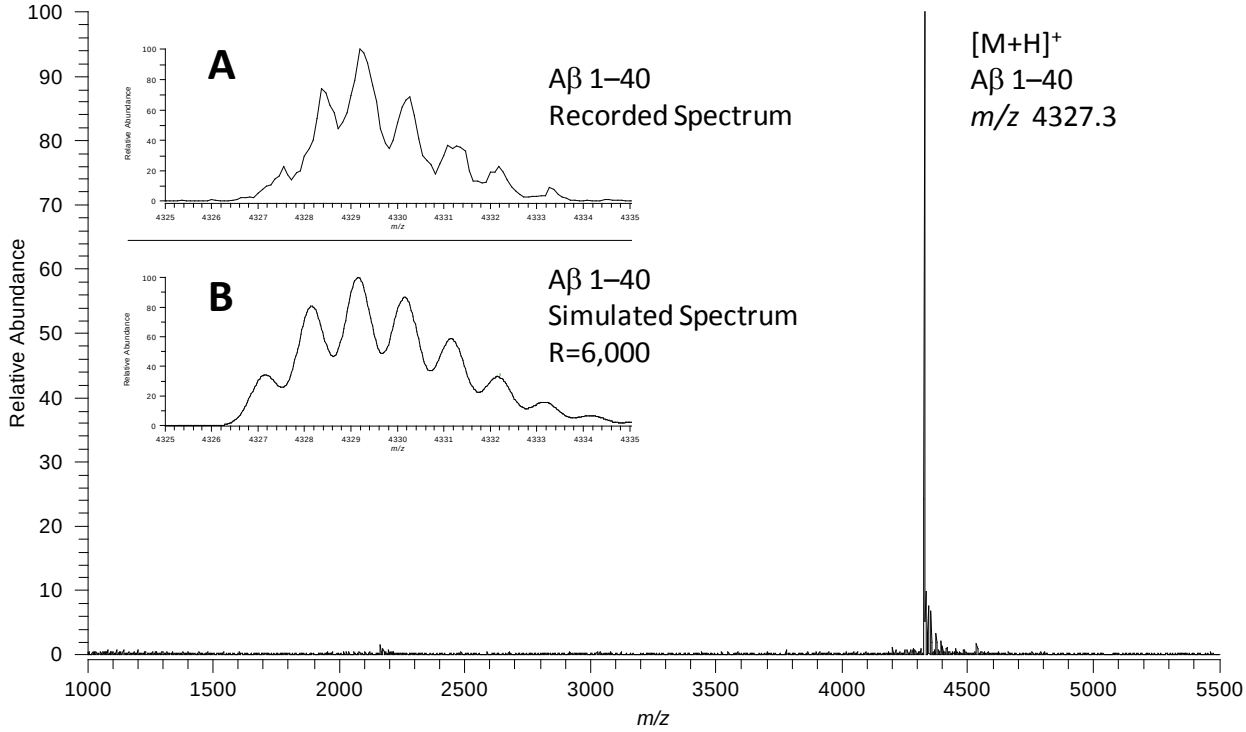

Figure 2-1. Full scan mass spectrum of Aβ 1–40. Inset A is an expansion around the Aβ 1–40 $[M+H]^+$ peak. The isotope distribution matches that of the simulated spectrum in inset B. The peptide sequence of Aβ 1–40 is DAEFRHDSGYEVHHQKLVFFAEDVGSNKGAIIGLMVGGVV.

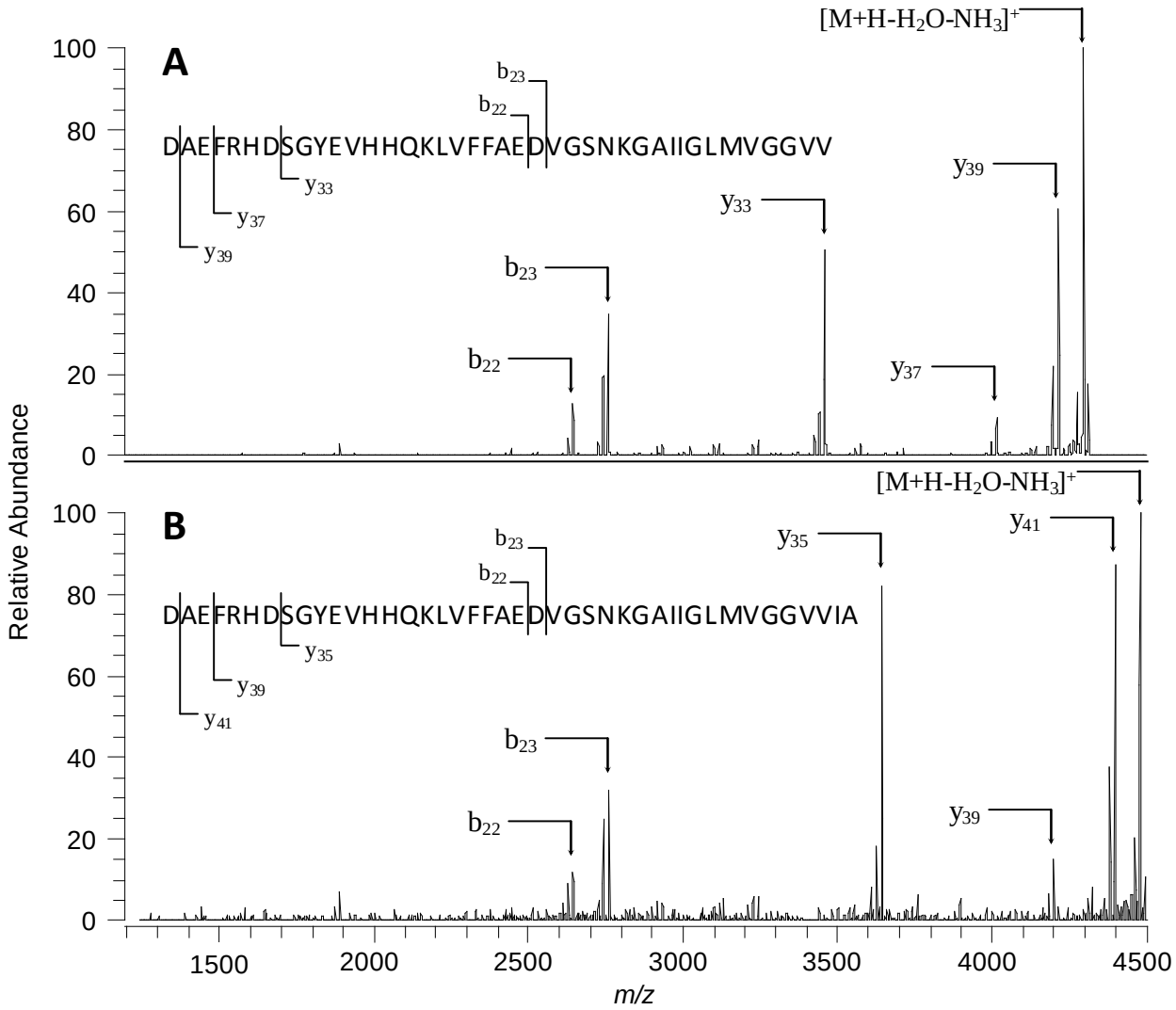

Figure 2-2. MS/MS spectra of the [M+H]+ ions of Aβ 1–40 (A) and Aβ 1–42 (B). The *m/z* values of the major peaks match the expected y and b series ions for their respective parent. Coverage of the Aβ peptide is incomplete due to preferential cleavage adjacent to acidic amino acid residues within the peptide.

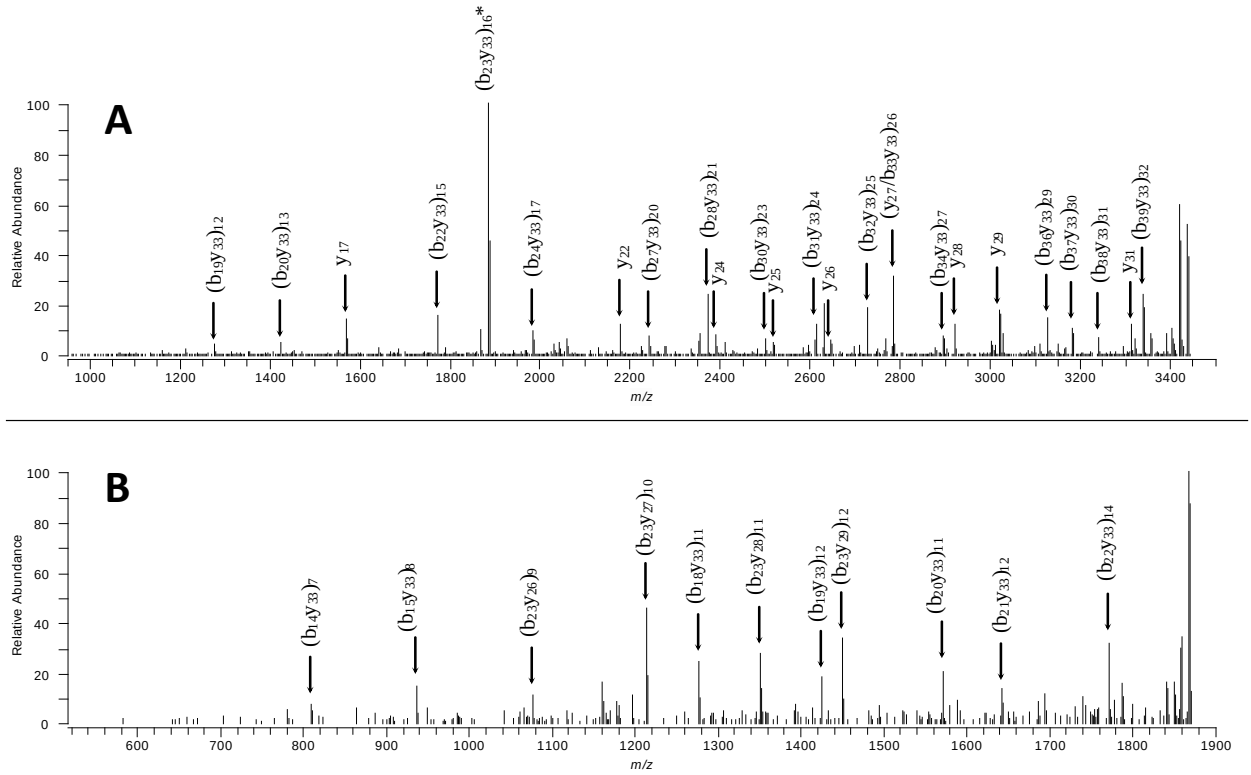

Figure 2-3. MS^3 (A) and MS^4 (B) experiments for the Aβ 1–40 ion. Further fragmentation of the Aβ 1–40 ion was performed for structural elucidation. The y_{33} ion was isolated and fragmented for the MS3 experiment. The $(b_{23}y_{33})_{16}$ ion (marked with asterisk in A) was isolated and fragmented to provide additional coverage of the Aβ peptide.

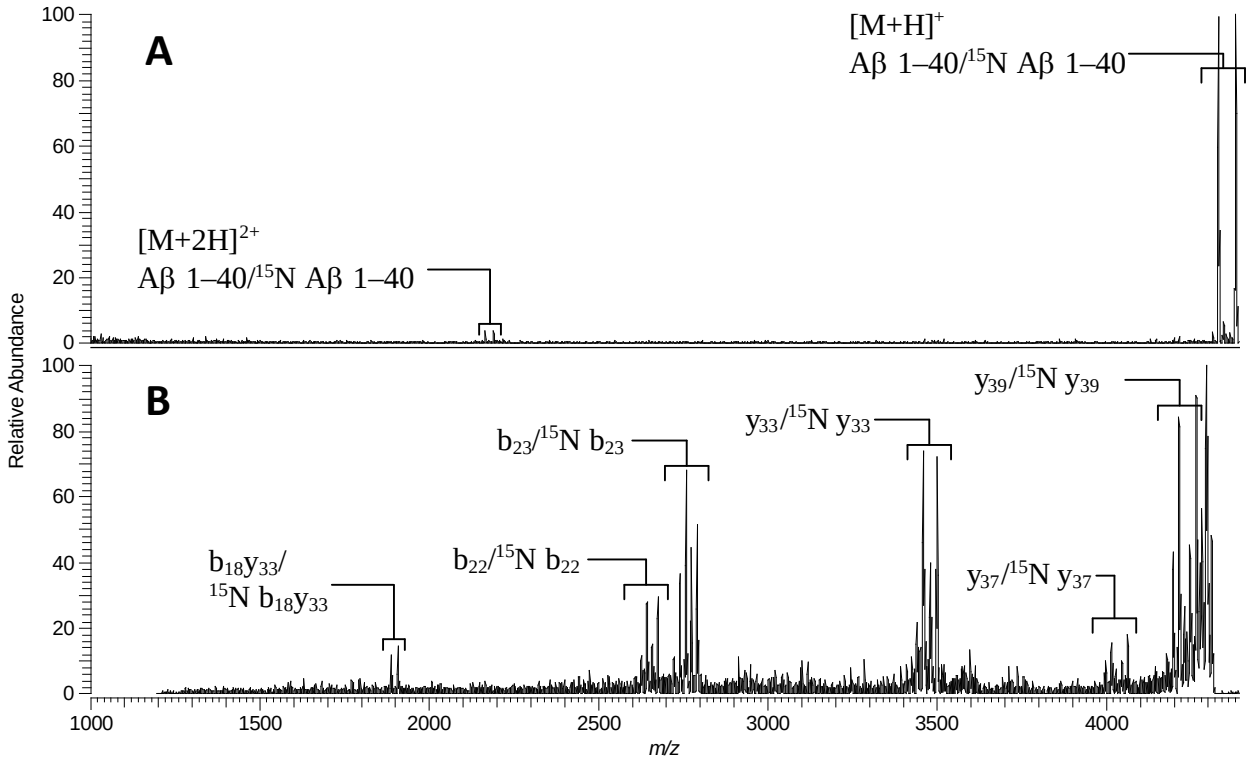

Figure 2-4. MS (A) and MS^2 (B) mass spectra of a 1:1 mixture of Aβ 1–40 and uniformly ^{15}N-labeled analog. For the MS^2 spectrum, the isolation window was an *m/z* range of 4315 to 4395 so as to include the $[M+H]^+$ ions of both the Aβ 1–40 and the uniformly ^{15}N-labeled analog.

CHAPTER 3
IN SITU ANALYSIS OF INTACT LARGE PEPTIDES BY MALDI-LIT-MS^N

Introduction

Alzheimer's Disease (AD) is a neurogenetive malady that affects over five million people in the United States [86]. This insidious disease leads to memory loss, deterioration of the thought process, and personality changes that may eventually end with the death of the AD patient. The hallmark characteristic of AD is the presence of neuritic plaques in the cortex and hippocampus regions of the brain [62]. These neuritic plaques consist of amyloid beta (Aβ) peptide fragments (lengths of 38 to 43 amino acid residues) that originate from the amyloid precursor protein (APP). These fragments are cleaved from APP by the aspartyl protease b-secretase (BACE) and the presenilin-dependent protease γ-secretase. At present, there is a need to localize Aβ fragments in brain tissue for AD research. Imaging techniques (e.g., optical microscopy and PET) offer avenues to determine the disposition of Aβ peptides within a tissue section [65]. This is especially useful for the determination of Aβ within live organisms [87]. However, these techniques offer limited chemical selectivity; rather, current imaging techniques rely on the selectivity of the molecular label (e.g., an antibody, stain, or radiolabel) for analyte detection.

Whereas a label's strength is its high affinity toward the label's targeted molecule, a label's weakness is its inability to aid in the detection of other molecules that may be medically relevant to determining the progression/treatment of a disease. For example, a common Aβ stain (Thioflavin S) will stain amyloid plaques blue, yellow, or green (depending upon the filter) in a tissue section [88]. However, if a lipid or other biologically relevant compound's disposition or concentration changed over the

progression of the disease, these changes would be invisible to the Aβ-specific stain. Thus, a complementary method that identifies both Aβ peptides and other AD relevant molecules is desirable.

Analyte identification based upon the molecular weight using mass spectrometry (MS) would be more selective than staining, especially if paired with tandem mass spectrometry to further increase molecular selectivity. For example, LC-MS is used to examine relative concentration of the various Aβ peptides [89]. However, the sampling preparation necessary for such an experiment requires tissue homogenization prior to analysis by LC-MS. Unfortunately, this necessary sample preparation prior to LC-MS analysis leads to a loss of spatial information.

One technique that offers the selectivity of MS, while retaining spatial information is mass spectrometric imaging (MSI) [3]. MSI is a micro-destructive, label-free imaging technique that utilizes a microprobe to collect mass spectra at discrete points across a tissue section. Upon collecting the mass spectra, the data are reprocessed using an imaging program and a resultant MS image is generated. The number of MS images that may be generated from a single MSI experiment is limited only by the mass range of the instrument, mass spectral resolution, and ionization efficiency of an analyte, as an MS image can be generated at each collected *m/z*.

The spatial resolution of a MSI experiment is dependent upon the spot size of the microprobe and the distance between each collected point (step size of the microprobe). Complete coverage over the tissue section is achieved by matching the step size to the microprobe spot size. However, analysis times can be decreased by increasing the micro probe step size (at the cost of degrading the MS image resolution).

Conversely spatial resolution can be increased by decreasing the microprobe step size in exchange for lengthening the experimental time.

Analysis times for an MSI experiment are dependent upon a number of factors—the spot size and step size of the microprobe, the type of MS experiment, the duty cycle of the MS instrument, and the area of the tissue surface to be examined—that must be balanced to avoid lengthy MSI experiments. Indeed, an MSI experiment can take anywhere from one hour to twelve hours, depending upon the factors above. However, two-hour experiments tend to be the norm for a tissue section with dimensions of ~7.5 mm by x 5 mm (i.e., the size of a sagittal mouse brain section) with a spot size and step size of 100 µm on an LIT system.

Detection and localization of Aβ in tissue by MSI offers complementary spatial information to existing imaging techniques. Previous AD MSI work has utilized a time of flight (ToF) mass spectrometer, both for its mass range and mass accuracy [68, 69, 90]. However, ToF MS instruments tend to lack structural elucidation capabilities (at best, two stages of tandem mass spectrometry is achieved if a ToF-ToF or Q-ToF is used). An alternative to a ToF-MS instrument for MSI experiments is a linear ion trap (LIT) mass spectrometer. LIT experiments offer multiple stages of mass analysis (MS^n) that enable structural elucidation of unknowns and enhance chemical selectivity through identification of characteristic product ions. However, the MALDI-LIT commercial instrument has an upper *m/z* cutoff of *m/z* 4000. This limits the instrument to examining compounds with a molecular weight of less than 4000 (assuming a singly charged ion). This poses a problem to the analysis of large peptides such as Aβ 1–40 and Aβ 1–42 that have molecular weights of 4329 and 4512 Da, respectively. A strategy to overcome

the upper *m/z* limitation is to extend the mass range of the LIT instrument [45]. This chapter will describe the methods developed to analyze Aβ peptides on an LIT. Images collected through the MSI experiments will be compared to a histological-stained serial section to determine the feasibility and limitations of this technique.

Experimental Methods

Chemicals and Materials

Trifluoroacetic acid (TFA) and MALDI matrix 2,5-dihydroxybenzoic acid (DHB), were purchased from Acros Organics (Morris Plains, NJ). The other two MALDI matrices, sinapinic acid (SA) and α-cyano-4-hydroxycinnamic acid (CHCA) along with Thioflavin S (for histology staining) were purchased from Sigma Aldrich (St. Louis, MO). Glacial acetic acid, ammonium bicarbonate, PBS, neutral buffered formalin, and HPLC-grade methanol and water were purchased from Fisher Scientific (Fairlawn, NJ). Distilled water from a Purelab Flex water system was used for histological staining. A standard of Aβ1–40 was purchased from rPeptide (Athens, GA). DHB MALDI matrix solutions were prepared at a concentration of 40 mg/mL in a 70:29.9:0.1 solution of methanol:water:TFA.

Animals

A generous donation of mice brains (female Tg2576 mice) were received from Bristol Myers Squibb (Wallingford, CT). These mice exhibit a fivefold increase of Aβ 1–40 and fourteen-fold increase of Aβ 1–42 over levels within young, unimpaired mice [91]. These mice were sacrificed at 30 months of age. Immediately after euthanization, brains were excised, flash frozen, and then stored at -80 °C.

Tissue Preparation

The left hemisphere of the mouse brain was mounted onto the target plate by surrounding the lower half of the brain with water and allowing the water to freeze the brain into place. OCT should not be used for MSI studies as the polymer may interfere and/or contaminate the MS spectrum. Sagittal sections of the mouse brain were collected using a Microm HM cryostat at a temperature of -25 °C. Brain sections were thaw-mounted onto glass microscope slide and then stored at -80 °C until analysis. Note that MSI experiments utilizing an LIT do not require the use of conductive glass slides as in MALDI-ToF experiments because charge build up will not affect mass analysis [6].

Prior to MALDI analysis, all tissue sections were placed in a vacuum desiccator for 30 minutes to remove excess water. Afterward, a series of washes was performed prior to MALDI matrix application to remove endogenous lipids and other endogenous compounds. The series of washes consisted of four steps:

1) 30 seconds in 70:30 ethanol:water

2) 30 seconds in 70:30 ethanol:water

3) 30 seconds in chloroform

4) 30 seconds in 90:9:1 ethanol:water:acetic acid.

After washing, the tissue section was placed in a vacuum desiccator for approximately 15 min to remove any residual moisture.

An important aspect to generating quality MSI spectra is matrix application [7]. Due to the size of the amyloid plaques, uniform coverage over the entire tissue surface along with matrix crystal lengths of less than 100 µm is desirable. Several different options for matrix application are available, including pneumatic spraying and inkjet

printing [6, 17]. For this work, matrix was applied using an artistic airbrush (Aztek A470, Testors, Rockford, IL) [6]. Visually, the airbrush offered a more uniform coating of MALDI matrix compared to dried droplet and inkjet printer deposition. The matrix solution consisted of 40 mg/mL DHB in 70:29.9:0.1 methanol:water:TFA. Approximately 20 passes were necessary to fully coat the tissue surface.

Instrumentation

A Thermo LTQ linear ion trap fitted with an intermediate pressure (70 mTorr) MALDI source (San Jose, CA) was used for all experiments. The MALDI source utilizes a N_2 laser (337 nm) with a repetition rate of 60 Hz and maximum energy of ~90 µJ/pulse and has a laser spot diameter size of approximately 100 µm. Experiments were typically performed with automatic gain control (AGC) off, using 2–3 laser shots per spot and approximately 6–8 µJ/pulse. The step size for these experiments was either 100 µm or 50 µm. For experiments examining intact Aβ peptides, the mass range of the instrument was extended past *m/z* 4000, up to *m/z* 5000, as described in a previous paper [45]. For MS^n experiments of intact peptides, an isolation window 15 AMU wide was used to capture the maximum number ions for tandem MS experiments. In addition, the laser energy was increased to 12 µJ/pulse to increase the number ions available for fragmentation. Although increasing the laser energy may lead to mass shifts during MS scans due to space-charging, there was less of a concern for space-charging due to the limited number of ions trapped during MS^n experiments.

Data Processing

Data were processed using ImageQuest v1.1 software (Thermo Fisher, San Jose, CA). A linear smoothing method was applied to the generated MS image. For MS images, the analyte response was divided by the total ion current (TIC) to generate an

m/z/TIC vs. position image. This was performed to normalize the analyte response across the tissue surface. For MS^n images, no normalization step was performed. Typically, a window of approximately 4 AMU wide was selected when constructing the MS image.

Optical Microscopy

For optical microscopy studies, frozen tissue sections were thawed (15 minutes) at room temperature prior to fixation. Formalin fixation was performed for ten minutes in 10% neutral buffered formalin. Following the fixation, slides were rehydrated in distilled water for 5 min. Sections were thrice washed in 40% ethanol for one minute. Afterward, the tissue sections were stained with 0.0125% Thioflavin/40% ethanol/phosphate buffered saline (PBS). Slides were then placed in 50% ethanol/PBS and transferred to PBS for thirty seconds each. After dipping the sections gently into distilled water to remove adherent salts, the sections were mounted with vecta stain.

Sections were examined on a Zeiss Pascal LSM5 (Zeiss; Oberkochen, Germany) confocal laser scanning microscope. A 488 nm absorbance wavelength and 505 nm emission wavelength was selected to examine the fluorescence of the Thioflavin S stain. Adobe Illustrator CS5 was used to merge the resultant images (~ 1.3 by 1.3 mm) to generate a single histological image.

Results and Discussion

Effects of Sample Preparation on MS Spectra

MSI analysis of large molecules is quite different from small molecule analysis. For example, MSI analysis of endogenous lipids or exogenous small drug molecules discourages the use of water/alcohol washes. Whereas alcohol/water washes remove endogenous salts, other soluble compounds of interest may undergo analyte migration

(or at worst, complete elimination of the analyte from the tissue section). However for the analysis of Aβ peptides, these endogenous compounds and salts may interfere (e.g., ion suppression, salt adduction, etc.) with MSI experiments. Figure 3-1 illustrates two Tg2576 brain sections that contain Aβ plaques in the cortex and hippocampus regions of the brain. Lipids dominate the low mass region of the mass spectrum collected from an unwashed tissue section (Figure 3-1A); in addition, response from Aβ plaques appears to be suppressed (inset of Figure 3-1A). However after washing, lipids in the *m/z* 700-1000 range that are present in the top half of the figure are dramatically reduced (Figure 3-1B). More importantly, ion suppression of the Aβ peptides is decreased after the wash procedure, allowing detection of the Aβ peptides (inset of Figure 3-1B). The increase in signal after the washing step may be explained by the removal of endogenous salts and lipids, whose presence may lead to ion suppression of the target analyte.

MSI of Intact Aβ Peptides using a Mass Range Extension

Sagittal sections of the anterior portion of a Tg2576 mouse brain were selected for MSI experiments. Several abundant ions were identified in the cortex region of the brain section (Figure 3-2). Three ions abundant in the frontal cortex region of the brain (*m/*z 4132, 4330, and 4515) correspond to the MW of Aβ peptides 1–38, 1–40, and 1–42, respectively. Table 3-1 lists the *m/z* of the $[M+H]^+$ ions of the observed Aβ peptides in the MS spectrum of Figure 3-2 along with the expected average MW weight of the peptides. The observed *m/z* of each of the peptides was within 0.1 Da of its corresponding expected *m/z*. The MS images illustrate a similar distribution in the

tissue section for all three ions. The Aβ distribution is consistent with the expected localization of plaques within the cortex region of this anterior brain section.

Lateral to the tissue section examined in Figure 3-2, two serial whole brain sections were examined for Aβ plaques (Figure 3-3). The same three abundant Aβ peptides (Aβ 1–38, 1–40, and 1–42) were imaged by MSI (Figure 3-3 A–C, respectively) in one sagittal brain section with an adjacent serial section stained with Thioflavin S (Figure 3-3E). Thioflavin S is a common histological stain that stains Aβ plaques green under the current experimental settings. MSI localization of the Aβ plaques matched that of the Thioflavin S stain, with localization predominately in the cortex and hippocampus regions of the brain. Although the image contrast for the Aβ 1–42 image is much lower compared to the Aβ 1–38 and Aβ 1–40 images, it is not surprising, given that the response for Aβ 1–42 is at least 20 times less than the Aβ 1–40 response.

In addition to the Aβ peptide distributions, the distribution of DHB MALDI matrix (Figure 3-3D) was examined. Uneven crystallization of MALDI matrix could lead to 'hot spots' in the MS image. The uniform response of the DHB ion (M^+, *m/z* 154) in the MS image of the tissue section indicates an even DHB crystallization across the tissue surface.

Earlier studies have demonstrated MSI imaging of Aβ peptides using a ToF instrument [68, 69, 90]. Although a ToF instrument is sufficient for performing single-stage MSI experiments, a ToF/ToF instrument would be required for any tandem mass spectrometry experiments. And at best, this instrument would be limited to two stages of mass spectrometry. The lack of tandem mass spectrometry limits structural identification of isobaric species (ions that fall at the same nominal mass). Multiple

stages of mass spectrometry may prove useful in further establishing the identity of the observed peptides.

To demonstrate the capabilities of the LIT for MS^n peptide imaging experiments, separate MSI experiments isolating and fragmenting the Aβ 1–40 ions were performed. The MS^2 spectra averaged over a region in the cortex region of the mouse brain section matched that of previous collected MS^2 spectrum of an Aβ 1–40 standard (Figure 3-4). The most abundant ion in both fragmentation spectra is the loss of 18 Da, water (Figure 3-4A). This ion results from a relatively uninformative neutral loss (many ions exhibit a loss of water upon fragmentation) and thus offers little structural information. The lack of the water neutral loss peak in the standard spectrum could be explained as a lack of isobaric compounds (which readily lose water) that are native to tissue. Therefore, other more informative ions were selected to generate MS images.

After the neutral loss of water, one of the next most abundant ions lies at *m/z* 3459. This MW corresponds to the y_{33} ion of a fragmented Aβ 1–40 ion. The distribution of this product ion (Figure 3-5A) further supports the identity of the parent ion as Aβ 1–40 because the y_{33} distribution matches that of the histological stain (Figure 3-5D).

Additional evidence supporting the identity of the Aβ 1–40 ion is provided by MS^3 experiments. For this set of MS^3 experiments, a different y-type ion (y_{39}, *m/z* 4512) was selected for dissociation by CID (Aβ 1–40→y_{39}→). This CID experiment produced two highly abundant product ions, *m/z* 3459 (Figure 3-5B) and *m/z* 2645 (Figure 3-5C). The first ion corresponds to y_{33} ions, originating from fragmented y_{39} ions. The second ion corresponds to a cleavage of the 1–22 residues on the N-terminus side of the Aβ 1–40

peptide resulting in a $(b_{23}y_{39})_{22}$ ion. The double backbone cleavage is preferred over continued fragmentation along the C-terminal side of the peptide due to the presence of internal acidic amino acid residues (in this case glutamic acid) in the peptide structure [83]. (Fragmentation adjacent to acidic amino acid residues is preferred over other sites on the peptide backbone).

The localization of both MS^3 product ions further supports the ion as Aβ 1–40 peptide, as the localization is similar to that of the histological stain (Figure 3-6). If the MS images offered a different localization, there would be some doubt to the identification of the peptides, as isobaric species could have a different distribution within the tissue. Although this technique lacks a separation step such as liquid chromatography or immunoprecipitation, tandem MSI offers a technique for peptide identification and localization complementary to traditional histological staining methods.

Histological versus MSI Image Resolution of Individual Plaques

Aβ plaques range in size from 50 µm to 200 µm (see Figure 1-11 for an example). Whereas larger plaques should not be difficult to image with current instrumentation, localization of smaller aggregations may prove more problematic. Figure 3-7A illustrates the localization of Aβ 1–40 taken with a raster step size of 100 µm. Two regions (indicated by the white boxes) have been expanded to examine individual amyloid plaque clusters (figure 3-7C and D).

The histological image, superimposed over the Figures 3-7 C and D, illustrates the difference in spatial resolution between a confocal microscope and an MSI instrument. The spatial resolution of the MSI instrument could be defined as being equal to the spot size of the laser (assuming the raster step size is equal to the spot

size and the size of the MALDI crystals are smaller than the spot size of the laser). Although the localization of the Aβ peptide fragments are generally similar to the histological image, close examination of individual plaque formations indicate a blurring of the MS image. This is due in part to the spot size of the laser being greater than the diameter of individual plaques. Moreover, the spot size of the laser is greater than the distances between individual plaque's in Figures 3-7 C and D. As a result, the smoothing function of the imaging software blurs the regions between the plaques such that it appears that one single plaque is present in each of the expanded areas.

To improve the spatial resolution, an MSI experiment with a reduced raster step size (50 µm rather than 100 µm) was performed. Figure 3-7B illustrates the localization of Aβ 1–40 taken with the reduced raster step size. The image quality and resolution of the 50 µm raster step size image are sharper than in the image with the 100 µm raster step size. Closer examination of the boxed areas supports the sharpened image conclusion (Figures 3-7 E and F). However, this improvement was at the cost of quadrupling of analysis time. For experiments that examine a whole body tissue section, this increase in analysis time may prove impractical; however for this application, oversampling may be useful since we are interested in a single organ. Although the spatial resolution of a confocal microscope (~200 nm) [92] is vastly superior to an MSI instrument, an MSI experiment can detect a wider range of compounds with a single MSI experiment while generating compound-specific spatial information for multiple analytes.

Conclusions

Mass spectrometric imaging offers many advantages over conventional histological stains. Primarily, more chemical information is available per experiment than in any single histological experiment. Using tandem mass spectrometry, analyte selectivity can be evaluated by matching fragment patterns of an ion to that of a standard. However MSI is not without limitations. The washing and fixation step used for these experiments may wash away endogenous lipids and/or wash soluble xenobotic analytes within the tissue. This could be problematic if, for example, the distributions of an AD drug and Aβ deposits were to be compared. Thus, two experiments on serial sections may be necessary if one wished to determine the disposition of the small drug molecule and the larger peptide.

Even if analyte migration is not an issue, the MSI technique does not offer the spatial resolution that an optical technique will achieve. This is especially true in these AD studies, as MSI does not have the resolution to distinguish between plaques and neurofibrillary tangles. Nevertheless, MSI of large peptides (such as Aβ peptides) on a linear ion trap provides valuable and complementary information to traditional imaging techniques.

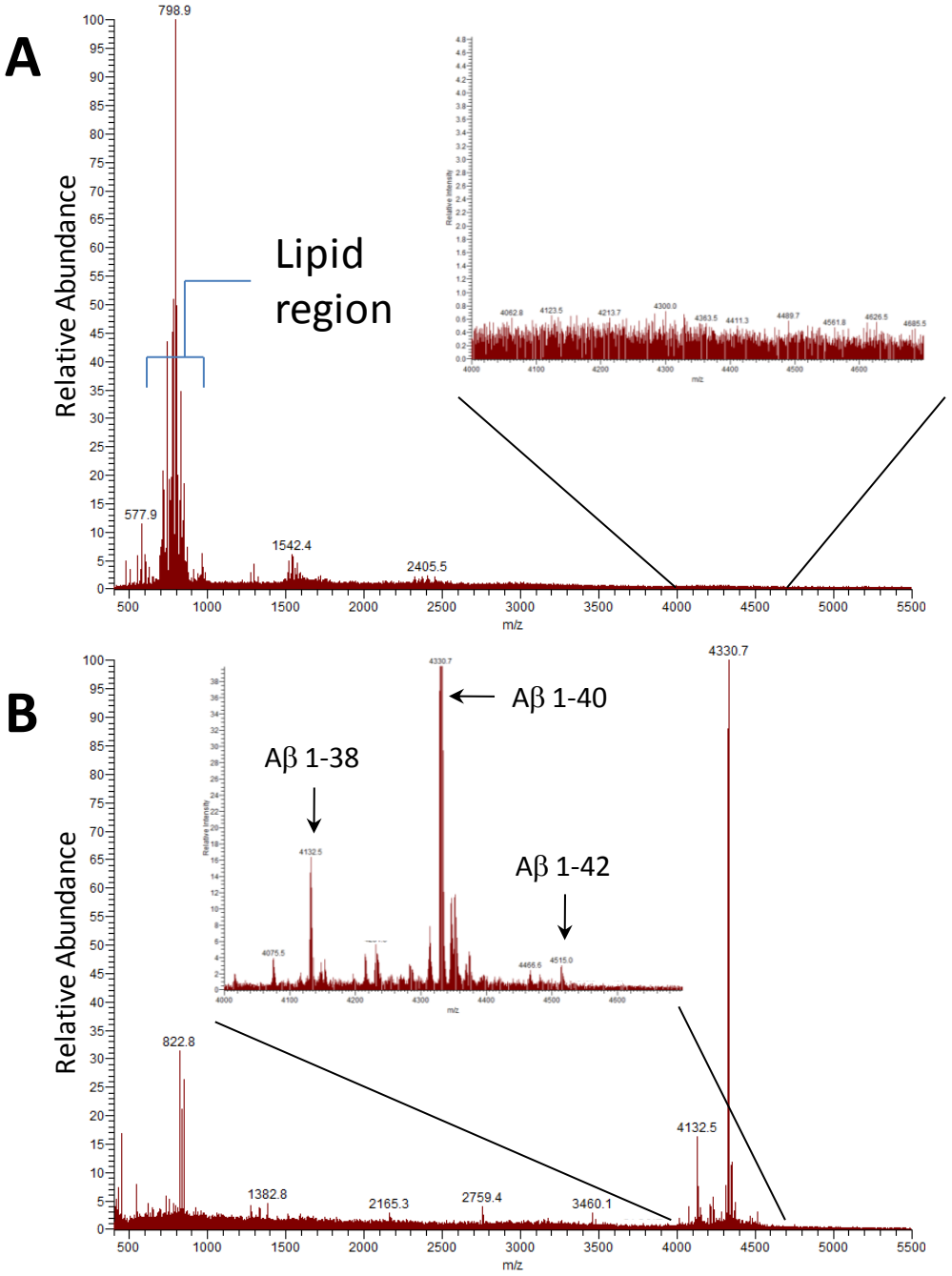

Figure 3-1. Effect of tissue washing on a Tg2576 mouse brain section. Lipids dominate the mass spectrum in A. There is a noticeable lack of signal in the region where the amyloid β peptides should reside. After washing however, B, most of the lipid signal has been eliminated. In addition, the ions corresponding to the amyloid β peptides are readily detected.

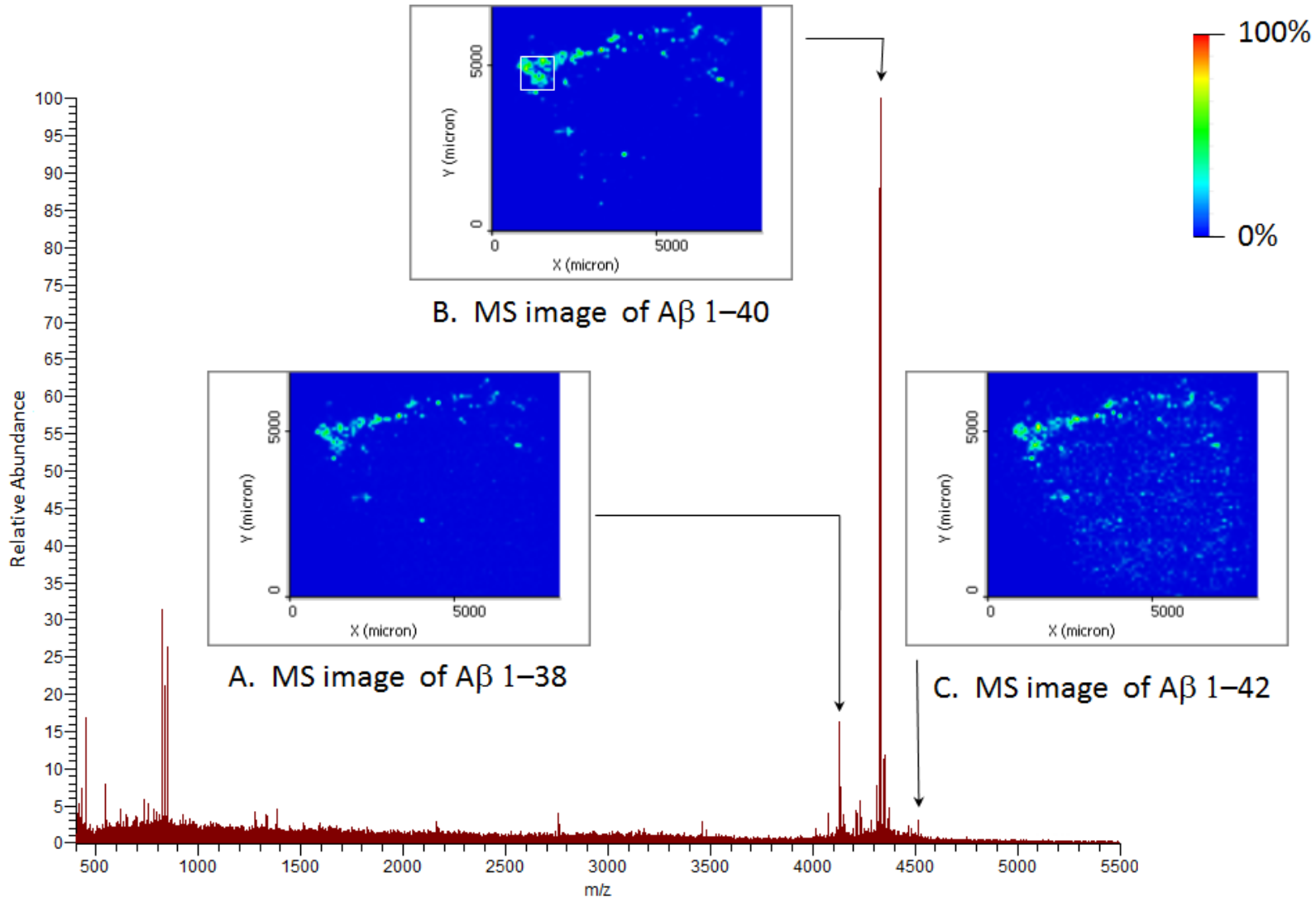

Figure 3-2. MSI images from the anterior portion of a sagittal Tg2576 mouse brain section. The three images illustrate the localization of a few prominent peptides that originate from APP, Aβ 1-38 (A, *m/z* 4130-4133), Aβ 1-40 (B, *m/z* 4329-4332), and Aβ 1-42 (C, *m/z* 4214-4217). The mass spectrum in this figure is the average over the area indicated by the white box of inset B.

Table 3-1. Observed amyloid β peptides in situ during MSI experiments

Peptide	Predicted average $[M+H]^+$ *(m/z)*	Observed $[M+H]^+$ *(m/z)*
1-37	4075.5	4075.4
1-38	4132.6	4132.5
1-40	4330.8	4330.7
1-40 Oxid	4346.8	4346.8
1-42	4515.1	4515.1

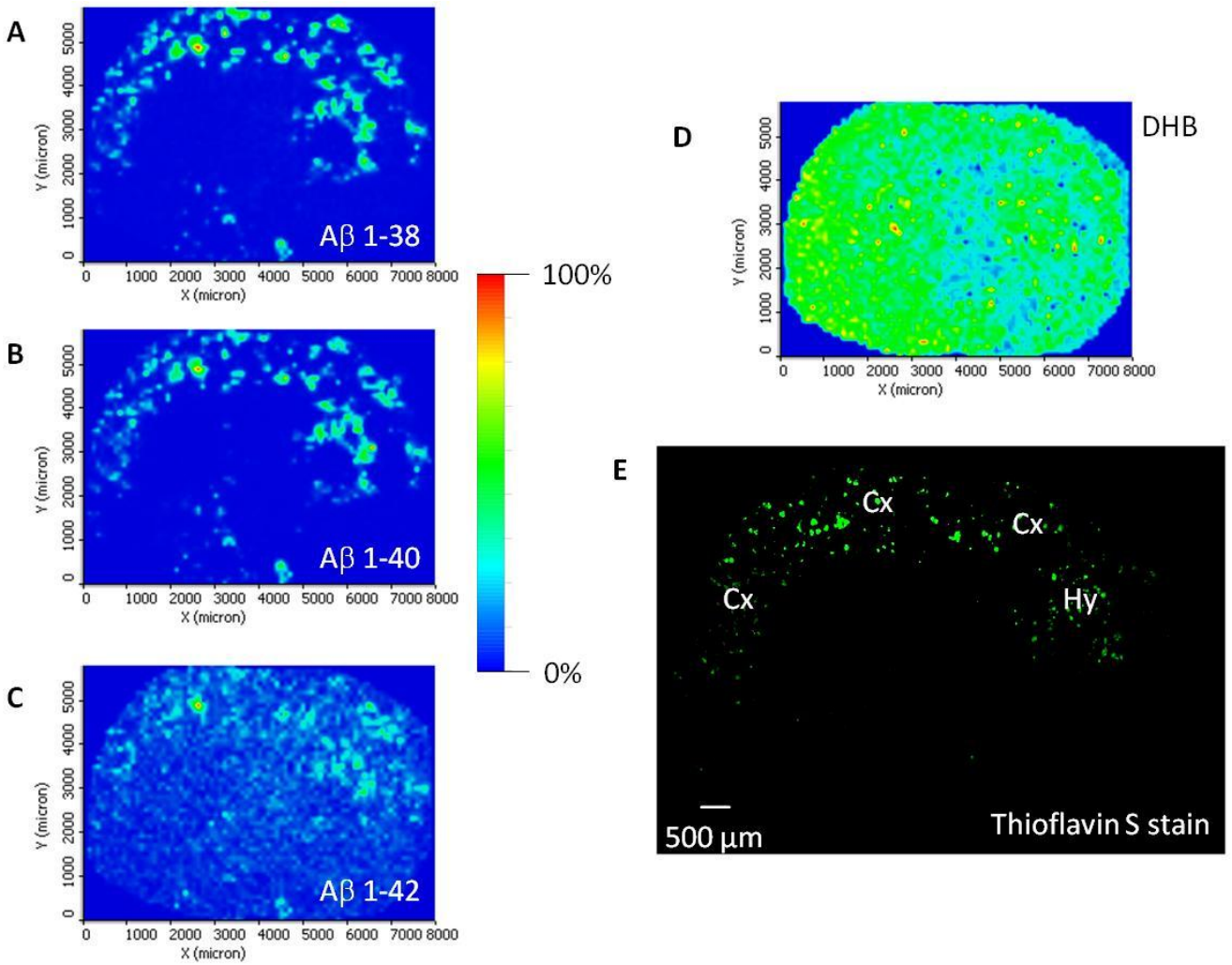

Figure 3-3. MSI images a sagittal Tg2576 mouse brain section. The first three images illustrate the localization of a three prominent peptides that originate from APP, Aß 1-38 (A, *m/z* 4130-4133), Aß 1-40 (B, *m/z* 4329-4332), and Aß 1-42 (C, *m/z* 4214-4217). Image D illustrates the distribution of DHB (*m/z* 154) across the tissue surface. Image E is an image of the histological stain of the serial section adjacent to the MS imaged tissue section. 'Cx' indicates the cortex region of the brain. 'Hy' indicates the hippocampus region of the brain.

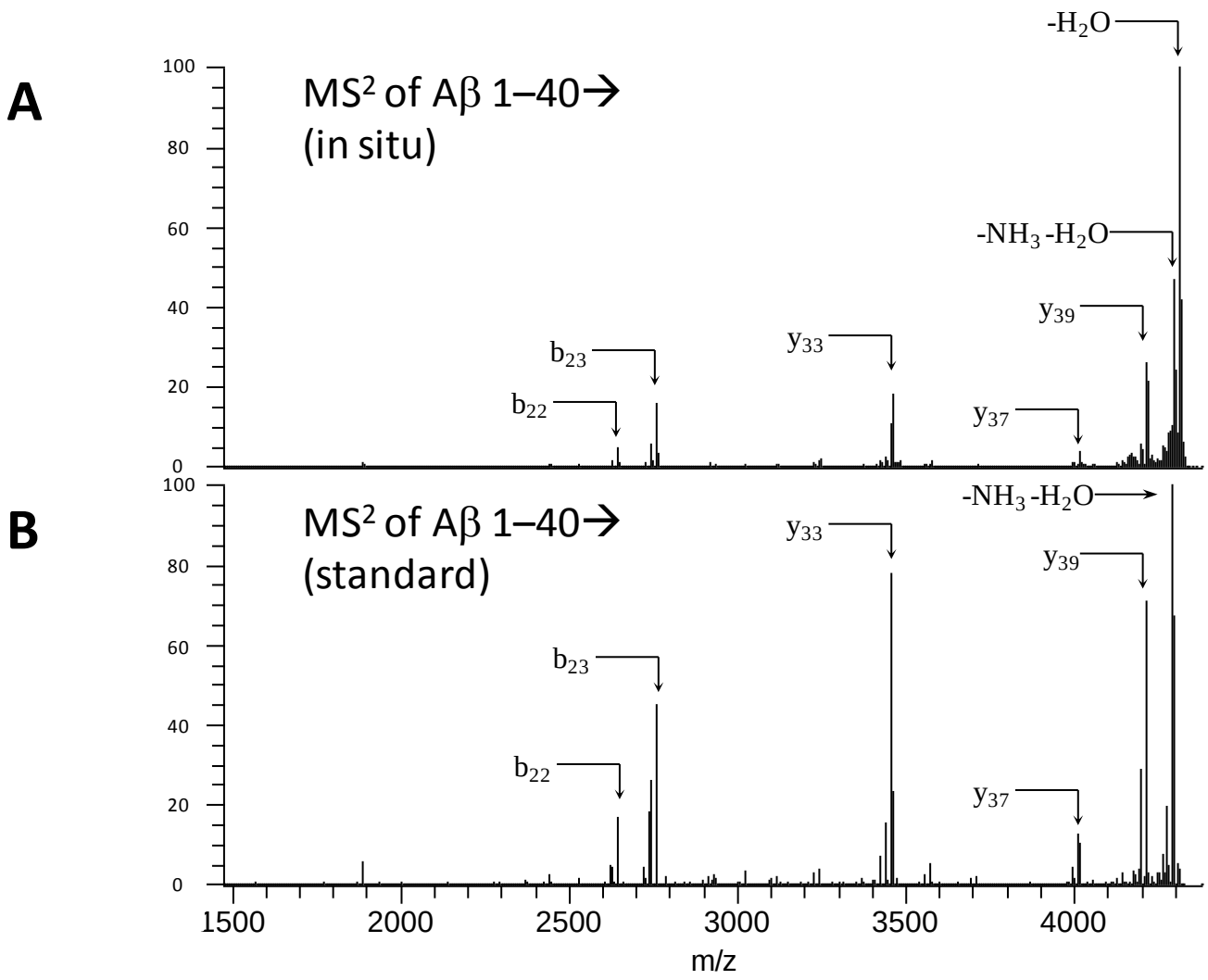

Figure 3-4. Comparison of MS^2 fragmentation of Aβ 1–40→ from tissue (A) and an Aβ 1–40 standard (B). Although the neutral loss of water is more abundant in A, the general fragmentation pattern is similar between both spectra.

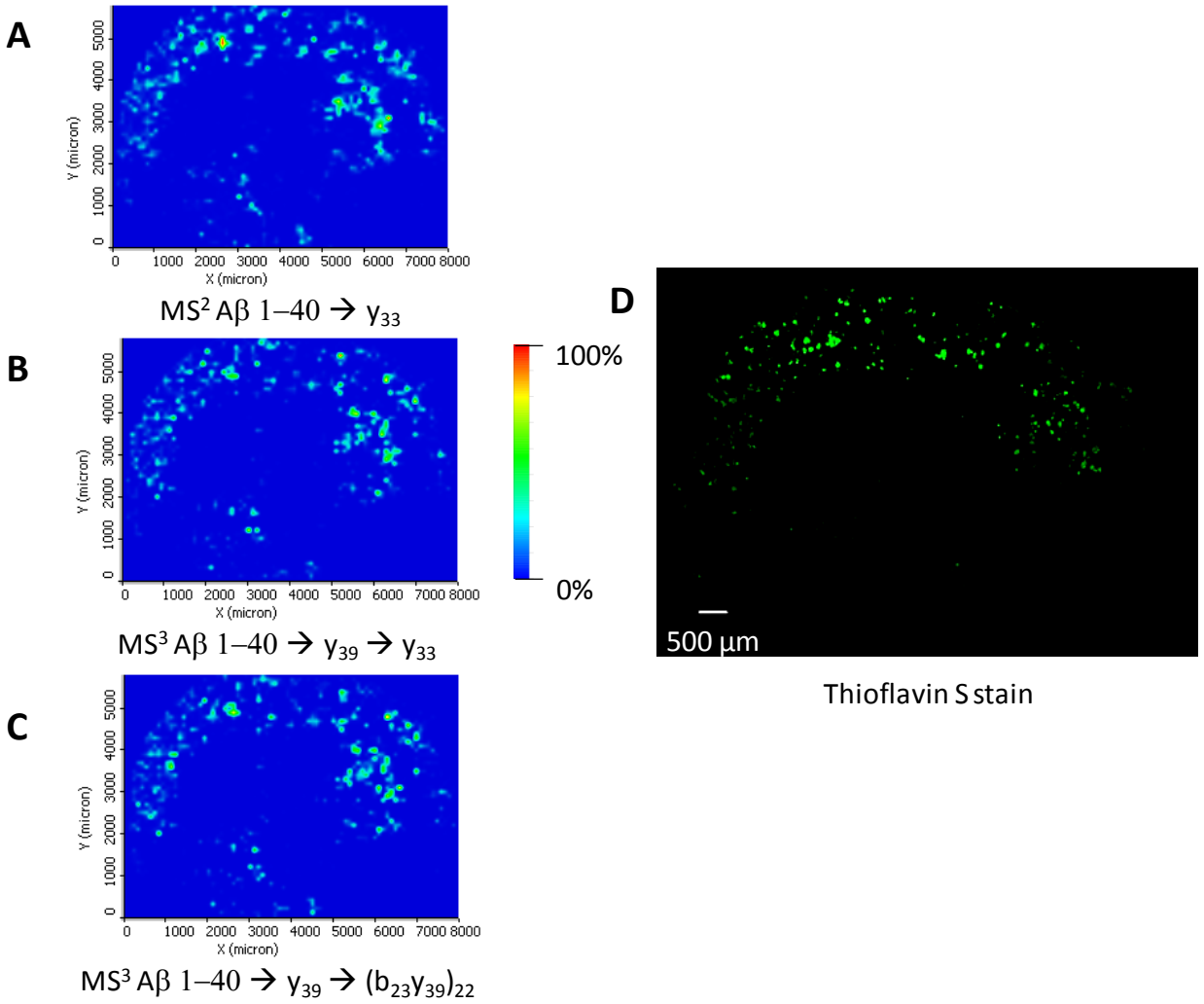

Figure 3-5. MS^n image maps of the fragmentation of endogenous Aβ 1–40. The localization of the y_{33} ion, A, illustrates a distribution similar to the histological image, D. The fragmentation of the y_{39} ion was performed to demonstrate the ability to construct images from ions found in the MS^3 spectra (y_{33},B, and $(b_{23}y_{39})_{22}$, C) For further information about the MS^n fragmentation of Aβ 1–40, see Chapter 2.

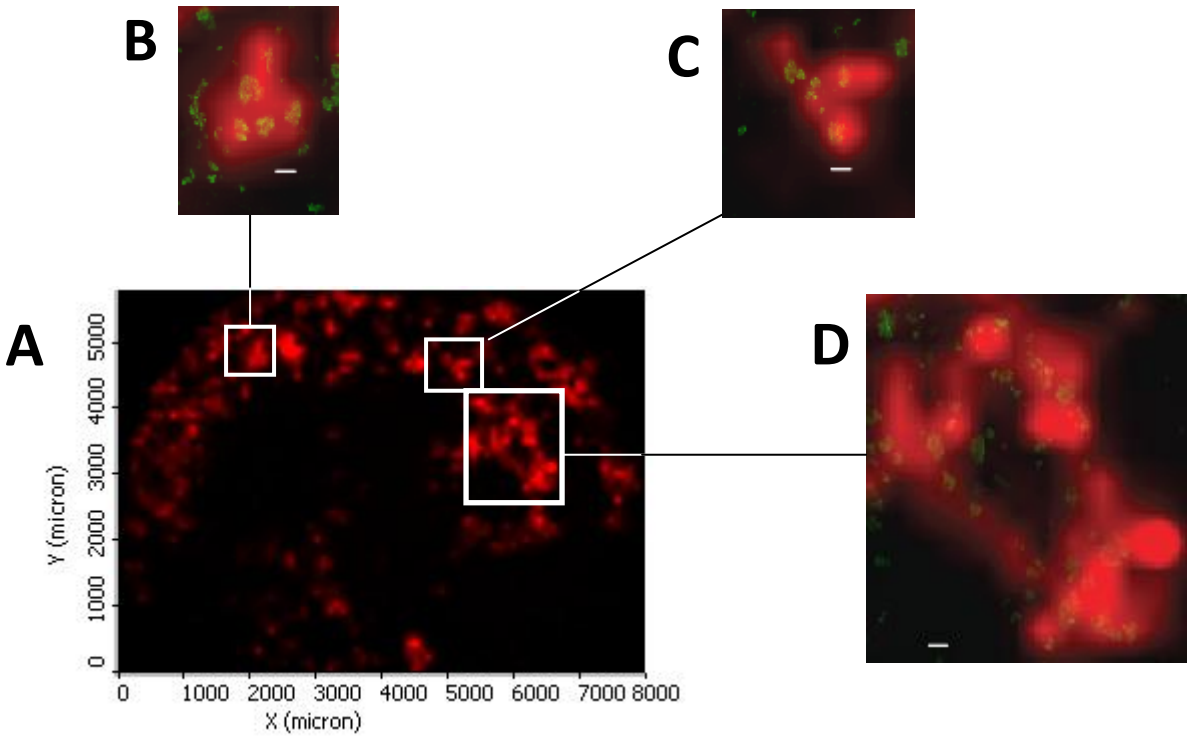

Figure 3-6. MS image of Aβ 1–40 ion, A, with three regions, indicated by the white boxes, expanded (B-D). The Thioflavin S histological image was superimposed atop the expanded MS images. The white scale bars in B–D indicate a length of approximately 100 µm. The raster step size employed for this MS image was 100 µm. Although the general MS image indicates regions of amyloid plaques analogous to the histological image, the MS image does not differentiate plaques that are in close proximity to each other.

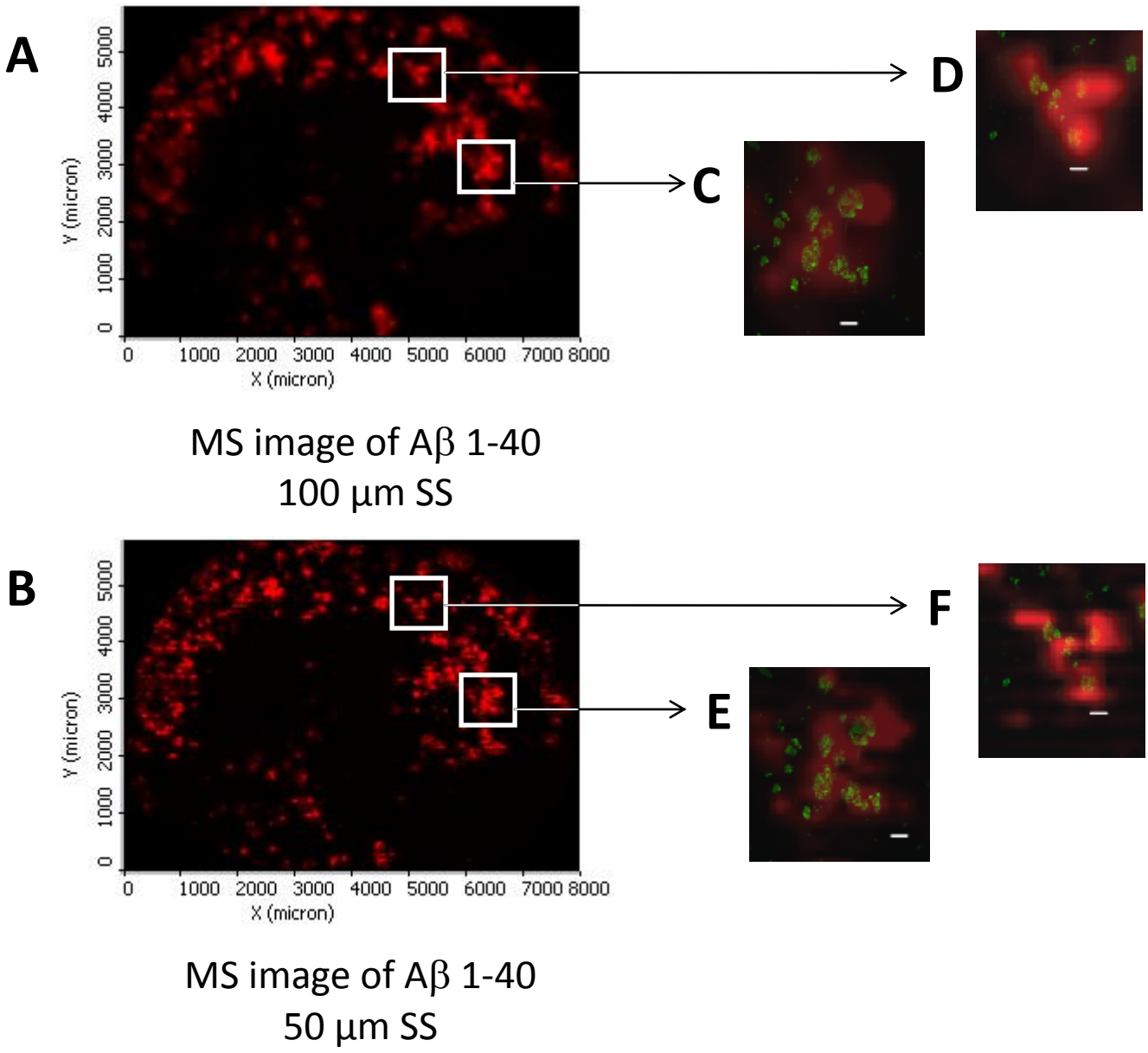

Figure 3-7. Effect of step size on an MSI experiment. Figures A and B illustrates the localization of Aβ 1–40 (red) across two different MSI experiments utilizing a 100 µm and 50 µm raster step size, respectively. Figures C through F are expansions of the indicated white boxes in A and B. The histological stain image (green) is superimposed over the MS images to demonstrate the differences in spatial resolution between the two techniques. The scale bars present in C through F represents a distance of approximately 100 µm.

CHAPTER 4
DIGESTION OF LARGE PEPTIDES IN SITU PRIOR TO MSI STUDIES

Introduction

The analysis of peptides and proteins offers scientists valuable information about the biological processes related to disease states within the body. Protein discovery and identification are typically performed by mass spectrometry due to the technique's high sensitivity and structural elucidation capabilities. Various MS platforms are available for peptide identification, e.g., LITs, ToFs, FT-ICRs, and orbitraps are MS instruments commonly found in MS proteomic cores. However, LITs have a distinct advantage over ToFs and orbitrap instruments because multiple stages of mass spectrometry (MS^n) enables identification of larger sections of the peptide sequence. FT-ICR instruments also offer MS^n capabilities; however, the cost of an FT-ICRs is much greater than that of an LIT.

MS experiments typically examine proteins and peptides as intact molecules (or as smaller fragments, if an enzymatic digestion step is performed prior to MS analysis). The previous chapter demonstrated the abilities of an LIT for the analysis of intact large peptides. However, no commercial LIT MS instruments have the capability to analyze peptide ions with an *m/z* greater than 4000. Thus an alternative is to enzymatically digest the samples prior to MS analysis.

Peptide/protein digestion is a technique that utilizes an enzyme to digest proteins into smaller peptides. One advantage of enzymatic digestions is that smaller peptides are easier to sequence versus larger compounds due to potentially poor ionization efficiencies and structural modifications on a protein [93]. Moreover, digestion of the proteins increases the likelihood of detection by MS. This is because a large protein is

likely to have an *m/z* greater than the upper *m/z* limit of the MS instrument and thus will not be discovered in an MS scan.

There are many different enzymes for protein digestion; however, trypsin is by far the most common protease for enzymatic digestion experiments [93]. Both its low cost and its specificity make it an attractive protease. Trypsin selectively cleaves proteins at the carboxy-terminal side of any arginine or lysine residues present in a protein molecule.

Tryptic digestions are performed on numerous sample types, e.g., cell cultures, tissue extracts, etc. For tryptic digestion of tissue samples, protein extraction precedes the digestion step. However, extraction from a tissue section will lead to a loss of spatial localization of the protein. Although protein identification is important, localization of the protein within a tissue section is equally important. Mass spectrometric imaging of proteins and peptides has been demonstrated to illustrate the localization of large proteins within tissue sections [3, 5]. But what if the protein of interest has an *m/z* greater than the upper *m/z* limit of the instrument and digestion is necessary?

In situ digestion of proteins atop intact tissue is feasible, albeit difficult [46, 94, 95]. Current equipment for in situ digestion of tissue sections utilizes automated spotters to dispense nL volumes of trypsin solution (diameter ~55 µm) to the tissue surface [96]. Unfortunately, equipment to dispense trypsin solution at these low volumes is expensive (> $50,000) and may pose a funding barrier to emerging (or even well established) research laboratories. Moreover, trypsin is not applied across the entire tissue surface. Rather, trypsin is applied at discrete spots, such that each spot is separate from its

neighbor. This deposition method is analogous to an undersampling experiment (see Figure 1-4B). Thus, this spotting method generates a series of trypsin digestion experiments that reduces the likelihood of analyte migration. However, this method is not useful for Aβ experiments, as demonstrated by the results in chapter 3. An oversampling experiment was necessary to achieve high levels of spatial resolution to identify closely-spaced amyloid plaques. The goal of this chapter is to demonstrate a cost effective enzymatic digestion alternative that will perform in situ tryptic digestion of Aβ peptides across the entire tissue surface.

Experimental Methods

Chemicals and Materials

Trifluoroacetic acid (TFA) and MALDI matrix 2,5-dihydroxybenzoic acid (DHB), were purchased from Acros Organics (Morris Plains, NJ). The other two MALDI matrices, sinapinic acid (SA) and α-cyano-4-hydroxycinnamic acid (CHCA) along with trypsin and octyl-α/β-glucoside (OcGlc), were purchased from Sigma Aldrich (St. Louis, MO). Glacial acetic acid, ammonium bicarbonate, ammonium hydroxide (NH_4OH), and HPLC-grade methanol and water were purchased from Fisher Scientific (Fairlawn, NJ). A standard of Aβ1–40 was purchased from rPeptide (Athens, GA). Aβ1–40 standards were resuspended at a concentration of 1 mg/mL in 1% NH_4OH. DHB MALDI matrix solutions were prepared at a concentration of 40 mg/mL in a 70:29.9:0.1 solution of methanol:water:TFA. Trypsin was prepared at a concentration of 125 ng/µL in either 10 mM ammonium bicarbonate, 0.1% OcGlc, or 70:30 ethanol:10mM ammonium bicarbonate solution.

Animals

A generous donation of aged female mice brains (Tg2576 mice are modified to express human Aβ peptides) and mature rat brains (male Sprague Dawley rats) were received from Bristol Myers Squibb (Wallingford, CT). The Tg2576 mice exhibit a fivefold increase of Aβ 1–40 and fourteen-fold increase of Aβ 1–42 over levels within young, unimpaired mice [91]. Immediately after euthanization, brains were excised, flash frozen, and stored at -80 °C.

Tissue Preparation

The left hemisphere of the mouse brain was mounted onto the target plate by surrounding the brain with water and allowing the water to freeze the brain into place. OCT should not be used for MSI studies as the polymer may interfere and/or contaminate MS spectra. Sagittal sections of the mouse brain were collected using a Microm HM cryostat at a temperature of -25 °C. For rat brains, coronal sections of the brain were collected. Brain sections were thaw-mounted onto glass microscope slide and then stored at -80 °C until analysis.

Prior to MALDI-MS analysis, all tissue sections were placed in a vacuum desiccator for 30 minutes to remove excess water. A series of washing steps was then performed prior to the digestion step to remove interfering lipids and salts. The washing step used for these experiments involved a 4-step wash:

1) 30 seconds in 70:30 ethanol:water
2) 30 seconds in 70:30 ethanol:water
3) 30 seconds in chloroform
4) 30 seconds in 90:9:1 ethanol:water:acetic acid

The washing steps involved repeatedly dipping the glass slide into and out of the wash solution over a period of thirty seconds for each solution. After the tissue washing step, the tissue section was placed in a vacuum desiccator for approximately 15 minutes to remove any residual moisture.

Enzymatic Digestion

Trypsin was applied to dried tissue sections using a micropipettor prior to MALDI matrix application. Approximately 15 µL of trypsin solution was required to completely cover the tissue section. After the trypsin application, the glass slide was placed into a container (five-slide holder) and then the container sealed with parafilm. After sealing the container, the incubation device was then placed in a sealed bag, similar to the setup described by Setout et al. [95] (Figure 4-1). The container held a wetted kimwipe (1 mL of DI water was added to the kimwipe) so as to maintain a humid environment within the sealed container. This apparatus was placed in an oven and incubated at 37 °C for approximately 2.5 h. After removal from the oven, the tissue section was placed in the vacuum desiccator to remove excess moisture. For digestions of Aβ 1–40 standards, equal volumes (1 µL each) of the standard and the trypsin solution were placed in 0.5 µL centrifuge tubes and allowed to digest for one to two hours.

MALDI Matrix Application

MALDI matrix was applied using a modified Epson R260 inkjet printer [17]. The inkjet cartridges were filled with 40 mg/mL DHB in 70:29.9:0.1 methanol:water:TFA. Approximately 40 passes were required to fully coat the tissue surface. For digested standards, a dried droplet method was employed to examine the peptide fragments.

Instrumentation

A Thermo LTQ linear ion trap, fitted with an intermediate pressure (70 mTorr) MALDI source (San Jose, CA), was used for all experiments. The MALDI source utilizes a N_2 laser (337 nm) with a repetition rate of 60 Hz and maximum energy of ~90 µJ/pulse. Experiments were typically performed using 2–3 laser shots per spot and approximately 6–8 µJ/pulse. The raster step size for these experiments was 100 µm. For enzymatic digestion experiments, the instrument was scanned from *m/z* 150 to 2000. For MS^n experiments involving digested peptides, an isolation window of 2 AMU and laser energy of 12 µJ/pulse was used. The increased laser energy was less of a concern for space-charging effects due to the limited number of ions trapped during MS^n experiments.

Data Processing

MSI images were generated using ImageQuest v1.1 software (Thermo Fisher, San Jose, CA). A linear smoothing method was applied to the generated MS image. Typically, a window of approximately 4 AMU wide was selected when constructing the MS image.

Results and Discussion

Effects of MALDI Matrix Choice for MS Analysis of Enzymatically-digested Tissue Sections

Trypsin digestion experiments are a powerful tool for AD studies. Trypsin cleaves peptides and proteins at the carboxy-terminal side any arginine (R) or lysine (L) residues present within a peptide. This specific cleavage permits in silico determination of peptide fragments resulting from a tryptic digestion. A web-based program, ProteinProspector [81], was utilized to predict fragments resulting from tryptically-

digested Aβ1-40, Figure 4-2. Although several tryptic peptides are generated during the enzymatic digestion, few of these fragments are useful for Aβ studies. Digestion and instrument parameters were optimized to achieve optimal signal of the fragments containing the C-terminus of Aβ 1–40. These fragments are shaded in Table 4-1 (the reasoning for the optimization based upon these select fragments is explained below.)

Peptide experiments by MALDI-MS tend to use one of three MALDI matrices, CHCA, DHB, or SA. Although any of these matrices are useable for the analysis of intact Aβ peptides, tryptic digestion experiments of Aβ peptides uncovered a drawback to using certain matrices. Figure 4-3 illustrates the mass spectrum of tryptically digested Aβ 1-40 using CHCA, SA and DHB. There are many similar peaks within each spectrum; however, several differences were noted. The experiment using CHCA offered the least amount of background noise (Figure 4-3A) especially when compared to SA (Figure 4-3B). The MS spectra utilizing DHB (Figure 4-3C) demonstrated Aβ fragments common to the CHCA and SA experiment. However DHB produced more sodiated (i.e., $[M+Na]^+$) ions than experiments utilizing CHCA or SA, complicating the MS spectrum. However, the CHCA-related spectrum is less informative than the DHB-related spectrum. This is due to the absence of Aβ 6–40, Aβ 17–40, and Aβ 29–40 fragments in the CHCA-related spectrum. Clinical AD samples will contain a number of different Aβ isoforms, differing by their C-terminal residues. For analysis of enzymatically digested Aβ to be effective, the C-terminus of the peptide must retain the charge; otherwise, it is difficult to distinguish the origin of a digested peptide fragment. For example if trypsin is added to a mixture of Aβ 1–38, 1–39, 1–40, 1–41, or 1–42 peptides, among the tryptic fragments, an Aβ 1–5 fragment is generated (cleavage

occurs after the fifth residue (arginine)). However, it would be impossible, without prior labeling, to determine the origin of the Aβ 1–5 fragment. Thus, fragments retaining the terminal 40th residue (valine) or 42nd residue (alanine) are more informative for MSI experiments than any of the other fragment ions that dominate all three spectra. Although the SA-related spectrum does contain the Aβ 29–40 fragment, the wide abundance of response throughout the mass spectrum potentially complicates the identification of unknown ions after a digestion.

The lack of $[M+H]^+$ ions containing the C-terminus of the Aβ peptide could be attributed to the lack of basic residues in the remaining fragment ion, as the presence of basic residues promotes protonation. Figure 4-4 illustrates a mass spectrum of a trypsin digestion of the Aβ 1–40 standard when more complete digestion is performed. Although the incubation time for digestion could be extended, the digestion period was not extended for fear of producing tryptic autocleavage peptides. The ion of interest was observed at *m/z* 1108, $[A\beta\ 29–40+Na]^+$. Sample preparation parameters will focus on optimizing the response of the $[A\beta\ 29–40+Na]^+$ ion because the response of the two fragments with missed cleavages, $[A\beta\ 17–40+Na]^+$ and $[A\beta\ 6–40+Na]^+$ unpredictably varied between experiments.

In situ Tryptic Digestion of Aβ Peptide Standards

Digestion of Aβ peptides offers the advantage of examining both Aβ peptides and other biologically relevant peptides in the process. However, after performing a tryptic digestion atop a tissue surface, the mass spectrum was complex. Figure 4-5A & B illustrates a tryptic digestion of an Aβ 1–40 standard deposited atop a Tg2576 mouse tissue surface and allowed to dry prior to tryptic digestion. The response for the [Aβ 29–

40+Na]$^+$ ion in Figure 4-5A is low compared to other peaks within the spectrum. Others have demonstrated the use of surfactants to enhance peptide signal for MSI studies [95, 97]. Use of a surfactant (OcGlc) appeared to decrease the lipid background response, by a factor of three; and as a result, Aβ fragments of interest were readily identified. Although the use of OcGlc appeared to aid detection of the tryptic Aβ peptides, further use was discarded due to the amount of OcGlc necessary for an experiment and a desire to generate results in a cost effective manner.

The previous chapter demonstrated the benefits of removing lipids though a washing step in MSI for intact Aβ peptides . Figure 4-6 illustrates this point for tryptic peptides. The wash protocol set forth in the experimental section was applied to a rat brain tissue section prior to tryptic digestion. After the washes, the lipid signal observed in the *m/z* 700–900 region (Figure 4-6A) is dramatically reduced compared to that of the unwashed tissue section (Figure 4-6B); note that the scale in A is 20X expanded over that in B. However even after washing, the response of [Aβ 29–40+Na]$^+$ is indistinguishable from the noise in these tissue sections that underwent tryptic digestion (a 1 µL droplet of Aβ 1–40 standard was applied to both brain sections prior to tissue washing). Despite this setback, other tools are available to tease out the [Aβ 29–40+Na]$^+$ ion from the noise.

Rather than performing an MS experiment as has been previously performed, what if the [Aβ 29–40+Na]$^+$ ion was isolated and fragmented by CID (Figure 4-7)? When a Aβ 1–40 standard was tryptically digested and the resulting solution co-crystallized with DHB the following MS^n spectra were collected. The most abundant ion in the MS^2 spectrum of [Aβ 29–40+Na]$^+$ (*m/z* 1107.6) → was *m/z* 1008.7, (Figure 4-7A).

This corresponds to a neutral loss of the terminal valine on the C-terminus side of the peptide. Note that the loss of a terminal valine on the C-terminus side of the peptide would result in a NL of 117 (not NL 99). Because the parent species is sodiated, the peptide fragment could experience a neutral loss of a valine residue and a gain water forming a $[b_{11}+Na+H_2O]^+$. Lin et al. observed a similar phenomenon when performing CID experiments on alkali-cationized peptides on a 3D ion trap [98]; however, they observed $[b_{n-1}+Na+OH]^+$ ions after CID rather than $[b_{n-1}+Na+H_2O]^+$ ions for the fragmentation of the Aβ 29–40 ion (a difference of one dalton). Unfortunately further experiments did not explain the discrepancy.

Unlike the MS^2 spectrum, the MS^3 spectrum is more straightforward. The spectrum illustrates a second neutral loss of valine on the C-terminal side of the peptide (Figure 4-7B). Note that an addition water is not gained during CID.

In situ Tryptic Digestion of Tg2576 Brain Tissue

An additional tactic to improve detection of tryptic peptides is to remove non-relevant analytes from the tissue section (i.e., remove the lipids from the tissue section). One would anticipate that washing the tissue prior to tryptic digestion is better than after digestion because analyte migration is more likely if washing is performed after digestion (lower MW trypic peptides will likely be more soluble than intact Aβ peptides). The comparison between washing before and after digestion is demonstrated in Figure 4-8. An Aβ 29–40 standard (1 µL droplet) was applied atop two blank rat brain sections. The washing steps described in the experimental section were applied to one tissue section prior to tryptic digestion and to another section after tryptic digestion. Both the droplets of the amyloid standards had similar diameters prior to washing and digestion.

However, washing appears to move the analyte in the tissue. Figures 4-8A and B illustrate an MS^3 image of an ion originating from Aβ 29–40 (*m/z* 909.6). Despite similar starting conditions, it appears that the Aβ 29–40 fragment has migrated in the y-direction (Figure 4-8B) if one compares response of the two spots in the y-direction (2.6 mm, Figure 4-8A, versus 3.1 mm, Figure 4-8B). The glass slides were raised and lowered into the wash solution along the y-axis, perhaps explaining why migration occurred along the y-axis.

After a tryptic digestion was performed on a Tg2576 mouse sample, CID was applied to the ion at $[A\beta\ 29–40+Na]^+$. Figure 4-9 illustrates the MS^2 and MS^3 images of the dominant ions that are present in each spectrum, *m/*z 1008.7 ($[b_{11}+Na+H_2O]^+$) and *m/z* 909.6 ($[b_{10}+Na+H_2O]^+$), respectively. The MS^2 image of *m/z* 1008.7 appears to localize across the anterior (left side of the image) and posterior (right) regions of the brain, with little localization in the top portion of the brain (top of the image). The MS^3 image of *m/*z 909.6 offers a weaker signal (poorer S/N) that perhaps suggests similar distribution as in the MS^3 image. The distribution of the Aβ 29–40 ion in the MS^2 and MS^3 images should not be the case as the amyloid plaques should be confined to the cortex and hippocampus regions of the brain, as demonstrated in the previous chapter.

Due to the length of time the sections are immersed in the trypsin solution (2.5 h), it is possible that soluble peptides migrate throughout the tissue section, which is feasible because the trypsin solution does not readily evaporate, but rather forms a ‘puddle’ atop the tissue section that stays wet for the duration of the experiment. (If the tissue section remains in a humid environment, the tissue can remain moist for over 12 hours). Indeed, it appears that the peptides have migrated from the cortex regions (see

Figure 3-3E of the brain to the anterior and posterior regions (left and right sides of the image). Other in situ digestion methods perform their digestions using a robotic spotter to deposit trypsin spots that are isolated from each other [46, 94, 95]. This could solve the analyte migration problem; however, the spots are typically 200 µm in diameter, with 200 µm separation between the spots. The size of the spots and the distance between the spots would be too large to determine the location of amyloid beta plaques, as even the largest plaques are usually 200 µm in diameter. Thus a different method must be employed.

Reduction of Analyte Migration within Tissue during in situ Peptide Digestion

Preliminary experiments have demonstrated that no digestion occurs if the tissue section is not damp throughout the digestion period. However, this does not mean a 'puddle' of trypsin solution must remain atop the tissue section. An alternative, is to apply a smaller volume trypsin solution atop the tissue surface, then allow the solution to evaporate, leaving trypsin atop the tissue section. Then, rehydration of the tissue can be effected by placing the tissue section in a humid environment. Initial experiments indicate that tryptic digestion occurs using this 'dry' digestion method. Figure 4-10 illustrates the results of the experiment. Trypsin in an ethanol solution was applied to tissue section previously spotted with 1µL of 1 mg/mL Aβ 1–40 standard. The right side of the figure illustrates a 'wet' digestion, where the trypsin solution is not allowed to dry, and the right side of the figure illustrates a 'dry' digestion, where the trypsin solution is allowed to dry prior to placement into the humid incubation chamber (a kimwipe wetted with 1 mL of DI water was placed in the slide holder). To maximize the opportunity for analyte migration, both samples were incubated for a longer period of time (16 hours).

The distribution of the Aβ 29–40 tryptic peptide ion in appears uniform across the entire image in the wet digestion case (Figure 4-10A), whereas the distribution appears to be confined to the circle where the Aβ 1–40 standard was applied in the 'dry' digestion (Figure 4-10B). If the MS^3 images (green) are superimposed over the MS images of the Aβ 1–40 ion (red), the overlay images supports the assertion that little analyte migration has occurred in the 'dry' digestion (Figure 4-10D) versus the wet' digestion experiment (Figure 4-10C).

Conclusions

Digestion in situ of neuropeptides followed by MSI analysis offers a method to simultaneously examine high mass peptides and proteins while retaining spatial integrity. Aβ standards and endogenous peptides have been identified using MS^3; however, initial experiments have indicated that analyte migration can limit the spatial resolution of the MS image. In situ digestion experiments found extensive analyte migration if the trypsin solution is puddle atop the tissue section. However, preliminary results have indicated that and if trypsin solution is applied then allowed to dry atop the tissue section and if the tissue section remains moist digestion still occurs (with less analyte migration occurring). Unfortunately, it appears that the trypsin digestion was incomplete as much of the intact Aβ standard remained. Further experiments are necessary to optimize the 'dry' digestion parameters before this method becomes a viable alternative to expensive automated spotters for in situ tryptic digestion of proteins and peptides.

Figure 4-1. Image of trypsin digestion apparatus. The tissue section-bearing microscope slide was placed in a five-slot microscope slide holder along with a wetted kimwipe. The slide holder was sealed with parafilm then placed in a sealed plastic bag. The kimwipe ensures a humid environment within the container; whereas the parafilm and plastic bag ensures that moisture will not escape from the container, thus drying out the tissue. The bag was then incubated within an oven to allow in situ tryptic digestion.

MS-Digest Search Results

[+] **Parameters**

Index Number: **1**
pI of Protein: **5.3**
Protein MW: **4330**
Amino Acid Composition: **A3 D3 E3 F3 G6 H3 I2 K2 L2 M1 N1 Q1 R1 S2 V6 Y1**

1 DAEFRHDSGY EVHHQKLVFF AEDVGSNKGA IIGLMVGGVV

Number	m/z (mi)	m/z (av)	Modifications	Start	End	Missed Cleavages	Sequence
1	637.2940	637.6739		1	5	0	(-)DAEFR(H)
1	679.3046	679.7114	1Acetyl	1	5	0	(-)DAEFR(H)
1	1085.6387	1086.3905		29	40	0	(K)GAIIGLMVGGVV(-)
1	1101.6336	1102.3899	1Oxidation	29	40	0	(K)GAIIGLMVGGVV(-)
1	1325.6736	1326.5010		17	28	0	(K)LVFFAEDVGSNK(G)
1	1336.6029	1337.4024		6	16	0	(R)HDSGYEVHHQK(L)
1	1954.8791	1956.0536		1	16	1	(-)DAEFRHDSGYEVHHQK(L)
1	1996.8896	1998.0911	1Acetyl	1	16	1	(-)DAEFRHDSGYEVHHQK(L)
1	2392.2945	2393.8687		17	40	1	(K)LVFFAEDVGSNKGAIIGLMVGGVV(-)
1	2408.2894	2409.8681	1Oxidation	17	40	1	(K)LVFFAEDVGSNKGAIIGLMVGGVV(-)
1	2643.2586	2644.8806		6	28	1	(R)HDSGYEVHHQKLVFFAEDVGSNK(G)
1	3261.5348	3263.5318		1	28	2	(-)DAEFRHDSGYEVHHQKLVFFAEDVGSNK(G)
1	3303.5454	3305.5693	1Acetyl	1	28	2	(-)DAEFRHDSGYEVHHQKLVFFAEDVGSNK(G)
1	3709.8795	3712.2484		6	40	2	(R)HDSGYEVHHQKLVFFAEDVGSNKGAIIGLMVGGVV(-)
1	3725.8744	3728.2478	1Oxidation	6	40	2	(R)HDSGYEVHHQKLVFFAEDVGSNKGAIIGLMVGGVV(-)

Figure 4-2. In silico digestion of Aβ 1-40 using ProteinProspector [81]. Although there are many fragments, only a few fragments are diagnostically relevant. Any fragments that do not terminate at the 40th residue (V) are not usable as they could have a contribution from a different amyloid isoform.

Table 4-1. MWs of tryptic fragments originating from Aβ 1–40

Peak	Predicted *m/z of* $[M+H]^+$	Predicted *m/z of* $[M+Na]^+$	Start	End	# of Missed Cleavages	Sequence
1	1085.6		29	40	0	(K) GAIIGLMVGGVV(-)
1*		1107.6	29	40	0	(K) GAIIGLMVGGVV(-)
2	1325.7		17	28	0	(K) LVFFAEDVGSNK(G)
3	1336.6		6	16	0	(R) HDSGYEVHHQK(L)
4	1954.9		1	16	1	(-) DAEFRHDSGYEVHHQK(L)
5	2392.3		17	40	1	(K) LVFFAEDVGSNKGAIIGLMVGGVV(-)
5*		2414.3	17	40	1	(K) LVFFAEDVGSNKGAIIGLMVGGVV(-)

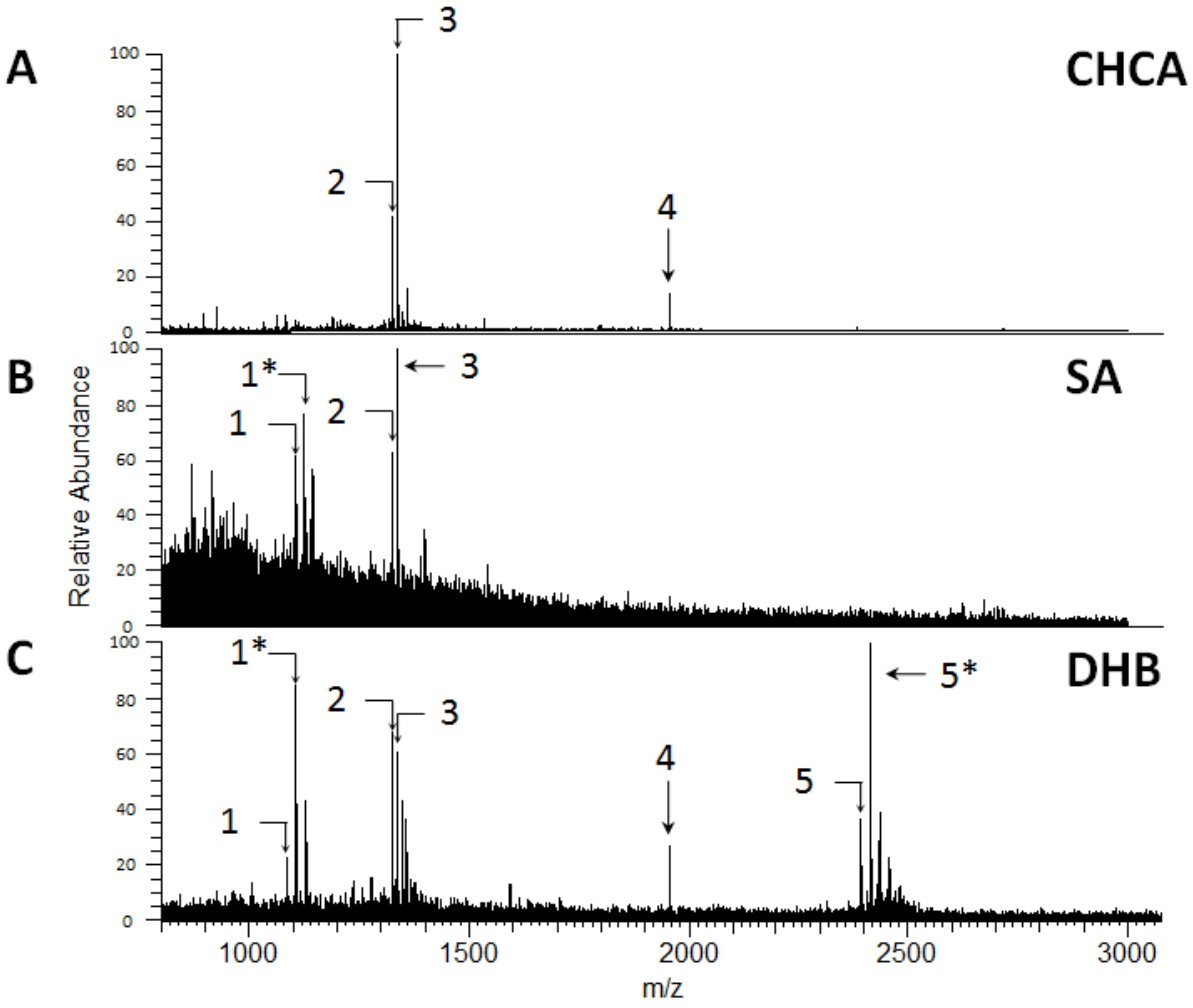

Figure 4-3. Comparison of MALDI matrices for analysis of Aβ tryptic fragments. An Aβ 1-40 standard was tryptically digested and the resulting solution was spotted and analyzed. $[M+H]^+$ ions derived from Aβ 1-40 are noted in the figure and the $[M+Na]^+$ ions are denoted with an asterisk (*). CHCA (A) offers the least amount of background ions, especially when compared to SA, (B). However, ions 2 and 3 are not informative as these fragments are common among amyloid beta fragments (e.g., 1-37, 1-38, 1-42, etc.) that have been tryptically digested. Peak 1 and its sodiated analog (1*) are peaks unique to Aβ 1–40, as it contains the terminal C-terminus. The molecular weights of the numbered peaks are found in Table 4-1.

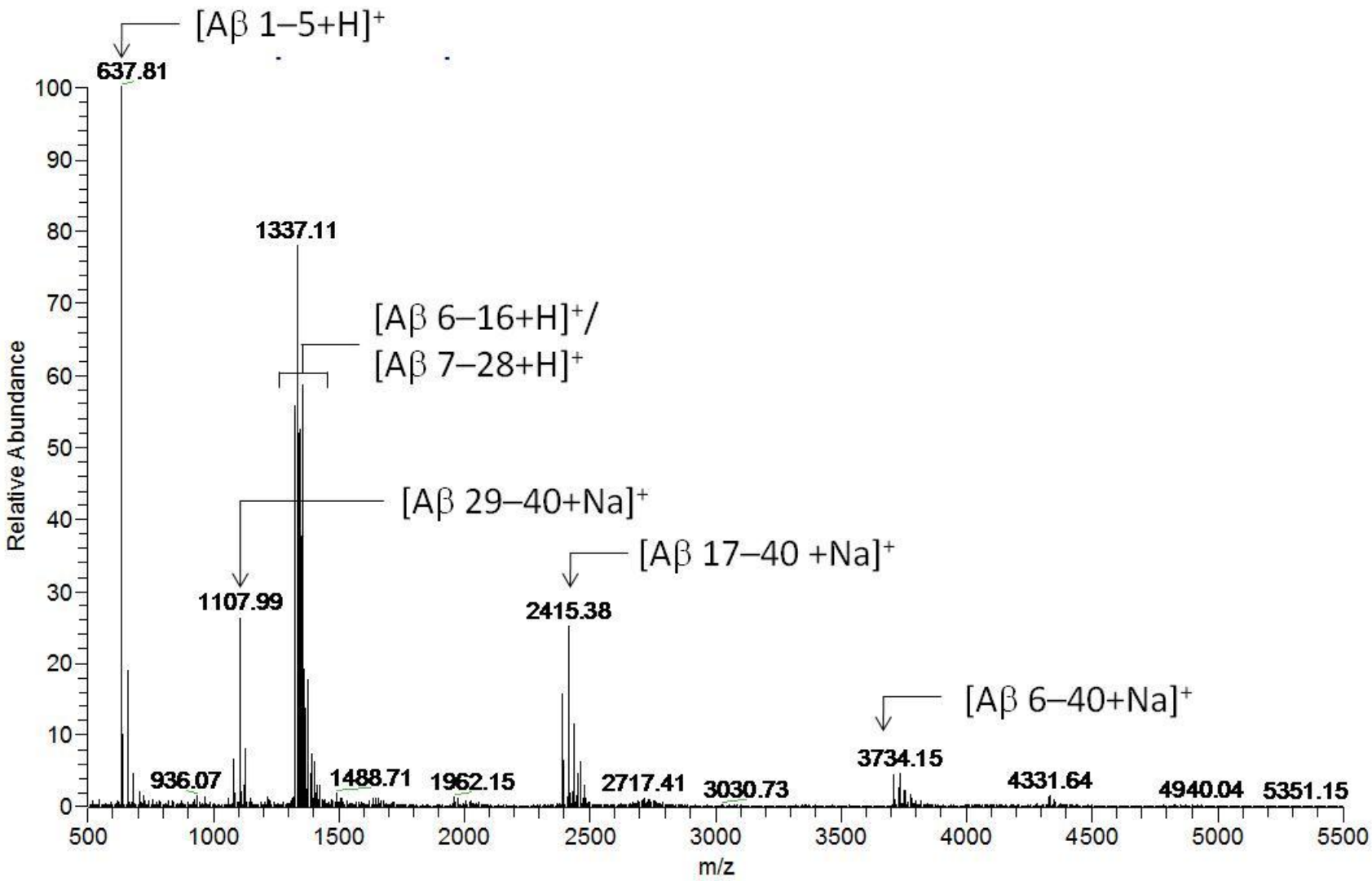

Figure 4-4. MALDI-MS spectrum of a tryptic digestion of Aβ 1–40 atop tissue using DHB as a MALDI matrix. Note the ions of interest (fragments that retain the terminal C-terminus) are the sodiated rather than protonated.

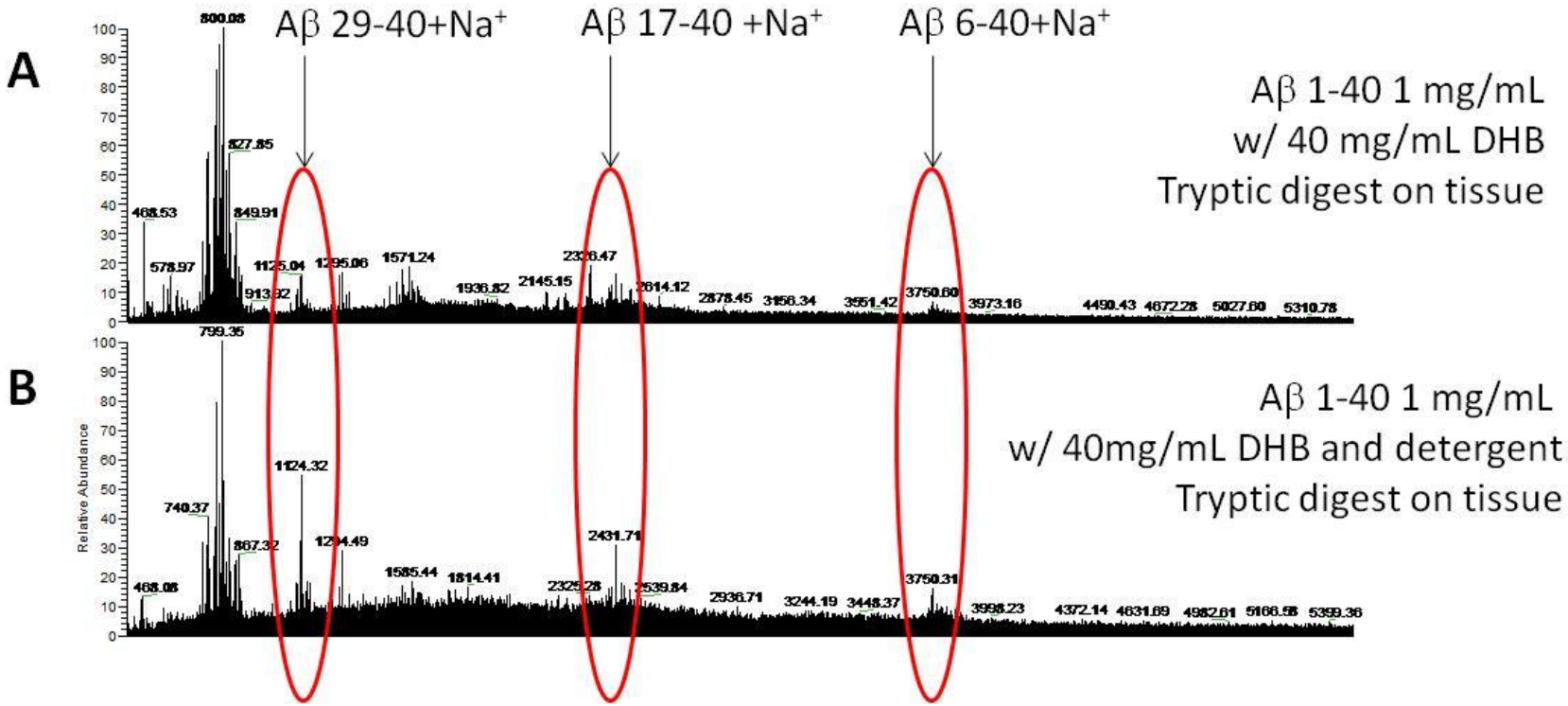

Figure 4-5. Mass spectrum of a series of tryptic digestion atop tissue. Digested fragments (circled in red) are difficult to distinguish from the noise, A. However, use of a detergent (OcGlc) may help improve analyte signal, B. The improvement of the signal could be due to the reduction of lipid response after treatment with OcGlc. The most abundant peak in A has $1.48e^5$ counts versus $3.65e^4$ for B. The response of Aβ 29–40 for both spectra remained nearly identical ($2.24e^4$ counts for A versus $2.04e^4$ counts for B).

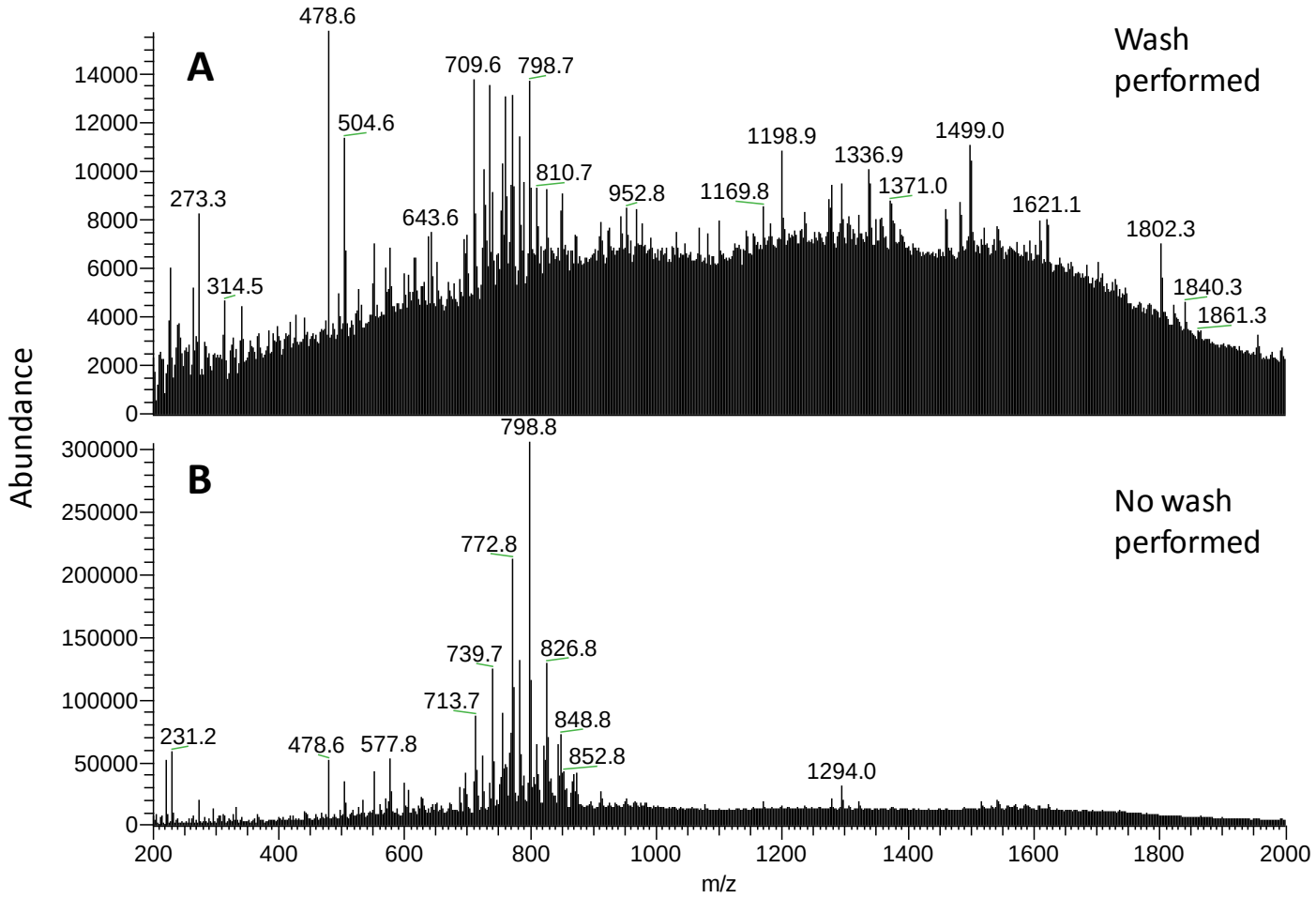

Figure 4-6. Comparison of mass spectra from two in situ digestion experiments. A, illustrates the MS spectrum after a series of washes (see experimental section for details) were performed. B, illustrates the MS if no washes are performed. Note the high abundance of lipid in the 700-900 region of the spectrum. Although the lipid response was dramatically reduced, response of the $[A\beta\ 29–40+Na]^+$ ion (*m/z* 1108) in A is not visible from the background.

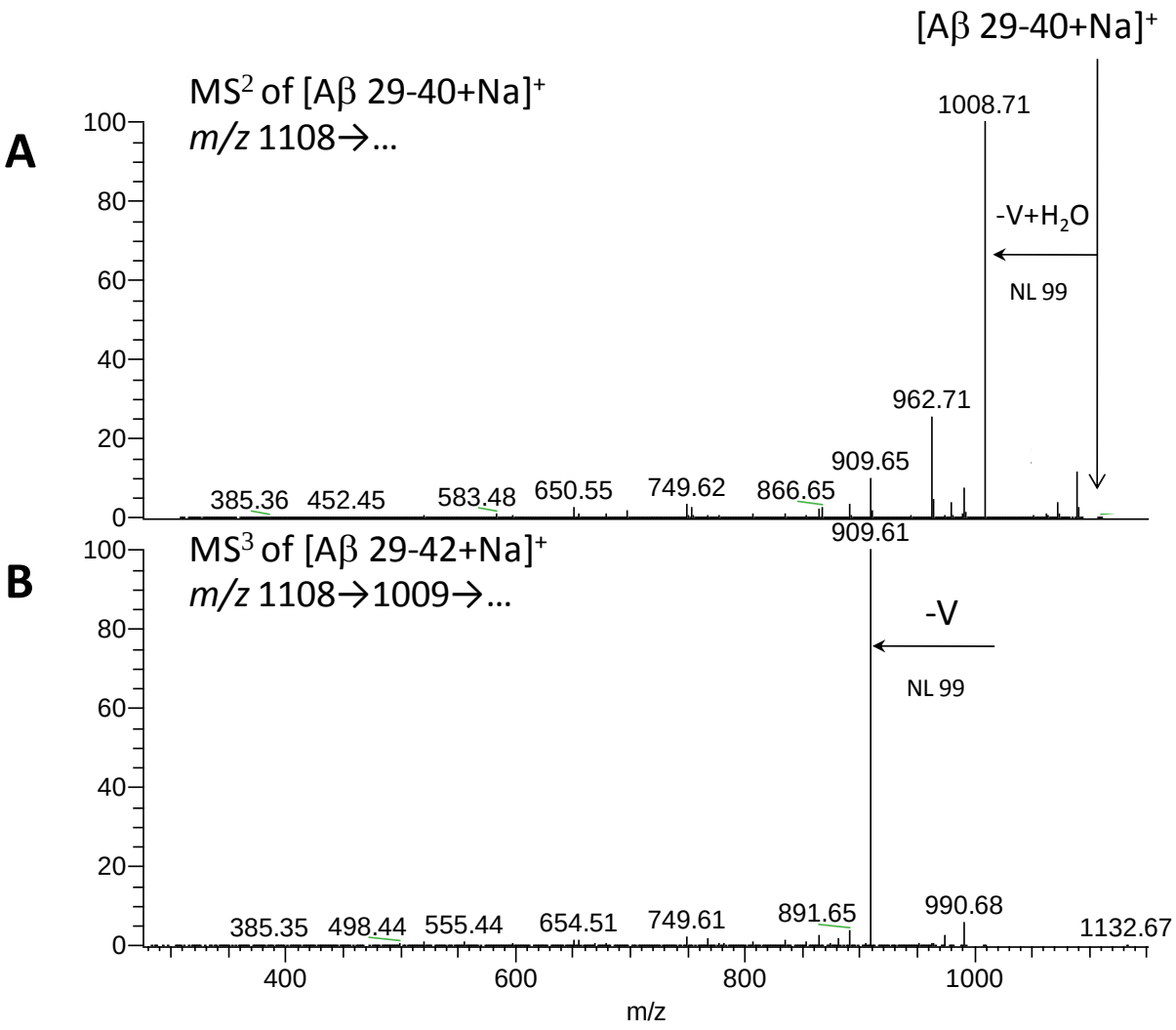

Figure 4-7. MS^2 and MS^3 spectra of the $[A\beta\ 29–40+Na]^+$ ion, *m/z* 1108.0. The top figure, A, illustrates the MS^2 fragmentation of $[A\beta\ 29–40+Na]^+$ (*m/z* 1108.0). The bottom figure, B, illustrates the MS^3 fragmentation of 1108.0→1008.7→… The major ion in each spectrum is due to a neutral loss of valine. The sequence of the Aβ 29–40 tryptic peptide is GAIIGLMVGGVV.

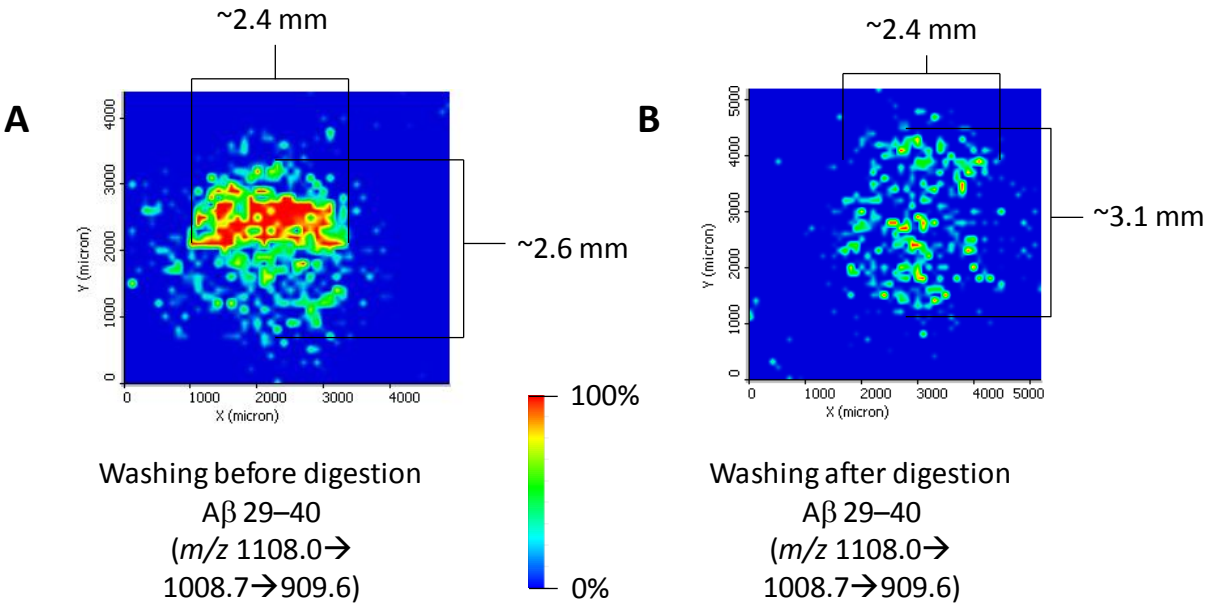

Figure 4-8. Comparison of washing a tissue section before and after tryptic digestion. Aβ standard (a 1 µL droplet) was applied atop two tissue sections. Although the Aβ droplet had similar diameters between the two sections, washing after digestion appears to promote analyte migration in the y-direction (the response of the tryptic peptide ion is 2.6 mm along the y-axis for A versus 3.1 mm for B).

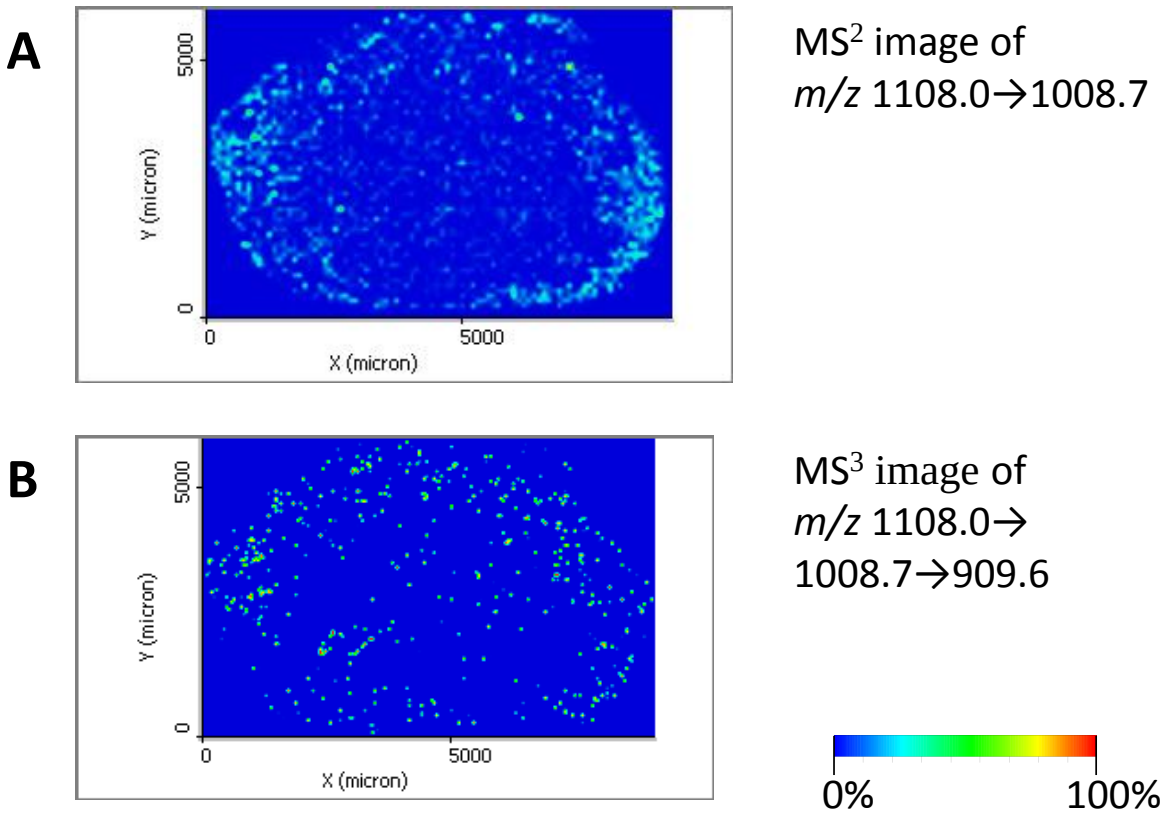

Figure 4-9. MS^2 and MS^3 images of Aβ 29–40 after digestion of Tg2576 mice brain sections. The MS^2 image of *m/z* 1008.7 exhibits a localization of signal in the anterior (left in the image) and posterior (right) sections of the image, A; whereas, more even distribution of signal is noted in the MS^3 image of *m/z* 1108.0→1008.7→909.6.

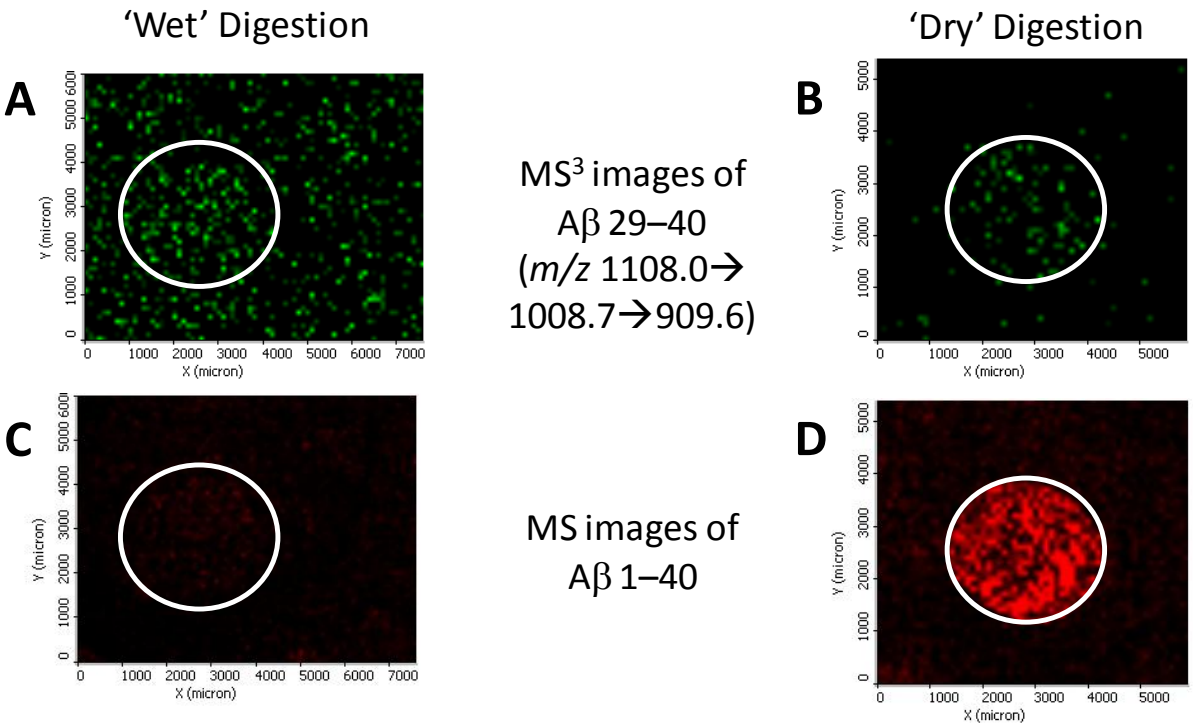

Figure 4-10. Comparison of 'wet' and 'dry' digestion techniques. The white circle in the figures indicates the area where the Aβ 1–40 standard was deposited. The images on the left hand side demonstrate a digestion where the trypsin is applied atop the tissue surface and promptly placed in the sealed, humid incubation chamber. The images on the right hand side illustrate a 'dry digestion' where the trypsin solution is allowed to evaporate prior to placement into the sealed, humid incubation chamber. The top set of images (A and B) illustrate the localization of *m/z* 909.6 after performing an MS^3 experiment isolating Aβ 29–40 tryptic peptide ion then monitoring the second successive loss of valine (see Figure 4-7 for more details). The bottom set of images (C and D) illustrate the localization of the intact Aβ 1–40 ion.

CHAPTER 5
CONCLUSIONS AND FUTURE WORK

Mass spectral imaging offers scientists a unique tool to determine the identity and distribution of a wide range of ions across a tissue section. Identification and localization of peptides within normal and diseased tissue can help determine their biological role. Analyses of large peptides are commonly performed on a ToF MS instrument. However, peptide structural elucidation and identification is more difficult without multiple stages of mass spectrometry. The goal of this work was to demonstrate the advantages and limitations of performing large peptide analysis with a MALDI LIT-MS for MSI studies.

The *m/*z range of a commercial LIT was extended past the normal upper limit of *m/*z 4000 to *m/*z 5500. MS spectra were collected for Aβ 1–40 and 1–42 peptides. Additionally, tandem mass spectrometry was performed on these large peptides. An experiment examining the feasibility of the instrument to perform tandem mass spectrometry over a wide window (>80 Da) proved successful. Wide window tandem mass spectrometry experiments may prove useful for future quantitation studies of endogenous Aβ peptides.

MSI studies offered greater potential to localize intact peptides. It was found that if no washing/fixation was performed during the sample preparation, lipid ions dominated the MS spectra and suppressed the ion signal of the Aβ peptides. A washing and fixation step prior to matrix application enhanced the response of the amyloid peptide fragments. Intact Aβ fragments 1–38, 1–40, and 1–42 ions were imaged in the tissue section and these MS image plots generally correlated with the Thioflavin S histological

images. MS^n fragmentation of Aβ 1–40 ions was performed and these product ions also correlated well with the histological image.

Although MS image plots offered general localization of the amyloid plaques, closely grouped, individual amyloid plaque formations were indistinguishable from one another in the MS image. The poor MS image resolution was due to the large spot size of the laser (~100 µm). The MS image resolution was improved when the raster step size was decreased from 100 µm to 50 µm. After this change, individual plaques, 100 µm apart, were identified in the MS image.

Experiments of peptides digested in situ proved more difficult than those of the intact species. MALDI matrix selection proved to be important for the study of digested Aβ peptides. DHB appeared to promote the ionization of Aβ fragments containing the C-terminus of the peptide. CHCA and SA lacked these diagnostic peaks and thus were discarded in favor for DHB for the remaining experiments.

Detection of tryptic peptides proved unviable unless a washing step and MS^n were used. The washing step should be performed prior to tryptic digestion; otherwise, peptides could migrate across the tissue section during the wash procedure. Unfortunately, this was not the only source of analyte migration.

In situ digestions of Tg2576 mice brain sections were performed. The distribution of Aβ tryptic peptides either indicated localization of amyloid plaques in the anterior and posterior regions of the brain (MS^2 image) or even distribution of the peptide across the tissue section (MS^3 image). This is in disagreement with known localization of the plaques in the cortex and hippocampus regions of the brain. These results suggest significant analyte migration occurred. This is likely due to a ‘puddle’ of trypsin solution

lying atop the tissue surface over the course of the incubation period (2.5 h). The 'puddle' was deemed necessary because no digestion was observed if the trypsin solution was allowed to evaporate and tissue was not kept damp. An alternative to this 'wet' trypsin digestion is to allow the trypsin to dry; afterward, the tissue section was placed into a humid environment to ensure the tissue section remained damp. Although full digestion of the Aβ 1–40 peptide was not achieved, analyte migration was minimized using this 'dry' digestion technique. Further work is needed to determine if this method is viable for in situ digestion of tissue sections.

This work would be valuable to pharmaceutical companies if a drug compound that targets a peptide biomarker and the biomarker itself could be localized. However, the washing and fixation steps would likely eliminate any traces of the drug molecule from the tissue surface. Future studies could involve examining methods to fix both the drug compound and the peptide in the tissue section to permit simultaneous analysis of both compounds; or, serial sections could be examined (one section washed and the adjacent section unwashed).

Another area of interest is the quantitation of peptide biomarkers. The best way to perform a quantitative study would be to apply a deuterated, or a uniformly N^{15}-labeled standard, to the tissue surface and ratio the response of the peptide to the standard to determine the analyte concentration. However, for this experiment, wide isolation MS^n windows would be necessary to isolate both the peptide and its isotopically labeled standard. And alternative to this would be to employ SWIFT waveforms to isolate the analyte and its standard and ignore any response in between the two peptides [99].

In addition to LTQ work, studies of large peptides on a hybrid LIT instrument (LTQ-ToF or LTQ-Orbitrap) could provide valuable complementary information. An LTQ-ToF instrument could offer analysis of Aβ peptides and tau proteins simultaneously. Tau proteins have been linked to AD, however, their molecular weight (~45–65 kDa) [100] is significantly greater than the expanded mass range of the LIT.

Whereas an LTQ-ToF would be used for its high MW range, the high resolution of an LTQ-Orbitrap instrument could prove helpful for distinguishing peptides from noise. Currently the orbitrap instrument will scan up to *m/z* 4000. However, according to private communications with the instrument engineers at Thermo, the orbitrap can detect ion up to *m/*z 5000. An orbitrap coupled to an LIT with an extended mass range could prove useful for the analysis of large peptides.

LIST OF REFERENCES

(1) Nelson, D.; Cox, M. *Principles of Biochemistry*, 3rd ed.; Worth Publishers: New York, 2000.

(2) Wouters, F. S.; Verveer, P. J.; Bastiaens, P. I. H. Imaging biochemistry inside cells. *Trends Cell Biol.* **2001**, *11*, 203-211.

(3) Caprioli, R. M.; Farmer, T. B.; Gile, J. Molecular imaging of biological samples: localization of peptides and proteins using MALDI-TOF MS. *Anal. Chem.* **1997**, *69*, 4751-4760.

(4) Troendle, F. J.; Reddick, C. D.; Yost, R. A. Detection of pharmaceutical compounds in tissue by matrix-assisted laser desorption/ionization and laser desorption/chemical ionization tandem mass spectrometry with a quadrupole ion trap. *J. Am. Soc. Mass Spectrom.* **1999**, *10*, 1315-1321.

(5) Seeley, E. H.; Caprioli, R. M. Molecular imaging of proteins in tissues by mass spectrometry. *Proc. Natl. Acad. Sci. U. S. A.* **2008**, *105*, 18126-18131.

(6) Garrett, T. J.; Prieto-Conaway, M. C.; Kovtoun, V.; Bui, H.; Izgarian, N.; Stafford, G.; Yost, R. A. Imaging of small molecules in tissue sections with a new intermediate-pressure MALDI linear ion trap mass spectrometer. *Int. J. Mass Spectrom.* **2007**, *260*, 166-176.

(7) Schwartz, S. A.; Reyzer, M. L.; Caprioli, R. M. Direct tissue analysis using matrix-assisted laser desorption/ionization mass spectrometry: Practical aspects of sample preparation. *J. Mass Spectrom.* **2003**, *38*, 699-708.

(8) Skoeld, K.; Svensson, M.; Nilsson, A.; Falth, M.; Svenningsson, P.; Andren, P. The importance of sample handling in neuropeptidomics, 2008; John Wiley & Sons, Inc.; 177-189.

(9) Landgraf, R. R.; Conaway, M. C. P.; Garrett, T. J.; Stacpoole, P. W.; Yost, R. A. Imaging of Lipids in Spinal Cord Using Intermediate Pressure Matrix-Assisted Laser Desorption-Linear Ion Trap/Orbitrap MS. *Anal. Chem.* **2009**, *81*, 8488-8495.

(10) Crossman, L.; McHugh, N. A.; Hsieh, Y.; Korfmacher, W. A.; Chen, J. Investigation of the profiling depth in matrix-assisted laser desorption/ionization imaging mass spectrometry. *Rapid Commun. Mass Spectrom.* **2006**, *20*, 284-290.

(11) Chaurand, P.; Schwartz, S. A.; Billheimer, D.; Xu, B. J.; Crecelius, A.; Caprioli, R. M. Integrating histology and imaging mass spectrometry. *Anal. Chem.* **2004**, *76*, 1145-1155.

(12) Scherl, A.; Zimmermann-Ivol, C. G.; Di, D. J.; Vaezzadeh, A. R.; Binz, P.-A.; Amez-Droz, M.; Cochard, R.; Sanchez, J.-C.; Glueckmann, M.; Hochstrasser, D. F. Gold coating of non-conductive membranes before matrix-assisted laser desorption/ionization tandem mass spectrometric analysis prevents charging effect. *Rapid Commun. Mass Spectrom.* **2005**, *19*, 605-610.

(13) Ayorinde, F. O.; Hambright, P.; Porter, T. N.; Keith, Q. L., Jr. Use of meso-Tetrakis(pentafluorophenyl)porphyrin as a Matrix for Low Molecular Weight Alkylphenol Ethoxylates in Laser Desorption/Ionization Time-of-Flight Mass Spectrometry. *Rapid Commun. Mass Spectrom.* **1999**, *13*, 2474-2479.

(14) Cohen, L. H.; Gusev, A. I. Small molecule analysis by MALDI mass spectrometry. *Anal. Bioanal. Chem.* **2002**, *373*, 571-586.

(15) Lemaire, R.; Tabet, J. C.; Ducoroy, P.; Hendra, J. B.; Salzet, M.; Fournier, I. Solid ionic matrixes for direct tissue analysis and MALDI imaging. *Anal. Chem.* **2006**, *78*, 809-819.

(16) Meriaux, C.; Franck, J.; Wisztorski, M.; Salzet, M.; Fournier, I. Liquid ionic matrixes for MALDI mass spectrometry imaging of lipids. *J. Proteomics* **2010**, *73*, 1204-1218.

(17) Baluya, D. L.; Garrett, T. J.; Yost, R. A. Automated MALDI Matrix Deposition Method with Inkjet Printing for Imaging Mass Spectrometry. *Anal. Chem.* **2007**, *79*, 6862-6867.

(18) Aerni, H.-R.; Cornett, D. S.; Caprioli, R. M. Automated Acoustic Matrix Deposition for MALDI Sample Preparation. *Anal. Chem.* **2006**, *78*, 827-834.

(19) Hankin, J. A.; Barkley, R. M.; Murphy, R. C. Sublimation as a Method of Matrix Application for Mass Spectrometric Imaging. *J. Am. Soc. Mass Spectrom.* **2007**, *18*, 1646-1652.

(20) Puolitaival, S. M.; Burnum, K. E.; Cornett, D. S.; Caprioli, R. M. Solvent-Free Matrix Dry-Coating for MALDI Imaging of Phospholipids. *J. Am. Soc. Mass Spectrom.* **2008**, *19*, 882-886.

(21) Kaletas, B. K.; van der Wiel, I. M.; Stauber, J.; Dekker, L. J.; Guzel, C.; Kros, J. M.; Luider, T. M.; Heeren, R. M. A. Sample preparation issues for tissue imaging by imaging MS. *Proteomics* **2009**, *9*, 2622-2633.

(22) Khatib-Shahidi, S.; Andersson, M.; Herman, J. L.; Gillespie, T. A.; Caprioli, R. M. Direct Molecular Analysis of Whole-Body Animal Tissue Sections by Imaging MALDI Mass Spectrometry. *Anal. Chem.* **2006**, *78*, 6448-6456.

(23) Solon, E. G.; Schweitzer, A.; Stoeckli, M.; Prideaux, B. Autoradiography, MALDI-MS, and SIMS-MS Imaging in Pharmaceutical Discovery and Development. *AAPS J.* **2010**, *12*, 11-26.

(24) Karas, M.; Hillenkamp, F. Laser desorption ionization of proteins with molecular masses exceeding 10,000 daltons. *Anal. Chem.* **1988**, *60*, 2299-2301.

(25) Hillenkamp, F.; Karas, M.; Beavis, R. C.; Chait, B. T. Matrix-assisted laser desorption/ionization mass spectrometry of biopolymers. *Anal. Chem.* **1991**, *63*, 1193A-1203A.

(26) Simpson, R. J. *Proteins and Proteomics: A Laboratory Manual*; Cold Spring Harbor Laboratory Press: New York, NY, 2003.

(27) Cooks, R. G.; Ouyang, Z.; Takats, Z.; Wiseman, J. M. Ambient Mass Spectrometry. *Science* **2006**, *311*, 1566-1570.

(28) Takats, Z.; Wiseman, J. M.; Gologan, B.; Cooks, R. G. Mass Spectrometry Sampling Under Ambient Conditions with Desorption Electrospray Ionization. *Science* **2004**, *306*, 471-473.

(29) Kertesz, V.; Van Berkel, G. J. Scanning and Surface Alignment Considerations in Chemical Imaging with Desorption Electrospray Mass Spectrometry. *Anal. Chem.* **2008**, *80*, 1027-1032.

(30) Takats, Z.; Wiseman, J. M.; Cooks, R. G. Ambient mass spectrometry using desorption electrospray ionization (DESI): Instrumentation, mechanisms and applications in forensics, chemistry, and biology. *J. Mass Spectrom.* **2005**, *40*, 1261-1275.

(31) Ifa, D. R.; Wiseman, J. M.; Song, Q.; Cooks, R. G. Development of capabilities for imaging mass spectrometry under ambient conditions with desorption electrospray ionization (DESI). *Int. J. Mass Spectrom.* **2007**, *259*, 8-15.

(32) Pasilis, S. P.; Kertesz, V.; Van Berkel, G. J. Surface Scanning Analysis of Planar Arrays of Analytes with Desorption Electrospray Ionization-Mass Spectrometry. *Anal. Chem.* **2007**, *79*, 5956-5962.

(33) Van Berkel, G. J.; Kertesz, V.; Koeplinger, K. A.; Vavrek, M.; Kong, A.-N. T. Liquid microjunction surface sampling probe electrospray mass spectrometry for detection of drugs and metabolites in thin tissue sections. *J. Mass Spectrom.* **2008**, *43*, 500-508.

(34) Kertesz, V.; Van Berkel, G. J. Fully automated liquid extraction-based surface sampling and ionization using a chip-based robotic nanoelectrospray platform. *J. Mass Spectrom.* **2010**, *45*, 252-260.

(35) Northen, T. R.; Yanes, O.; Northen, M. T.; Marrinucci, D.; Uritboonthai, W.; Apon, J.; Golledge, S. L.; Nordstrom, A.; Siuzdak, G. Clathrate nanostructures for mass spectrometry. *Nature* **2007**, *449*, 1033-1036.

(36) Patti, G. J.; Woo, H.-K.; Yanes, O.; Shriver, L.; Thomas, D.; Uritboonthai, W.; Apon, J. V.; Steenwyk, R.; Manchester, M.; Siuzdak, G. Detection of Carbohydrates and Steroids by Cation-Enhanced Nanostructure-Initiator Mass Spectrometry (NIMS) for Biofluid Analysis and Tissue Imaging. *Anal. Chem.* **2010**, *82*, 121-128.

(37) Reyzer, M. L.; Hsieh, Y.; Ng, K.; Korfmacher, W. A.; Caprioli, R. M. Direct analysis of drug candidates in tissue by matrix-assisted laser desorption/ionization mass spectrometry. *J. Mass Spectrom.* **2003**, *38*, 1081-1092.

(38) Cornett, D. S.; Frappier, S. L.; Caprioli, R. M. MALDI-FTICR Imaging Mass Spectrometry of Drugs and Metabolites in Tissue. *Anal. Chem.* **2008**, *80*, 5648-5653.

(39) Stoeckli, M.; Staab, D.; Schweitzer, A. Compound and metabolite distribution measured by MALDI mass spectrometric imaging in whole-body tissue sections. *Int. J. Mass Spectrom.* **2007**, *260*, 195-202.

(40) Bouslimani, A.; Bec, N.; Glueckmann, M.; Hirtz, C.; Larroque, C. Matrix-assisted laser desorption/ionization imaging mass spectrometry of oxaliplatin derivatives in heated intraoperative chemotherapy (HIPEC)-like treated rat kidney. *Rapid Commun. Mass Spectrom.* **2010**, *24*, 415-421.

(41) Chen, J.; Hsieh, Y.; Knemeyer, I.; Crossman, L.; Korfmacher, W. A. Visualization of first-pass drug metabolism of terfenadine by MALDI-imaging mass spectrometry. *Drug Metab. Lett.* **2008**, *2*, 1-4.

(42) Li, F.; Hsieh, Y.; Kang, L.; Sondey, C.; Lachowicz, J.; Korfmacher, W. A. MALDI-tandem mass spectrometry imaging of astemizole and its primary metabolite in rat brain sections. *Bioanalysis* **2009**, *1*, 299-307.

(43) Atkinson, S. J.; Loadman, P. M.; Sutton, C.; Patterson, L. H.; Clench, M. R. Examination of the distribution of the bioreductive drug AQ4N and its active metabolite AQ4 in solid tumours by imaging matrix-assisted laser desorption/ionisation mass spectrometry. *Rapid Commun. Mass Spectrom.* **2007**, *21*, 1271-1276.

(44) Trim, P. J.; Henson, C. M.; Avery, J. L.; McEwen, A.; Snel, M. F.; Claude, E.; Marshall, P. S.; West, A.; Princivalle, A. P.; Clench, M. R. Matrix-Assisted Laser Desorption/Ionization-Ion Mobility Separation-Mass Spectrometry Imaging of Vinblastine in Whole Body Tissue Sections. *Anal. Chem.* **2008**, *80*, 8628-8634.

(45) Magparangalan, D. P.; Garrett, T. J.; Drexler, D. M.; Yost, R. A. Analysis of Large Peptides by MALDI Using a Linear Quadrupole Ion Trap with Mass Range Extension. *Anal. Chem.* **2010**, *82*, 930-934.

(46) Groseclose, M. R.; Andersson, M.; Hardesty, W. M.; Caprioli, R. M. Identification of proteins directly from tissue: in situ tryptic digestions coupled with imaging mass spectrometry. *J. Mass Spectrom.* **2007**, *42*, 254-262.

(47) Schwartz, J. C.; Senko, M. W.; Syka, J. E. P. A two-dimensional quadrupole ion trap mass spectrometer. *J. Am. Soc. Mass Spectrom.* **2002**, *13*, 659-669.

(48) Perchalski, R. *Characteristics and Application of a Laser Ionization/Evaporation Source for Tandem Mass Spectrometry*, University of Florida, Gainesville, FL, 1985.

(49) Sleno, L.; Volmer, D. A. Some fundamental and technical aspects of the quantitative analysis of pharmaceutical drugs by matrix-assisted laser desorption/ionization mass spectrometry. *Rapid Commun. Mass Spectrom.* **2005**, *19*, 1928-1936.

(50) Gobey, J.; Cole, M.; Janiszewski, J.; Covey, T.; Chau, T.; Kovarik, P.; Corr, J. Characterization and performance of MALDI on a triple quadrupole mass spectrometer for analysis and quantification of small molecules. *Anal. Chem.* **2005**, *77*, 5643-5654.

(51) Hopfgartner, G.; Varesio, E.; Stoeckli, M. Matrix-assisted laser desorption/ionization mass spectrometric imaging of complete rat sections using a triple quadrupole linear ion trap. *Rapid Commun. Mass Spectrom.* **2009**, *23*, 733-736.

(52) Kertesz, V.; Van Berkel, G. J.; Vavrek, M.; Koeplinger, K. A.; Schneider, B. B.; Covey, T. R. Comparison of Drug Distribution Images from Whole-Body Thin Tissue Sections Obtained Using Desorption Electrospray Ionization Tandem Mass Spectrometry and Autoradiography. *Anal. Chem.* **2008**, *80*, 5168-5177.

(53) Strupat, K.; Kovtoun, V.; Bui, H.; Viner, R.; Stafford, G.; Horning, S. MALDI Produced Ions Inspected with a Linear Ion Trap-Orbitrap Hybrid Mass Analyzer. *J. Am. Soc. Mass Spectrom.* **2009**, *20*, 1451-1463.

(54) Watson, J. T.; Sparkman, O. D. *Introduction to Mass Spectrometry: Instrumentation, Applications, and Strategies for Data Interpretation*, 4th ed.; Wiley: Hoboken, NJ, 2007.

(55) Wong, P. S. H.; Cooks, R. G. Ion trap mass spectrometry. *Curr. Separations* **1997**, *16*, 85-92.

(56) March, R. E.; Todd, J. F. J. *Quadrupole Ion Trap Mass Spectrometry*, 2nd ed.; Wiley: Hoboken, NJ, 2005.

(57) Todd, J. F. J. Introduction to practical aspects of ion trap mass spectrometry. In *Pract. Aspects Ion Trap Mass Spectrom.*; CRC, 1995; Vol. 1, pp 3-24.

(58) Douglas, D. J.; Frank, A. J.; Mao, D. M. Linear ion traps in mass spectrometry. *Mass Spectrom. Rev.* **2005**, *24*, 1-29.

(59) Stafford, G. C., Jr.; Kelley, P. E.; Syka, J. E. P.; Reynolds, W. E.; Todd, J. F. J. Recent improvements in and analytical applications of advanced ion trap technology. *Int. J. Mass Spectrom. Ion Processes* **1984**, *60*, 85-98.

(60) Mikesh, L. M.; Ueberheide, B.; Chi, A.; Coon, J. J.; Syka, J. E. P.; Shabanowitz, J.; Hunt, D. F. The utility of ETD mass spectrometry in proteomic analysis. *Biochim. Biophys. Acta* **2006**, *1764*, 1811-1822.

(61) Zubarev, R. A. Electron-capture dissociation tandem mass spectrometry. *Curr. Opin. Biotechnol.* **2004**, *15*, 12-16.

(62) Selkoe, D. J. Degenerative disorders: Alzheimer disease. In *Molecular and Genetic Basis of Neurologic and Psychiatric Disease (4th Edition)*; Rosenberg, R. N., Dimauro, S., Paulson, H. L., Ptacek, L., Nestler, E. J., Eds.; Lippincott Williams & Wilkins: Philadelphia, PA, 2008, pp 317-329.

(63) National Institute on Aging (http://www.nia.nih.gov/Alzheimers/) (Accessed June 20, 2010).

(64) Ford, M. J.; Cantone, J. L.; Polson, C.; Toyn, J. H.; Meredith, J. E.; Drexler, D. M. Qualitative and quantitative characterization of the amyloid beta peptide (Abeta) population in biological matrices using an immunoprecipitation-LC/MS assay. *J. Neurosci. Methods* **2008**, *168*, 465-474.

(65) Geula, C. Pathological Diagnosis of Alzheimer's Disease. In *Early Diagnosis of Alzheimer's Disease*; Scinto, L. F. M., Daffner, K. R., Eds.; Humana Press, Inc.: Totowa, NJ, 2000, pp 65-82.

(66) Deshpande, A.; Mina, E.; Glabe, C.; Busciglio, J. Different Conformations of Amyloid beta Induce Neurotoxicity by Distinct Mechanisms in Human Cortical Neurons. *J. Neurosci.* **2006**, *26*, 6011-6018.

(67) Stoeckli, M.; Staab, D.; Staufenbiel, M.; Wiederhold, K. H.; Signor, L. Molecular imaging of amyloid beta peptides in mouse brain sections using mass spectrometry. *Anal. Biochem.* **2002**, *311*, 33-39.

(68) Rohner, T. C.; Staab, D.; Stoeckli, M. MALDI mass spectrometric imaging of biological tissue sections. *Mech. Ageing Dev.* **2005**, *126*, 177-185.

(69) Stoeckli, M.; Knochenmuss, R.; McCombie, G.; Mueller, D.; Rohner, T.; Staab, D.; Wiederhold, K. H. MALDI MS imaging of amyloid. In *Amyloid, Prions, and Other Protein Aggregates, Pt B*; Elsevier Academic Press Inc: San Diego, 2006; Vol. 412, pp 94-106.

(70) Petricoin, E.; Wulfkuhle, J.; Espina, V.; Liotta, L. A. Clinical proteomics: Revolutionizing disease detection and patient tailoring therapy. *J. Proteome Res.* **2004**, *3*, 209-217.

(71) Li, W.; Nemirovskiy, O.; Fountain, S.; Mathews, W. R.; Szekely-Klepser, G. Clinical validation of an immunoaffinity LC-MS/MS assay for the quantification of a collagen type II neoepitope peptide: A biomarker of matrix metalloproteinase activity and osteoarthritis in human urine. *Anal. Biochem.* **2007**, *369*, 41-53.

(72) Pisitkun, T.; Johnstone, R.; Knepper, M. A. Discovery of urinary biomarkers. *Mol. Cell. Proteomics* **2006**, *5*, 1760-1771.

(73) Wu, S.-L.; Amato, H.; Biringer, R.; Choudhary, G.; Shieh, P.; Hancock, W. S. Targeted proteomics of low-level proteins in human plasma by LC/MSn: Using human growth hormone as a model system. *J. Proteome Res.* **2002**, *1*, 459-465.

(74) Taylor, S. W.; Andon, N. L.; Bilakovics, J. M.; Lowe, C.; Hanley, M. R.; Pittner, R.; Ghosh, S. S. Efficient High-Throughput Discovery of Large Peptidic Hormones and Biomarkers. *J. Proteome Res.* **2006**, *5*, 1776-1784.

(75) Kaiser, R. E., Jr.; Cooks, R. G.; Stafford, G. C., Jr.; Syka, J. E. P.; Hemberger, P. H. Operation of a quadrupole ion trap mass spectrometer to achieve high mass/charge ratios. *Int. J. Mass Spectrom. Ion Processes* **1991**, *106*, 79-115.

(76) Masters, C. L.; Simms, G.; Weinman, N. A.; Multhaup, G.; McDonald, B. L.; Beyreuther, K. Amyloid plaque core protein in Alzheimer disease and Down syndrome. *Proc. Natl. Acad. Sci. U. S. A.* **1985**, *82*, 4245-4249.

(77) Hardy, J.; Selkoe, D. J. The amyloid hypothesis of Alzheimer's disease: progress and problems on the road to therapeutics. *Science* **2002**, *297*, 353-356.

(78) Selkoe, D. J.; Schenk, D. Alzheimer's disease: Molecular understanding predicts amyloid-based therapeutics. *Annu. Rev. Pharmacol. Toxicol.* **2003**, *43*, 545-584.

(79) Schupf, N.; Tang, M. X.; Fukuyama, H.; Manly, J.; Andrews, H.; Mehta, P.; Ravetch, J.; Mayeux, R. Peripheral Abeta subspecies as risk biomarkers of Alzheimer's disease. *Proc. Natl. Acad. Sci. U. S. A.* **2008**, *105*, 14052-14057.

(80) Graff-Radford Neill, R.; Crook Julia, E.; Lucas, J.; Boeve Bradley, F.; Knopman David, S.; Ivnik Robert, J.; Smith Glenn, E.; Younkin Linda, H.; Petersen Ronald, C.; Younkin Steven, G. Association of low plasma Abeta42/Abeta40 ratios with increased imminent risk for mild cognitive impairment and Alzheimer disease. *Arch. Neurol.* **2007**, *64*, 354-362.

(81) ProteinProspector (http://prospector.ucsf.edu/) (Accessed July 25, 2009).

(82) Grasso, G.; Mineo, P.; Rizzarelli, E.; Spoto, G. MALDI, AP/MALDI and ESI techniques for the MS detection of amyloid beta -peptides. *Int. J. Mass Spectrom.* **2009**, *282*, 50-55.

(83) Qin, J.; Chait, B. T. Preferential Fragmentation of Protonated Gas-Phase Peptide Ions Adjacent to Acidic Amino Acid Residues. *J. Am. Chem. Soc.* **1995**, *117*, 5411-5412.

(84) Garrett, T. J.; Yost, R. A. Analysis of Intact Tissue by Intermediate-Pressure MALDI on a Linear Ion Trap Mass Spectrometer. *Anal. Chem.* **2006**, *78*, 2465-2469.

(85) Reich, R. F.; Cudzilo, K.; Yost, R. A. Quantitative Imaging of Cocaine and Its Metabolites in Postmortem Brain Tissue by Intermediate-Pressure MALDI/Linear Ion Trap Tandem Mass Spectrometry, *Proceedings of the 56th ASMS Conference on Mass Spectrometry*, Denver, CO, June 1-5 2008.

(86) Centers for Disease Control and Prevention (http://www.cdc.gov) (Accessed June 20, 2010).

(87) Klunk, W. E.; Engler, H.; Nordberg, A.; Wang, Y. M.; Blomqvist, G.; Holt, D. P.; Bergstrom, M.; Savitcheva, I.; Huang, G. F.; Estrada, S.; Ausen, B.; Debnath, M. L.; Barletta, J.; Price, J. C.; Sandell, J.; Lopresti, B. J.; Wall, A.; Koivisto, P.; Antoni, G.; Mathis, C. A.; Langstrom, B. Imaging brain amyloid in Alzheimer's disease with Pittsburgh Compound-B. *Ann. Neurol.* **2004**, *55*, 306-319.

(88) Westermark, G. T.; Johnson, K. H.; Westermark, P. Staining methods for identification of amyloid in tissue. In *Methods Enzymol.*; Academic Press, 1999; Vol. 309, pp 3-25.

(89) Pype, S.; Moechars, D.; Dillen, L.; Mercken, M. Characterization of amyloid Î² peptides from brain extracts of transgenic mice overexpressing the London mutant of human amyloid precursor protein. *J. Neurochem.* **2003**, *84*, 602-609.

(90) Stoeckli, M.; Farmer, T. B. MALDI-MS imaging in biomedical research. In *Biomed. Appl. Proteomics*; Sanchez, J.-C., Corthals, G. L., Hochstrasser, D. F., Eds.; Wiley-VCH: Weinheim, 2004, pp 373-388.

(91) Hsiao, K.; Chapman, P.; Nilsen, S.; Eckman, C.; Harigaya, Y.; Younkin, S.; Yang, F.; Cole, G. Correlative Memory Deficits, Abeta Elevation, and Amyloid Plaques in Transgenic Mice. *Science* **1996**, *274*, 99-103.

(92) Jakobs, S. High resolution imaging of live mitochondria. *Biochim. Biophys. Acta, Mol. Cell. Res* **2006**, *1763*, 561-575.

(93) Steen, H.; Mann, M. The abc's (and xyz's) of peptide sequencing. *Nat. Rev. Mol. Cell Biol.* **2004**, *5*, 699-711.

(94) Lemaire, R.; Desmons, A.; Tabet, J. C.; Day, R.; Salzet, M.; Fournier, I. Direct Analysis and MALDI Imaging of Formalin-Fixed, Paraffin-Embedded Tissue Sections. *J. Proteome Res.* **2007**, *6*, 1295-1305.

(95) Setou, M.; Hayasaka, T.; Shimma, S.; Sugiura, Y.; Matsumoto, M. Protein denaturation improves enzymatic digestion efficiency for direct tissue analysis using mass spectrometry. *Appl. Surf. Sci.* **2008**, *255*, 1555-1559.

(96) CHIP-1000 (http://www.ssi.shimadzu.com/products/literature/Biotech/CHIP-1000.pdf) (Accessed December 1, 2010).

(97) Djidja, M.-C.; Francese, S.; Loadman, P. M.; Sutton, C. W.; Scriven, P.; Claude, E.; Snel, M. F.; Franck, J.; Salzet, M.; Clench, M. R. Detergent addition to tryptic digests and ion mobility separation prior to MS/MS improves peptide yield and protein identification for in situ proteomic investigation of frozen and formalin-fixed paraffin-embedded adenocarcinoma tissue sections. *Proteomics* **2009**, *9*, 2750-2763.

(98) Lin, T.; Payne, A. H.; Glish, G. L. Dissociation pathways of alkali-cationized peptides: opportunities for C-terminal peptide sequencing. *J. Am. Soc. Mass Spectrom.* **2001**, *12*, 497-504.

(99) Reich, R. F.; Cromwell, K. N.; Yost, R. A. MALDI-MS^n Quantitation by Selective Isolation of Analyte and Internal Standard Ions Using a Multi-Notch SWIFT Waveform, *Proceedings of the 57th ASMS Conference on Mass Spectrometry*, Philadelphia, PA, May 31-June 4 2009.

(100) Buée, L.; Bussière, T.; Buée-Scherrer, V.; Delacourte, A.; Hof, P. R. Tau protein isoforms, phosphorylation and role in neurodegenerative disorders. *Brain Research Reviews* **2000**, *33*, 95-130.

BIOGRAPHICAL SKETCH

Daniel Patrick Magparangalan was born in 1977 to Danilo and Anita Magparangalan, the first of three children. Shortly after his birth, his family moved to St. Louis, where Daniel spent the majority of his years. Daniel attended Saint Louis University for his undergraduate studies and majored in Chemistry. After graduation, Daniel was employed at Mallinckrodt, Inc., in various positions. Initially, he worked as a peptide chemist performing peptide synthesis to support development efforts. Later, he moved to the quality control portion of the group. Later, he moved from analyzing large biomolecules to HPLC method development of small drug molecules. It was here that he was first introduced to mass spectrometry. Wanting to learn more about MS, he eventually left Mallinckrodt left to study at the University of Florida. Daniel joined the chemistry program in 2005 under the advisement of Dr. Richard A. Yost.